ATTACHMENT I

QUALITY ASSURANCE

The Quality Assurance Programs for FPL and Combustion Engineering are described in this section.

FPL Quality Assurance Program

The FPL Quality Assurance Program is addressed in "FPL Topical Quality Assurance Report" (FPL TQAR 1-76A), Revsion 6, June 10, 1983. The Topical Quality Assurance Report is an integral part of Corporate Quality Assurance Manual (FPL-NQA-100A).

The control programs described in the following specific NQA-100A Quality Procedures have and will continue to be utilized to monitor repair of the core support barrel:

a. QP 4.4, "Review of Procurement Documents for Items and Services Other Than Spare Parts." Under the provisions of this document, the FPL Quality Assurance organization reviews and approves all procurement documents issued to Combustion Engineering (C-E) Avery associated with repair of the core support barrel.

b. QP 18.1, "Conduct of Quality Assurance Department Quality Audits." Under the provisons of this document, the FPL Quality Assurance organization audits on-site activities to ensure that documented procedures are developed and implemented for such operations as plugging, patching and cleaning of the core support barrel.

Combustion Engineering Quality Assurance Program

The C-E Avery Division Quality Assurance Program is described in its Quality Assurance Manual, Rev. 03, June 18, 1982. Compliance with the requirements of this manual was audited by the FPL Quality Assurance organization in November, 1983 with satisfactory results.

TABLE OF CONTENTS

CHAPTER 1

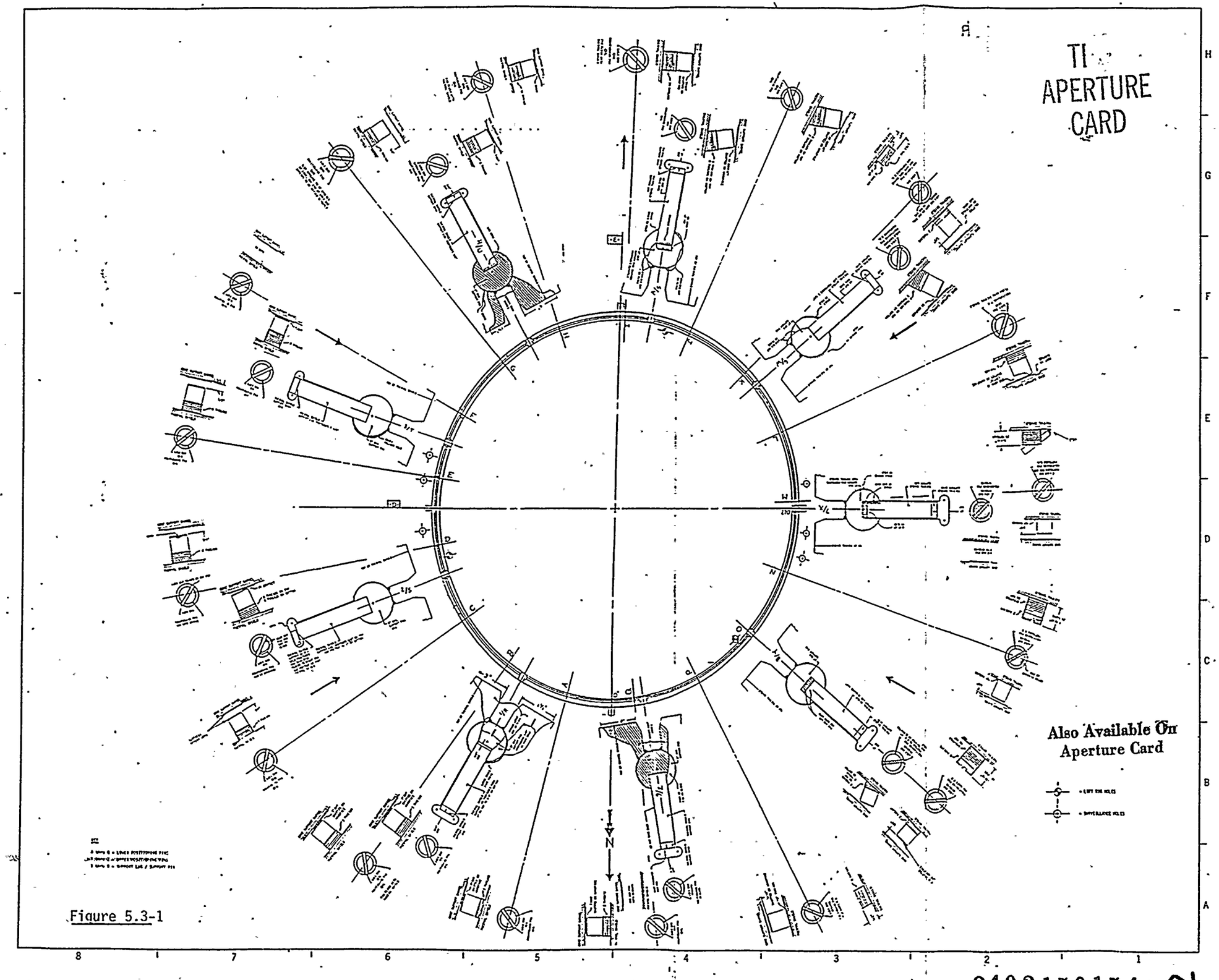

Figure 5.3-1

Also Available On
Aperture Card

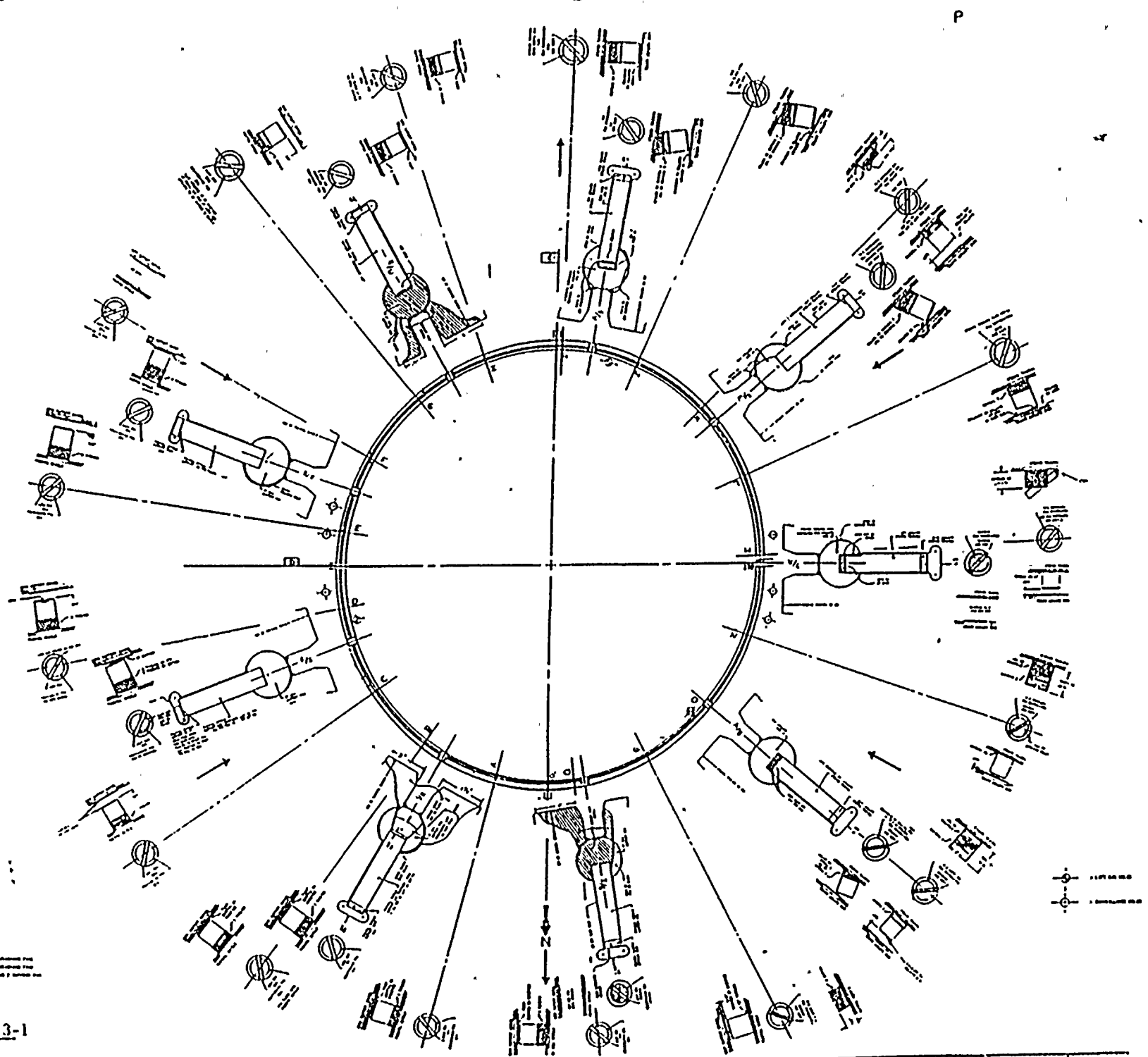

Figure 5.3-1

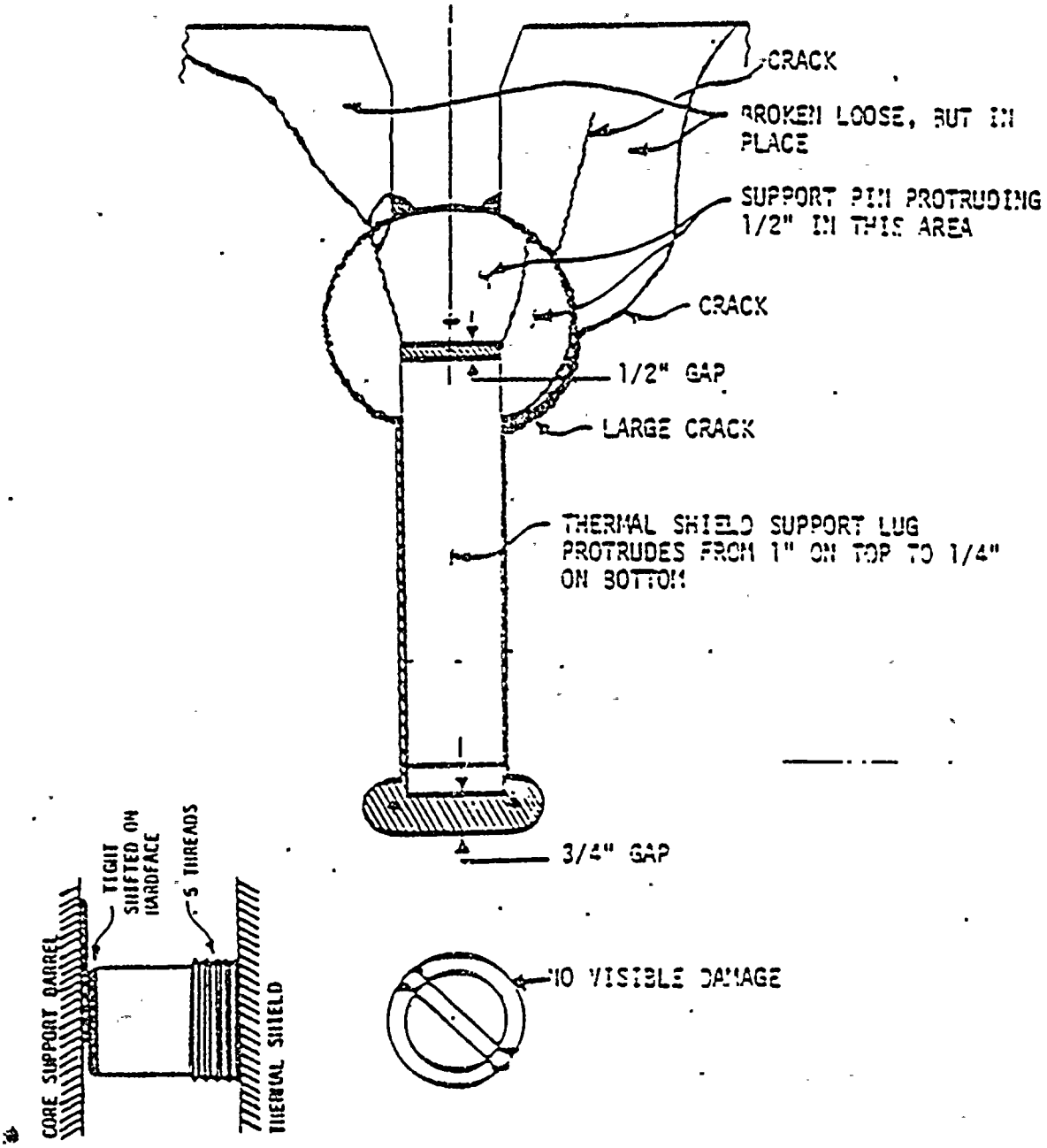

Figure 5.3-2

THERMAL SHIELD POSITION I/R (30°)

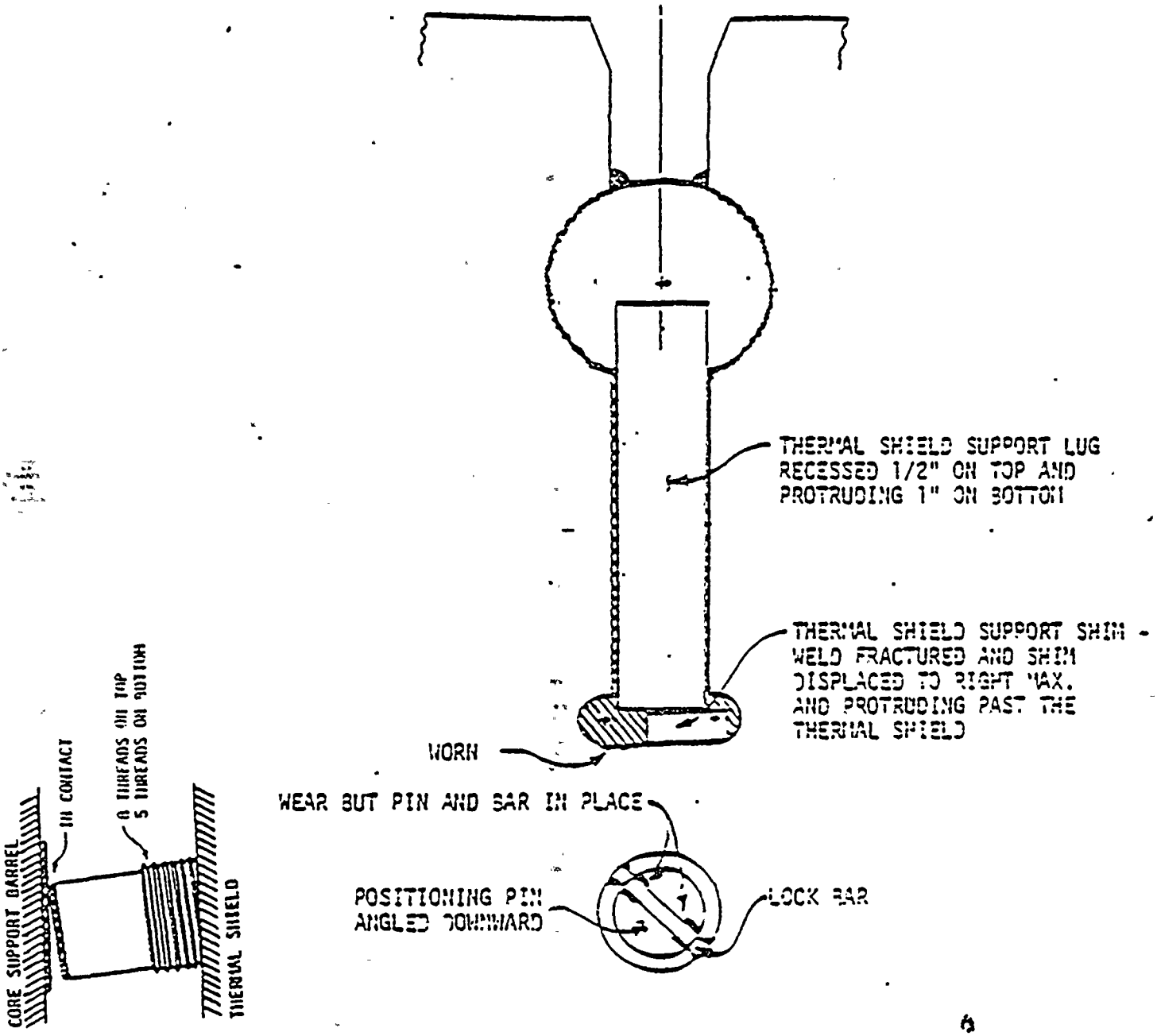

Figure 5.3-3

THERMAL SHIELD POSITION 2/S (70°)

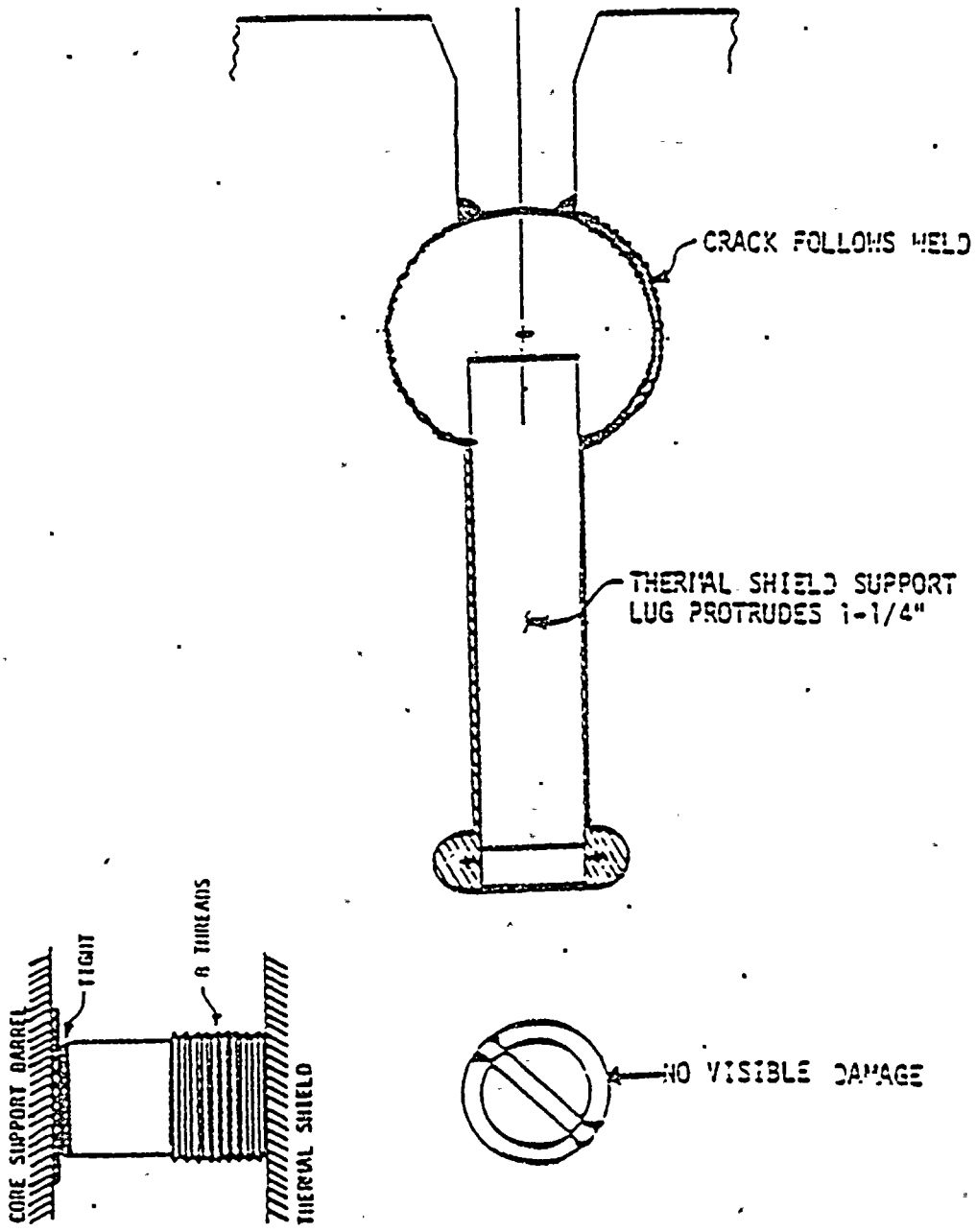

Figure 5.3-4

THERMAL SHIELD POSITION 3/T (110°)

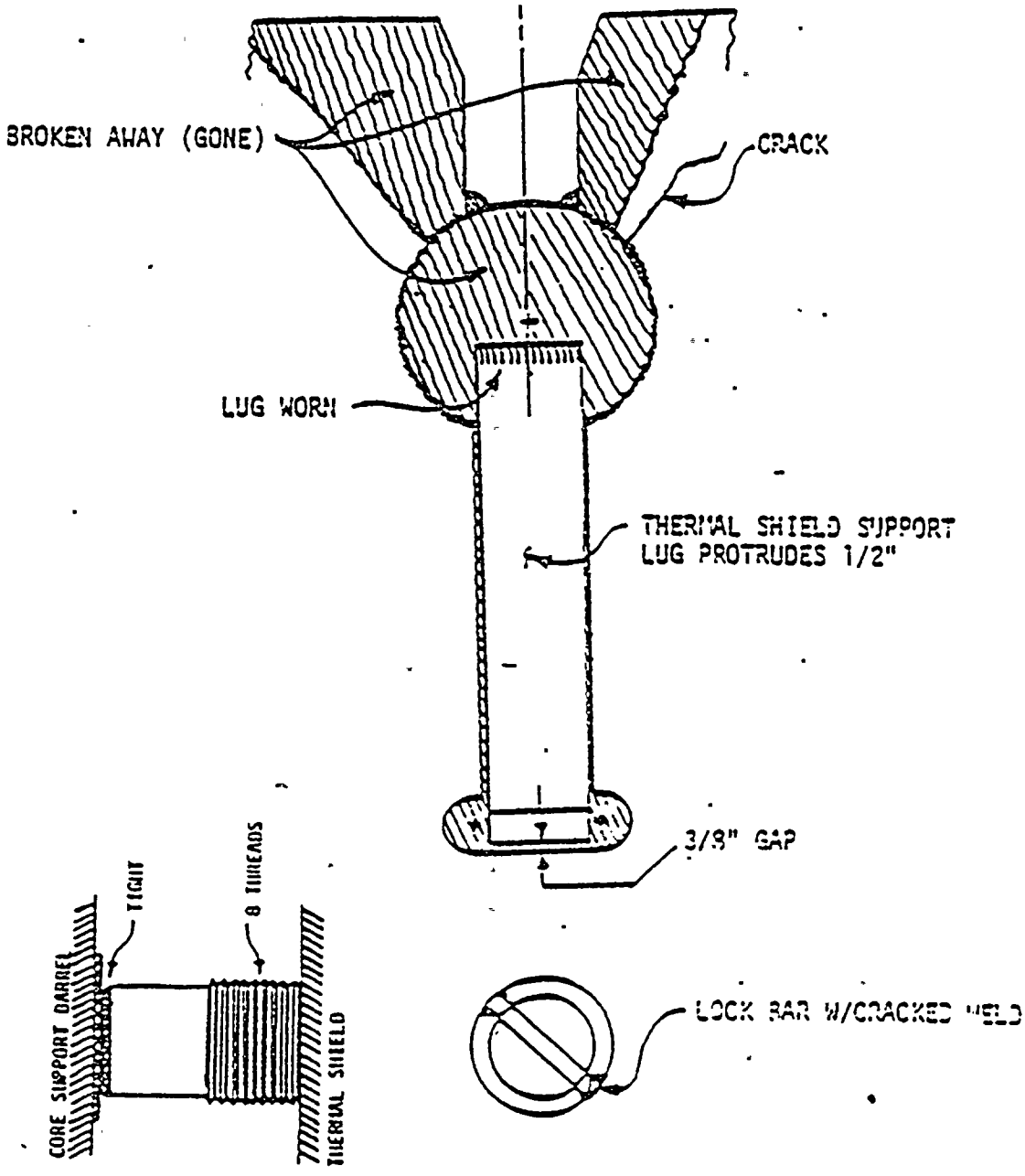

Figure 5.3-5

THERMAL SHIELD POSITION 4/U (180°)

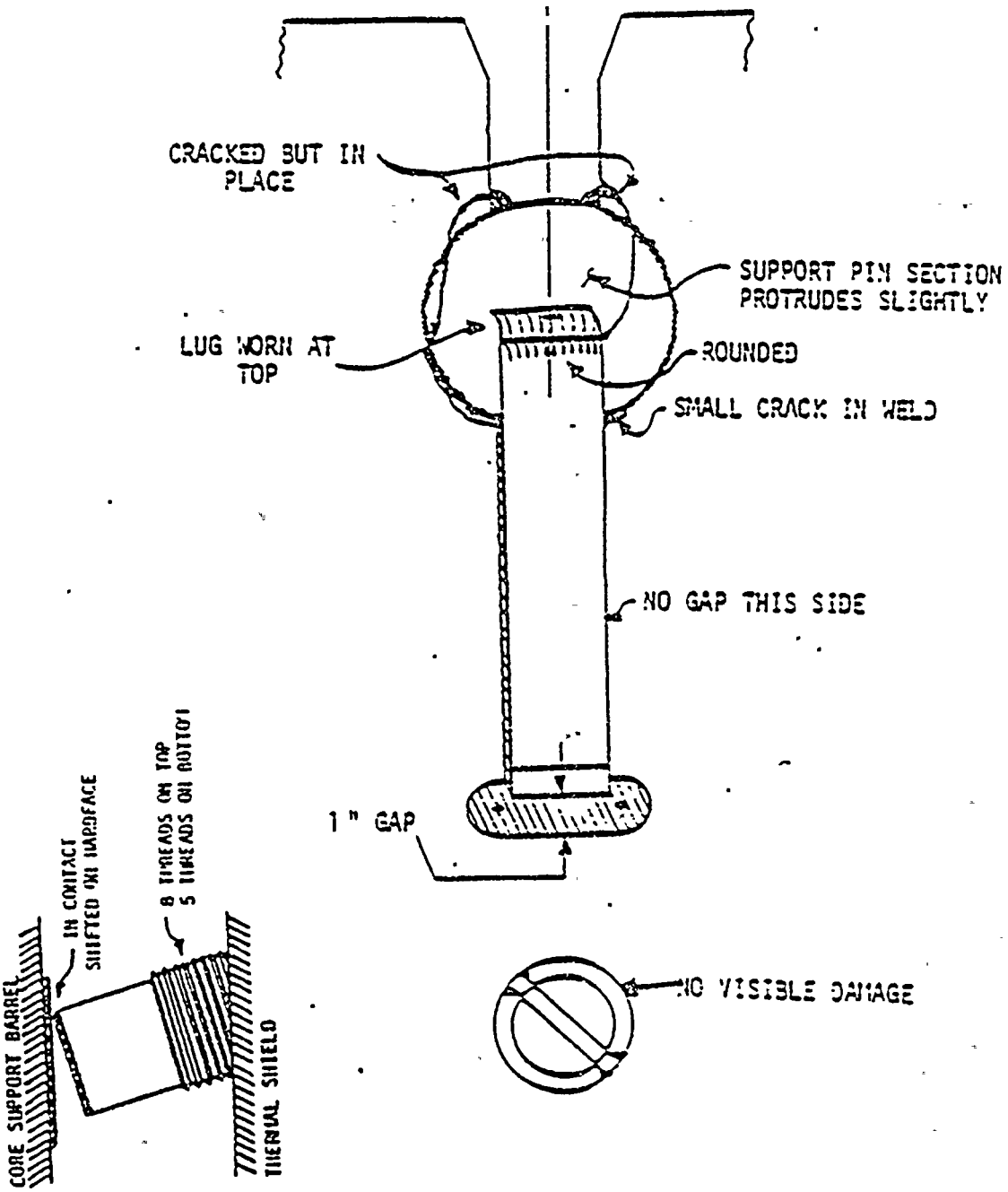

Figure 5.3-6

THERMAL SHIELD POSITION S/V (190°)

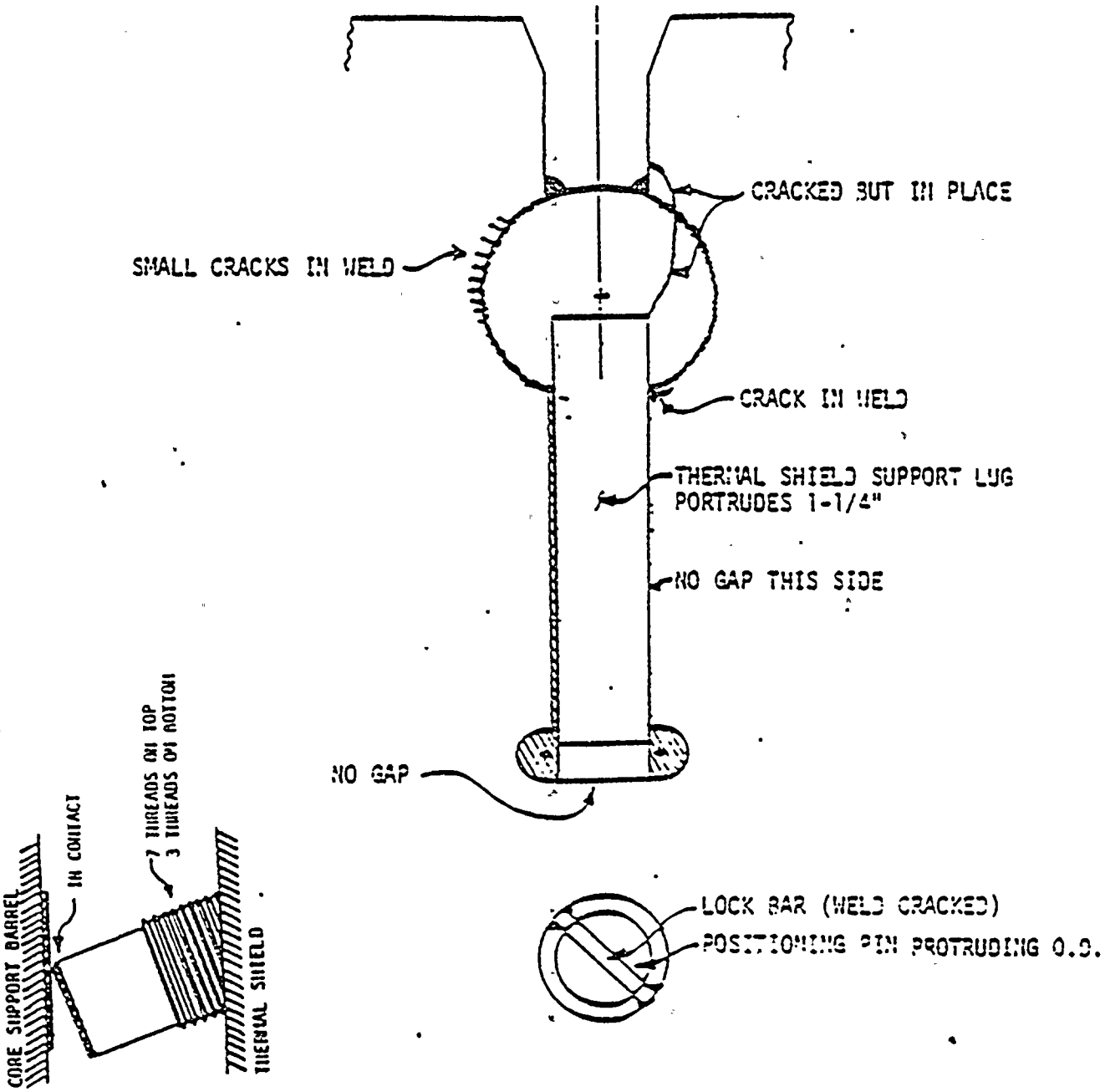

Figure 5.3-7

THERMAL SHIELD POSITION o/W (230°)

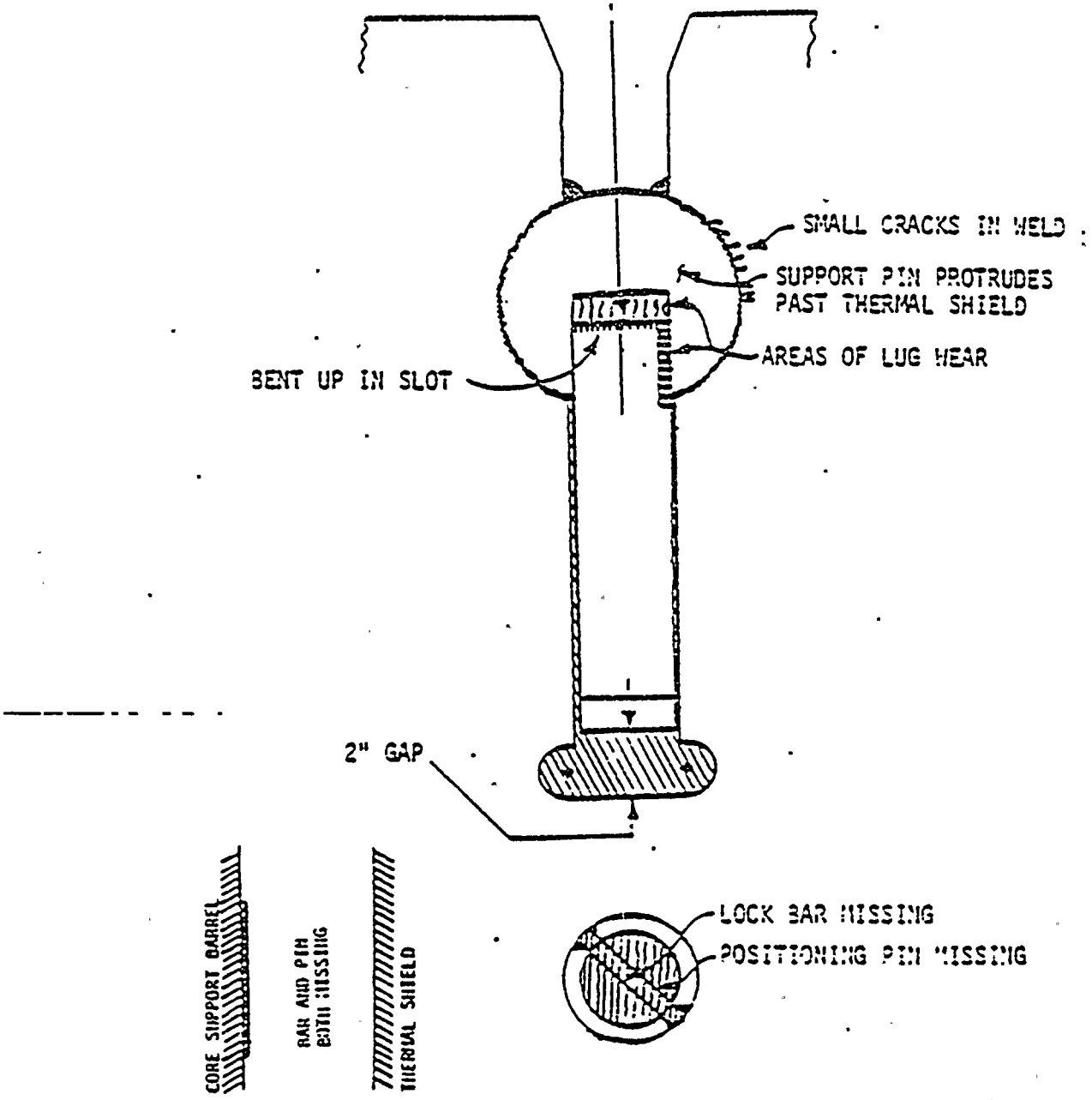

Figure 5.3-8

THERMAL SHIELD POSITION 7/X ($<70^{\circ}$)

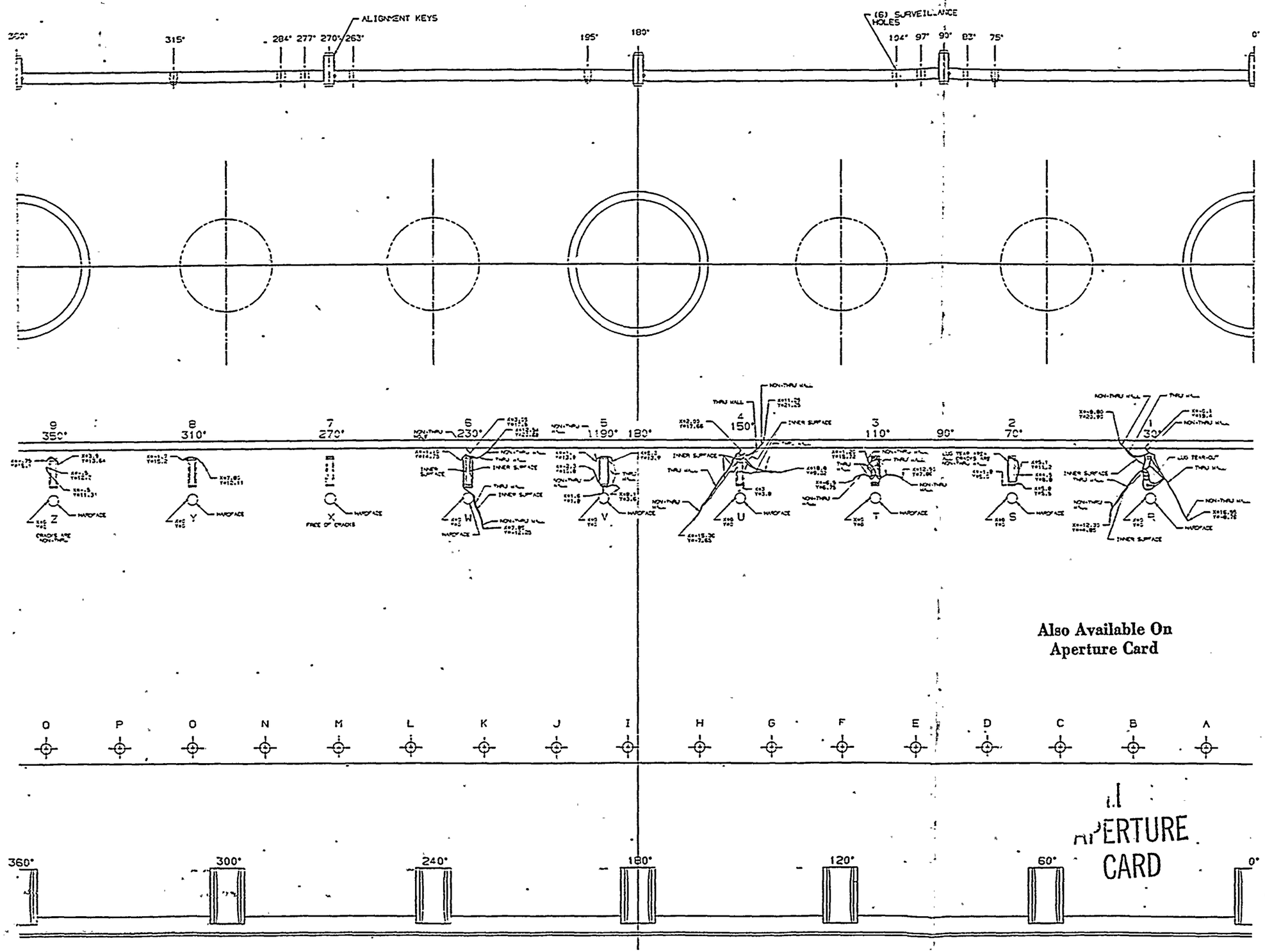

Also Available On Aperture Card

Figure 5.4-1

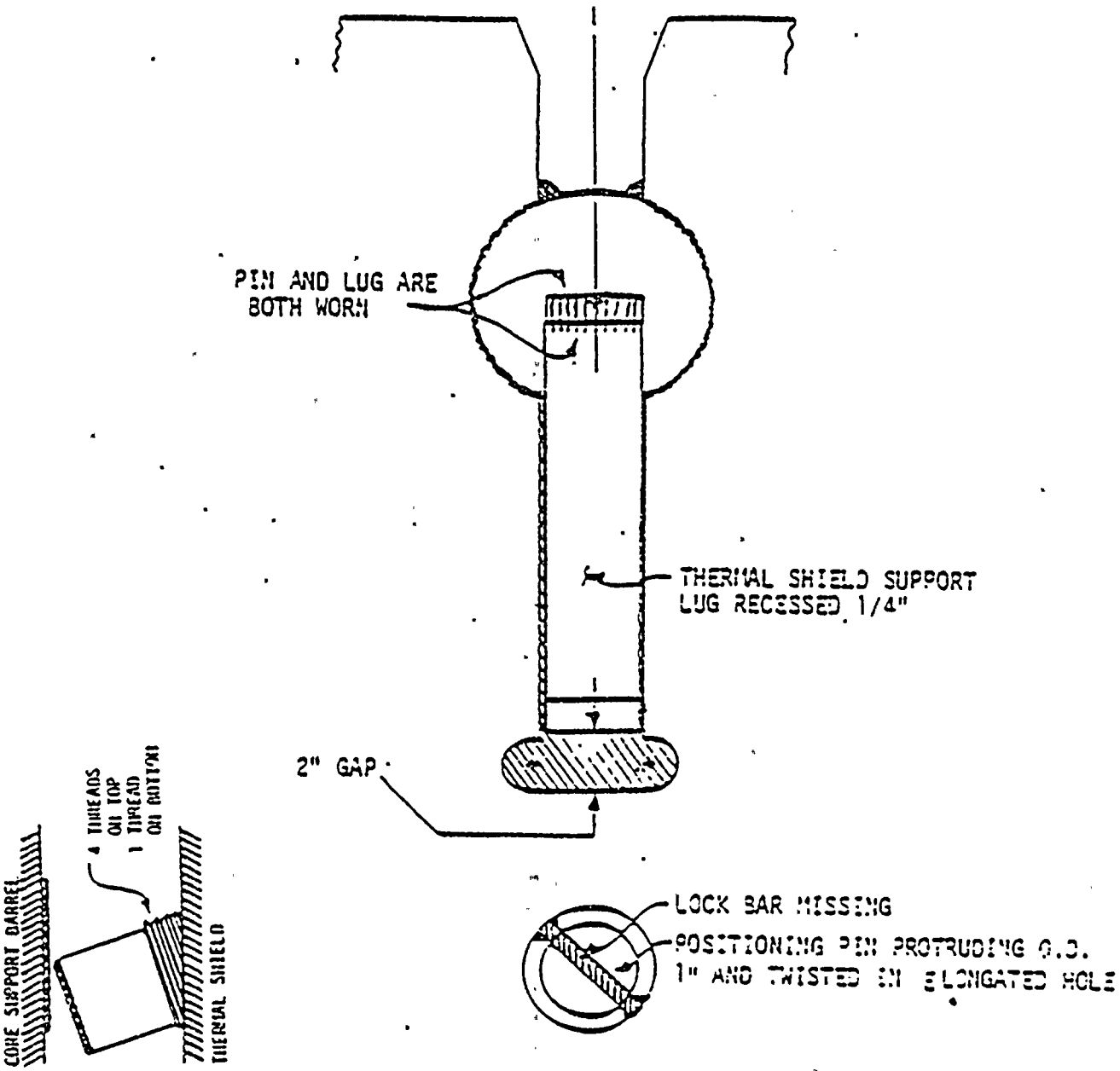

Figure 5.3-9

THERMAL SHIELD POSITION B/Y (310°)

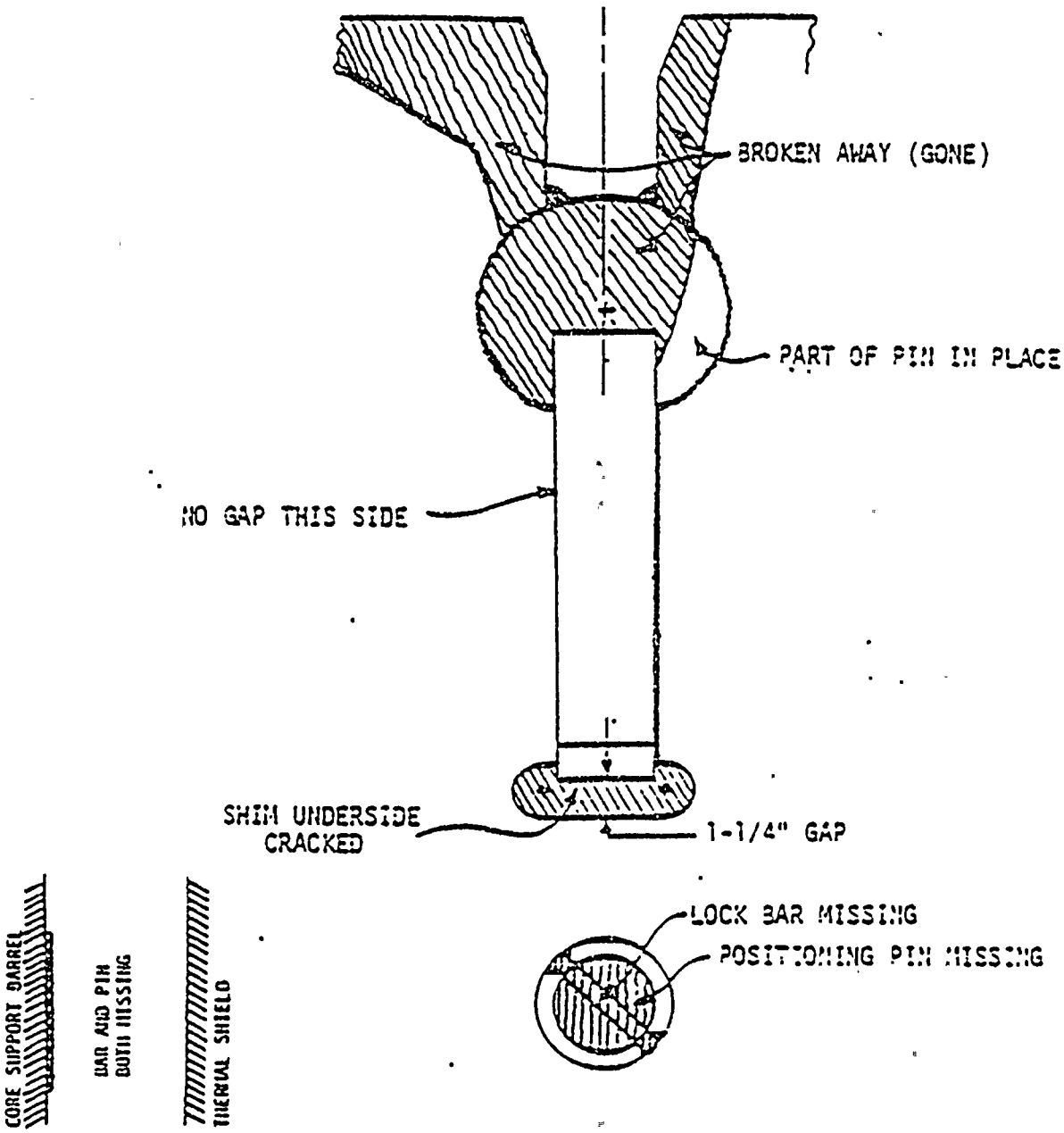

Figure 5.3-10

THERMAL SHIELD POSITION 9/I (360°)

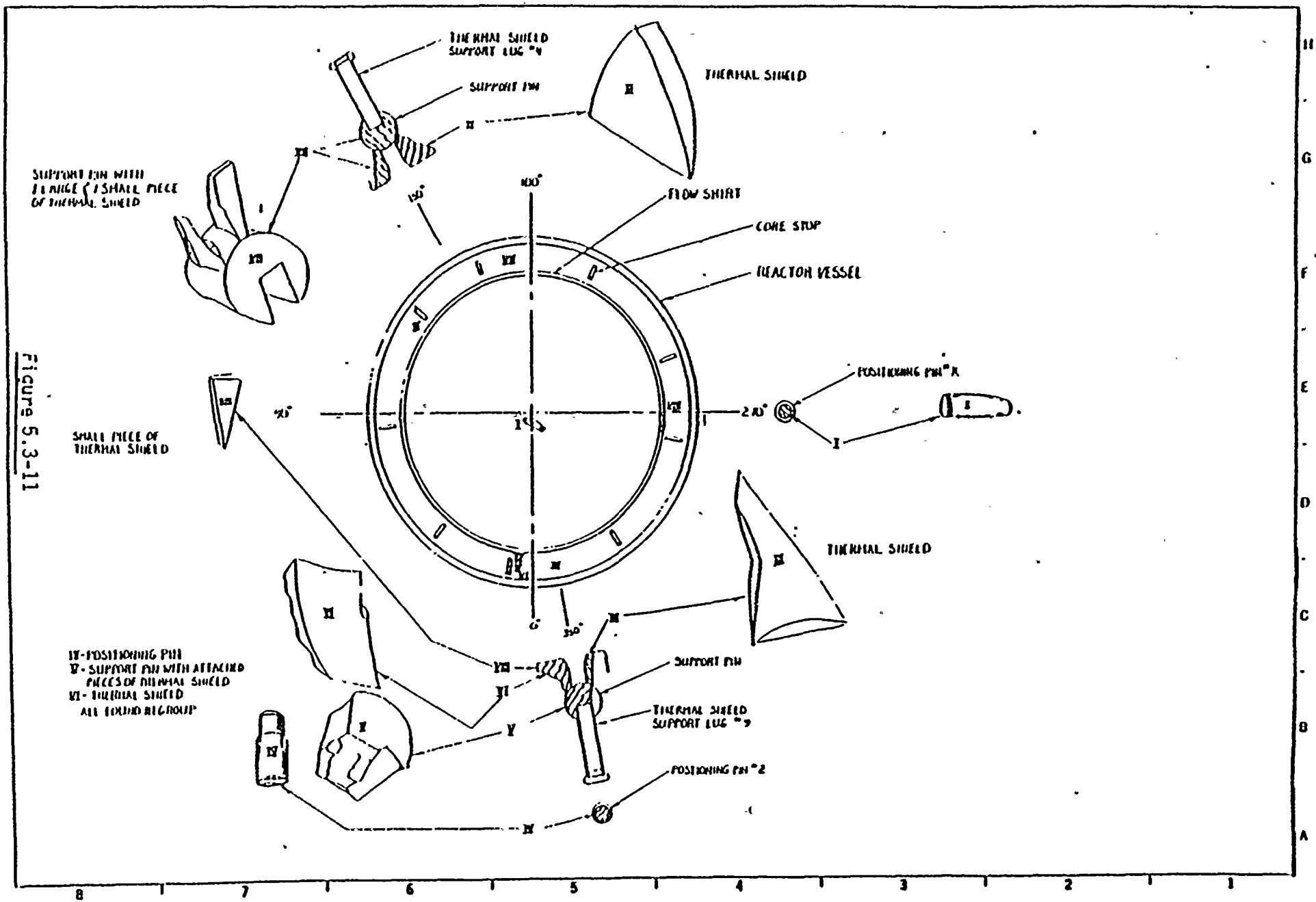
THERMAL SHIELD SUPPORT LUG "4
SUPPORT PIN
THERMAL SHIELD
SUPPORT PIN WITH FLANGE & SMALL PIECE OF THERMAL SHIELD
FLOW SHIRT
CORE STOP
REACTOR VESSEL
POSITIONING PIN "1
SMALL PIECE OF THERMAL SHIELD
THERMAL SHIELD
SUPPORT PIN
THERMAL SHIELD SUPPORT LUG "3
POSITIONING PIN "2
IV-POSITIONING PIN
V- SUPPORT PIN WITH ATTACHED PIECES OF THERMAL SHIELD
VI- THERMAL SHIELD
ALL WELDED ASSEMBLY

Figure 5.3-11

INSPECTED CONDITION OF DISPLACED POSITIONING PINS

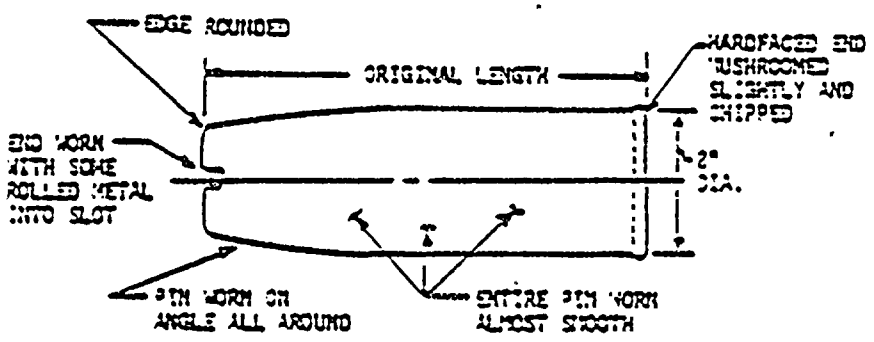

PIN 4 LOCATED AT 270°, RETRIEVED FROM THE CENTER OF THE BOTTOM OF THE REACTOR VESSEL.

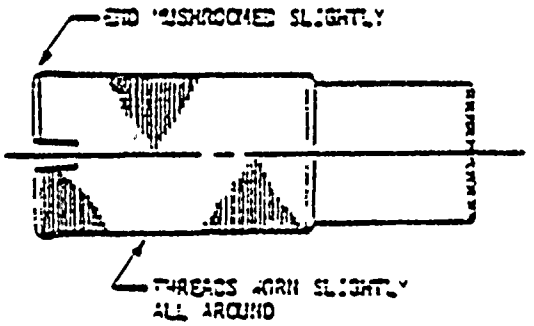

PIN 3 LOCATED AT 7°, RETRIEVED FROM THE ANNULUS BETWEEN THE REACTOR VESSEL AND THE FLOW SKIRT.

Figure 5.3-12

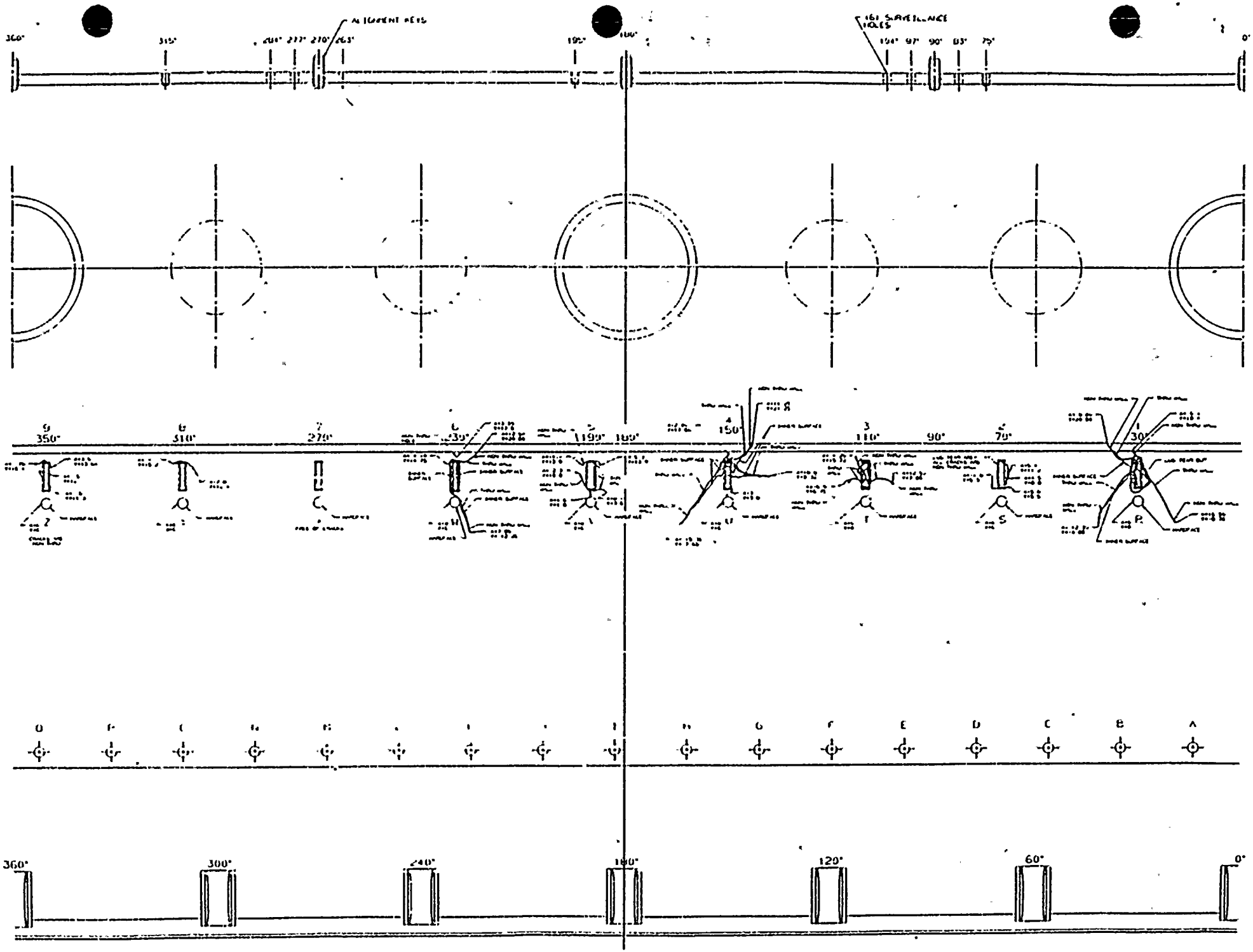
ALIGNMENT HOLES
161 SURVEILLANCE HOLES
360°
315°
270°
195°
180°
150°
120°
90°
75°
30°
0°
300°
240°
60°

Figure 5.4-1

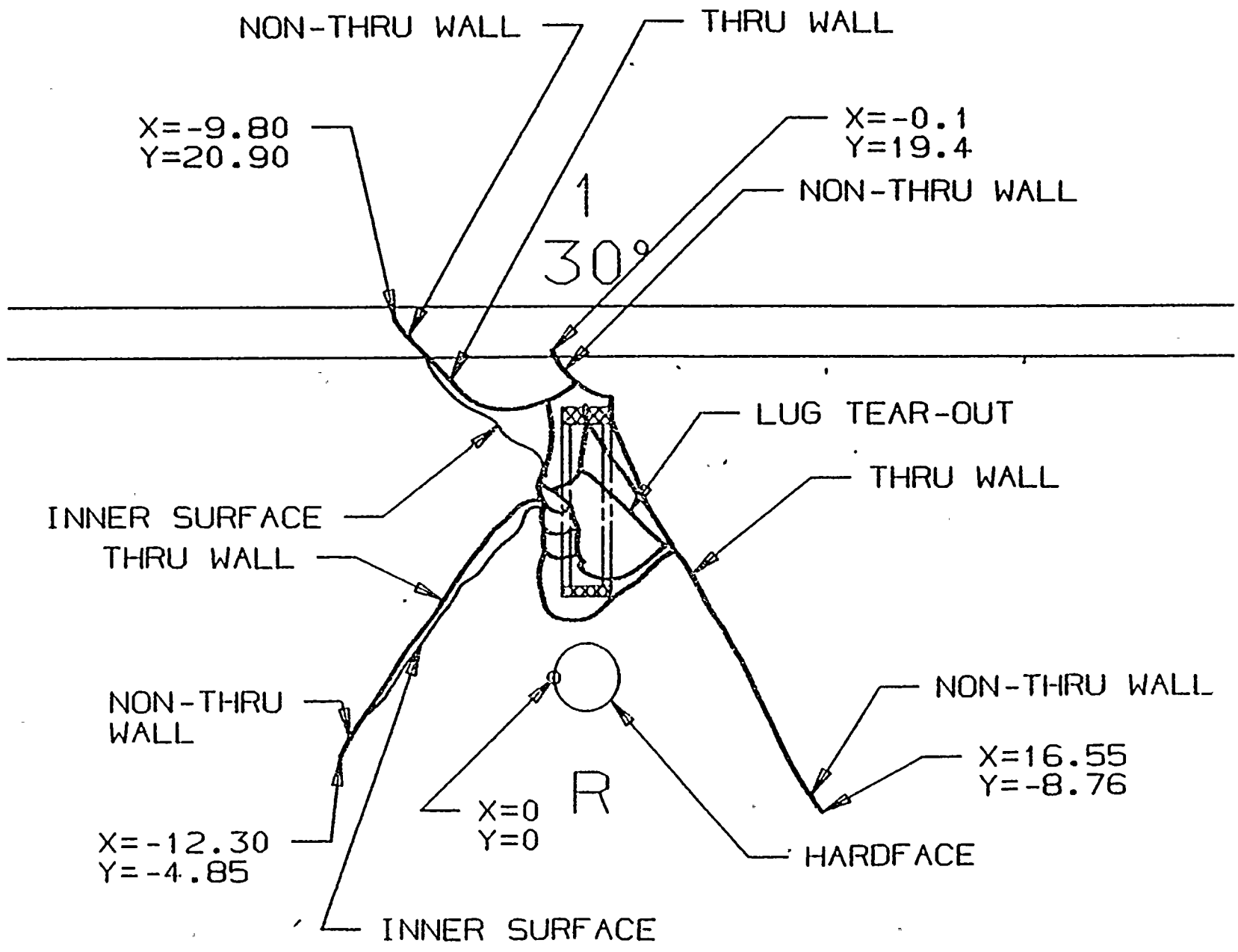

Figure 5.4-2
LUG W/R

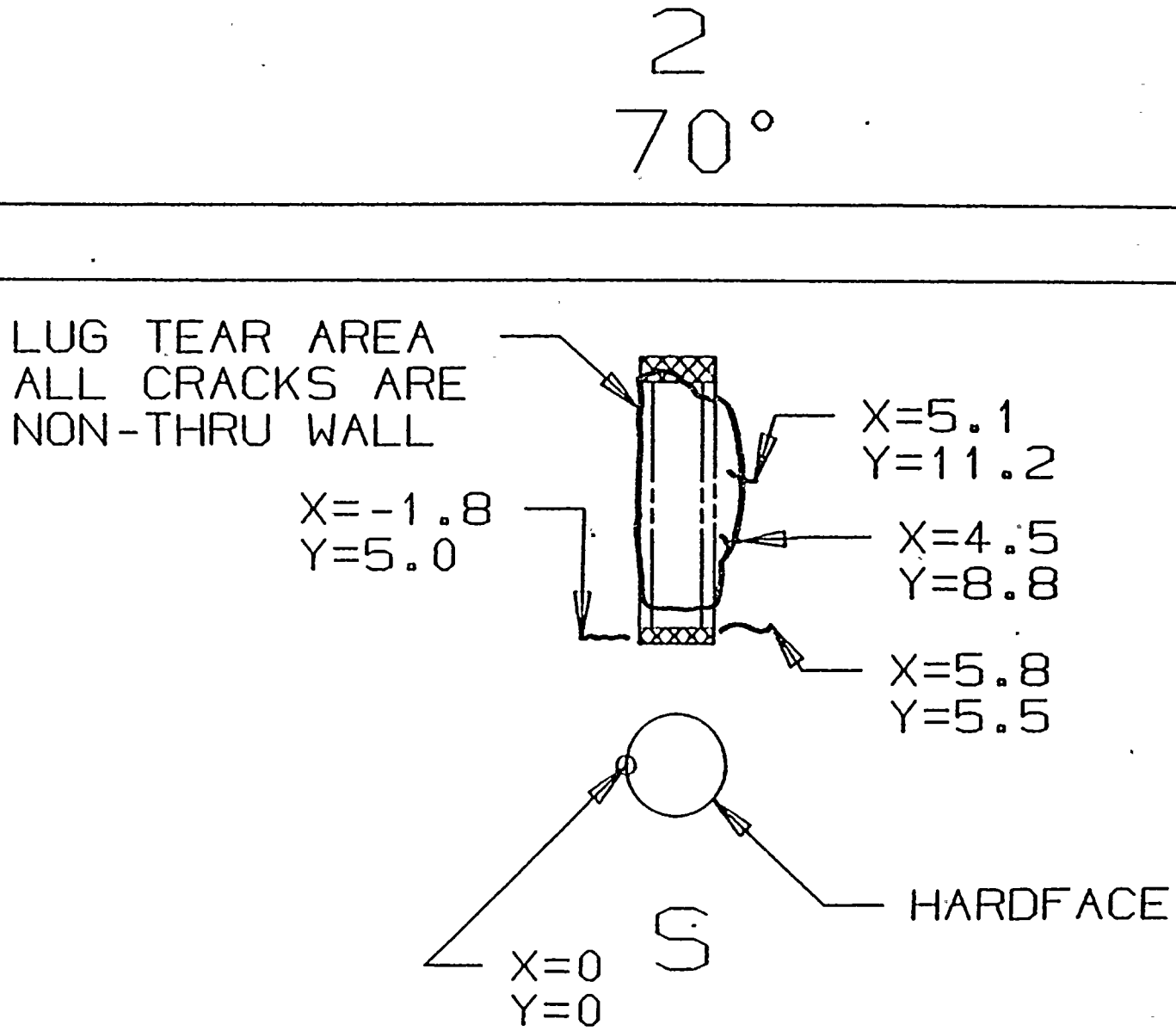

Figure 5.4-3
LUG 2/S

3

110°

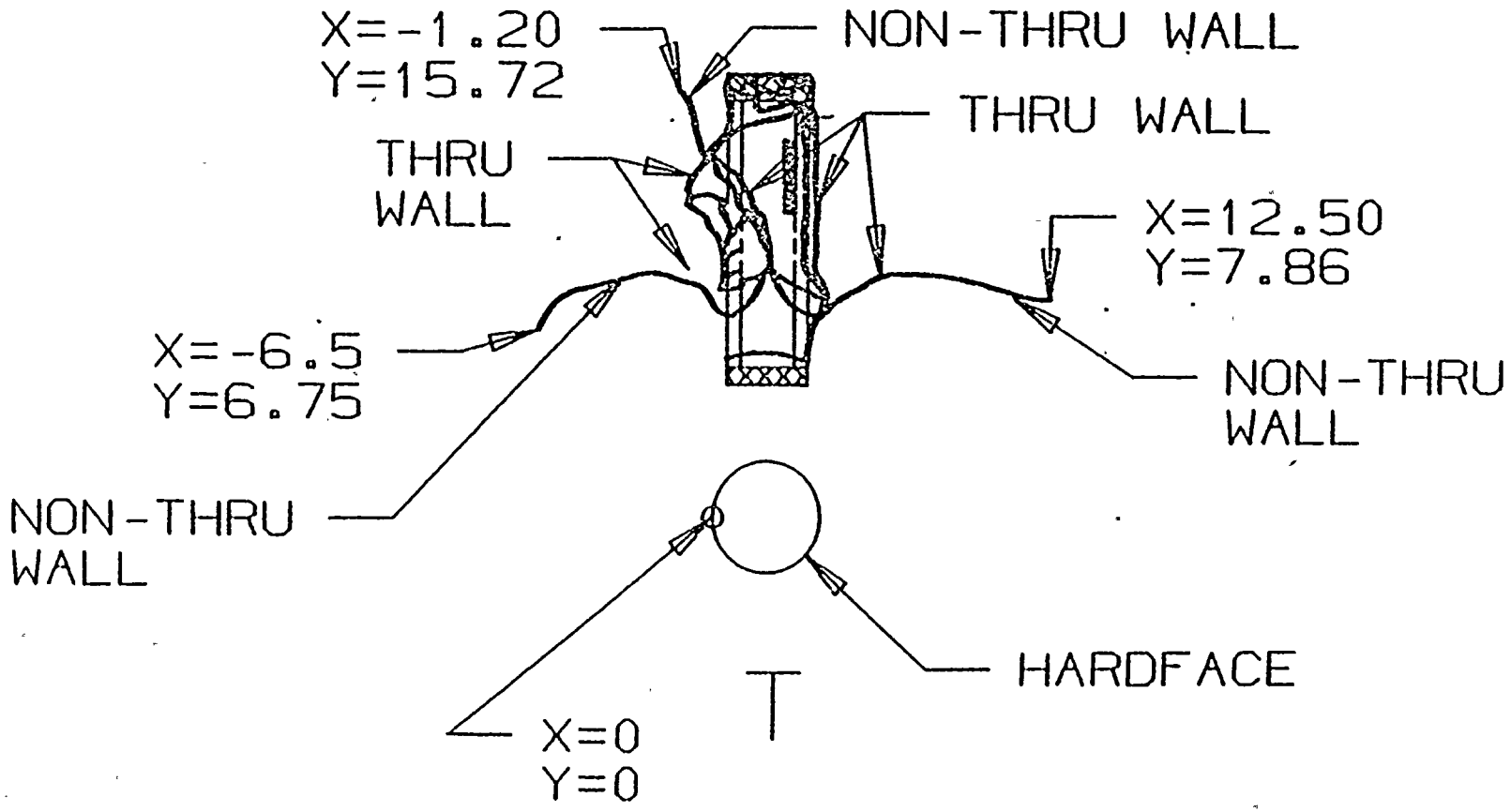

Figure 5.4-4
LUG 3/T

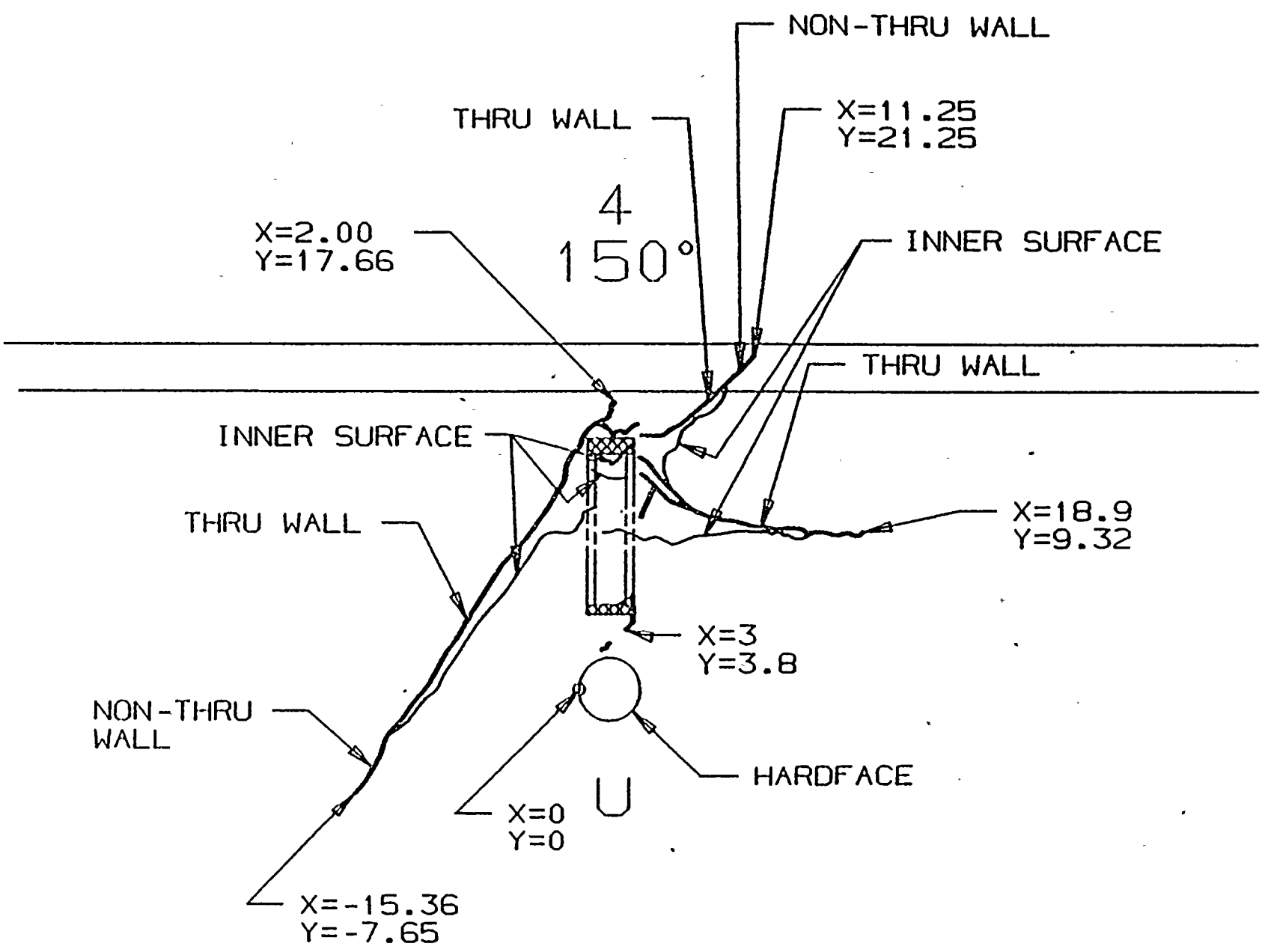

Figure 5.4-5
LUG 4/U

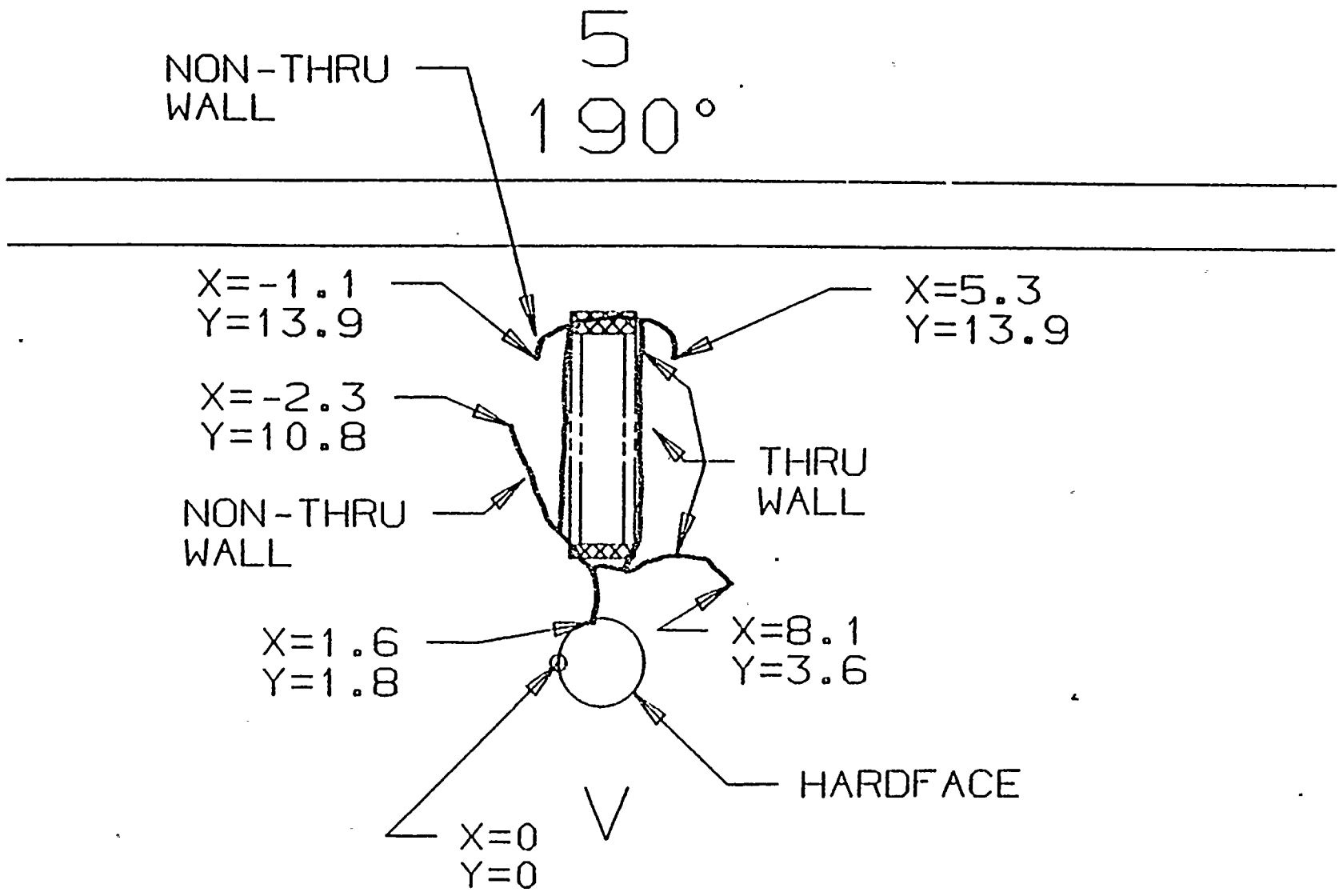

Figure 5.4-6
LUG 5/V

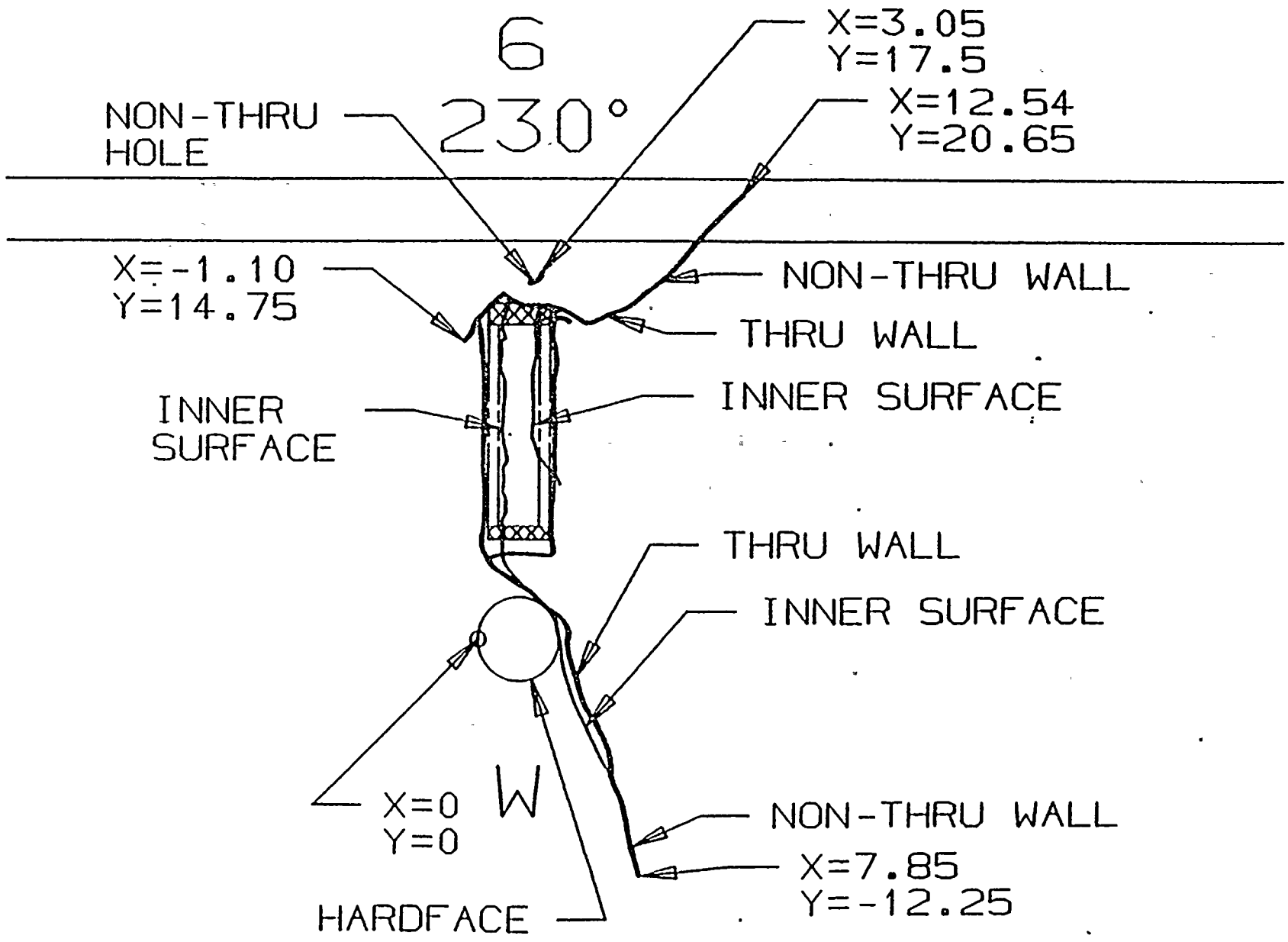

Figure 5.4-7
LUG 6/W

7

270°

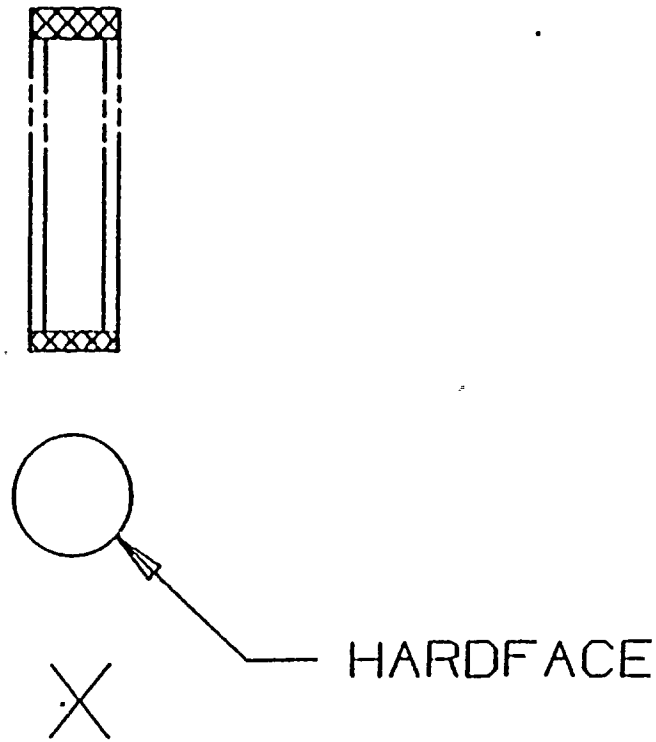

Figure 5.4-8
LU[illegible]/X

8

310°

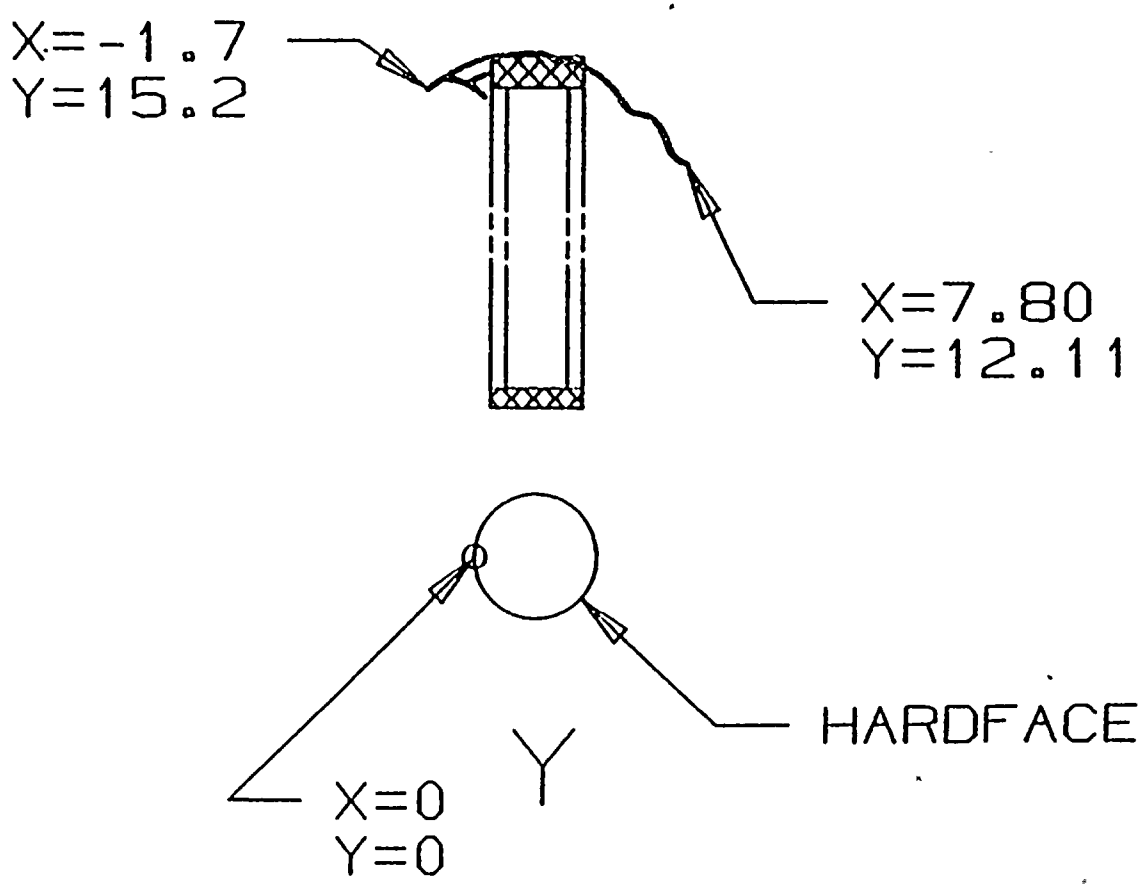

Figure 5.4-9
LUG 8/Y

9

350°

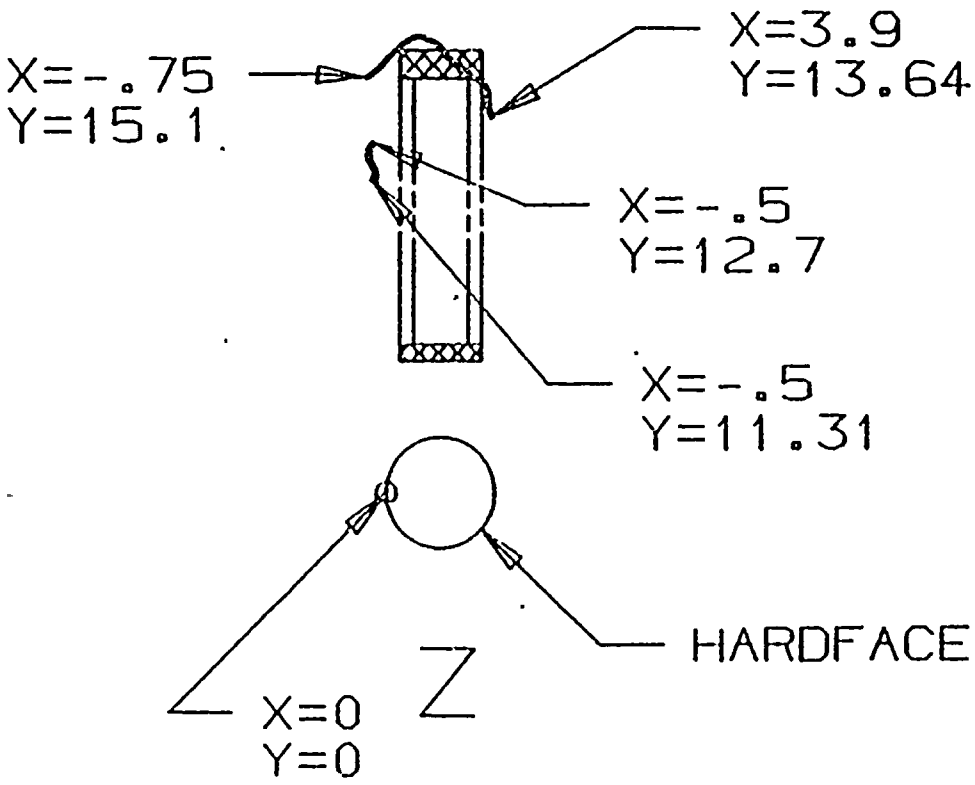

CRACKS ARE
NON-THRU

Figure 5.4-10
LUG 0/Z

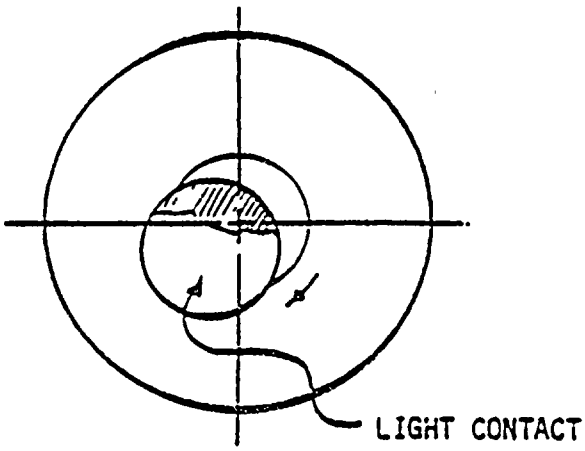

Figure 5.4-11
HARDFACE R (30°)

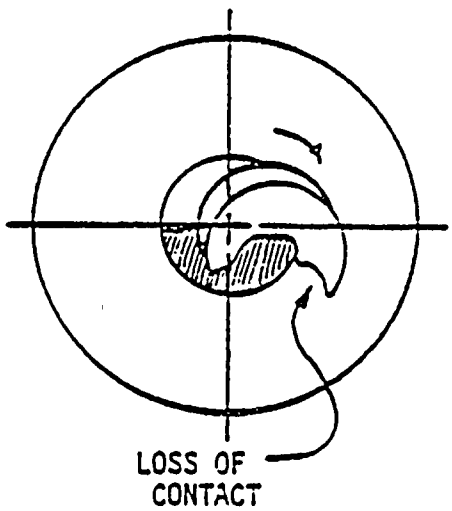

Figure 5.4-12
HARDFACE S (70°)

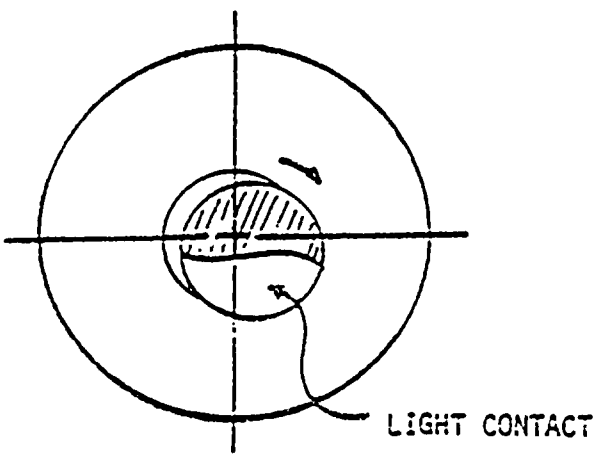

Figure 5.4-13
HARDFACE T (110°)

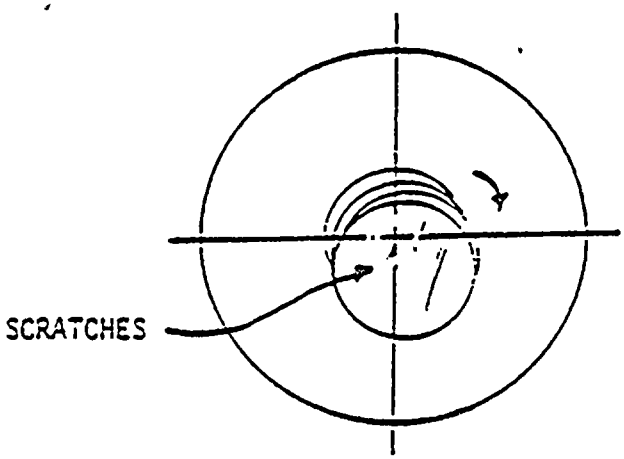

Figure 5.4-14
HARDFACE U (150°)

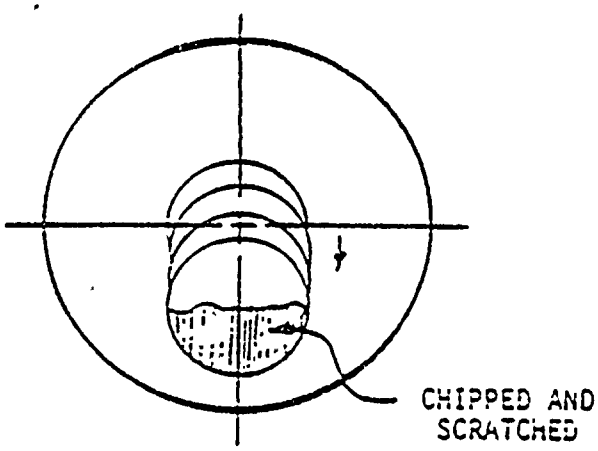

Figure 5.4-15
HARDFACE V (190°)

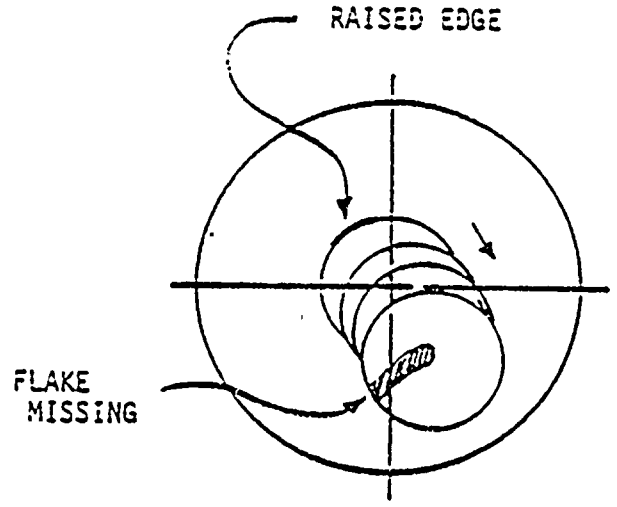

Figure 5.4-16
HARDFACE W (230°)

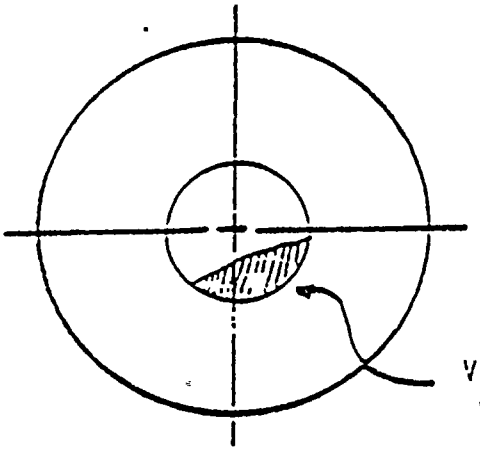

Figure 5.4-17
HARDFACE X (270°)

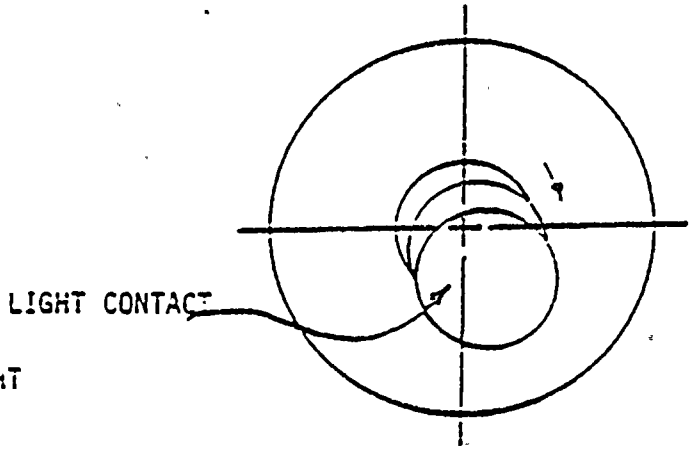

Figure 5.4-18
HARDFACE Y (110°)

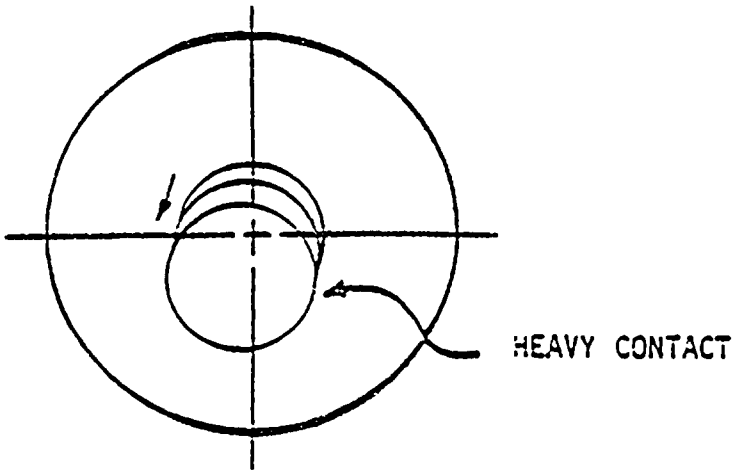

Figure 5.4-19

HARDFACE Z (350°)

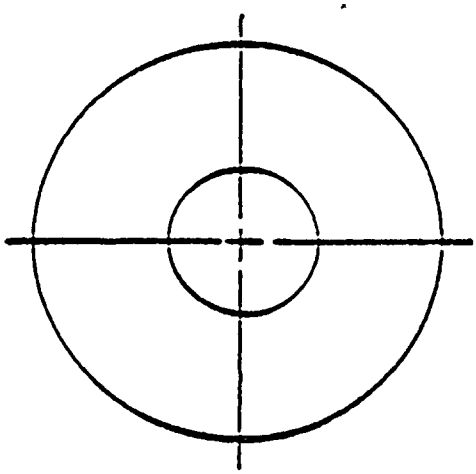

Figure 5.4-20

HARDFACE A (14°)

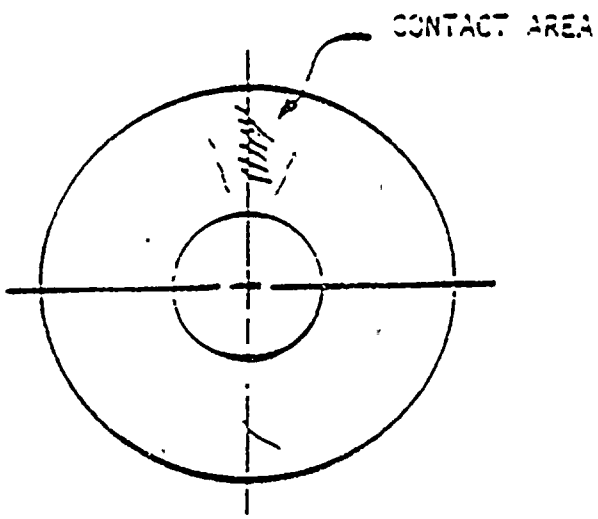

Figure 5.4-21

HARDFACE B (35°)

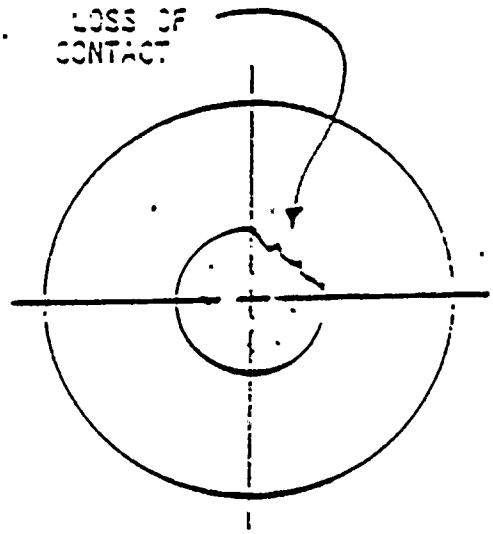

Figure 5.4-22

HARDFACE C (56°)

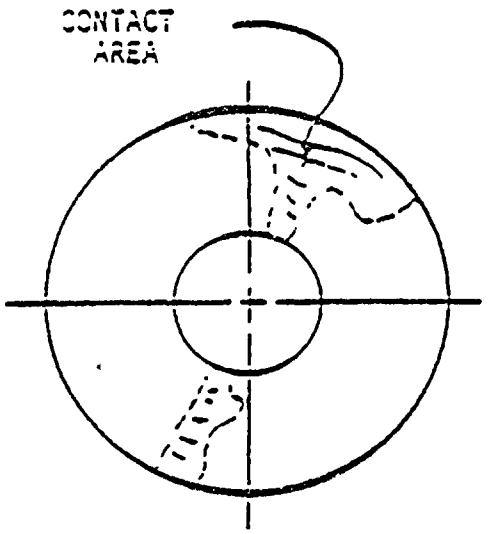

Figure 5.4-23
HARDFACE D (77°)

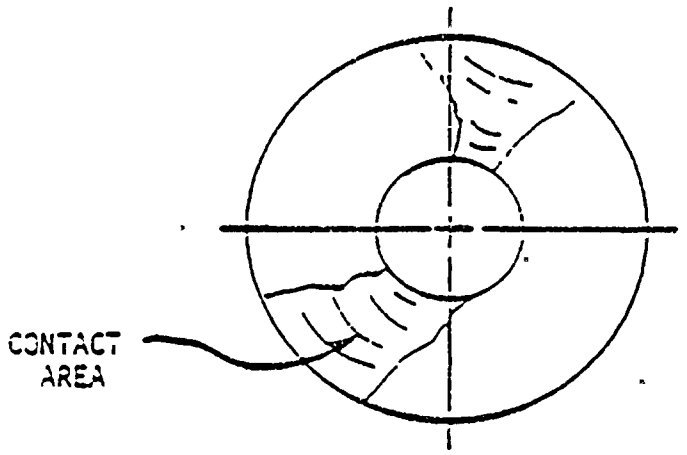

Figure 5.4-24
HARDFACE E (98°)

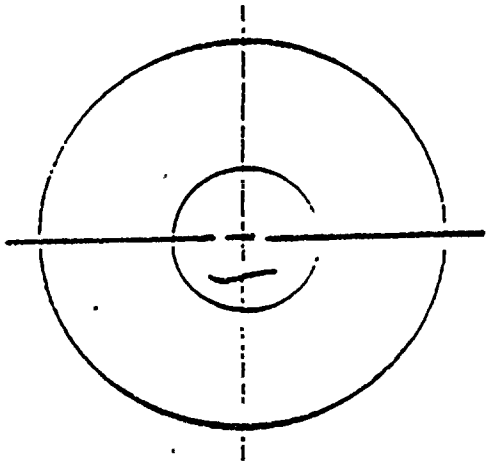

Figure 5.4-25
HARDFACE F (

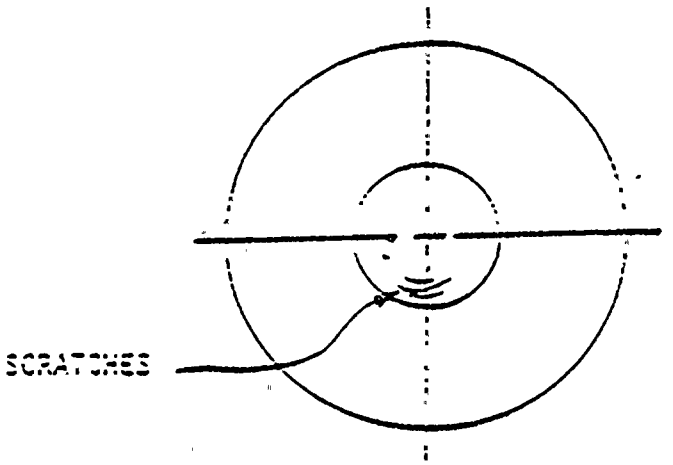

Figure 5.4-26
HARDFACE G (

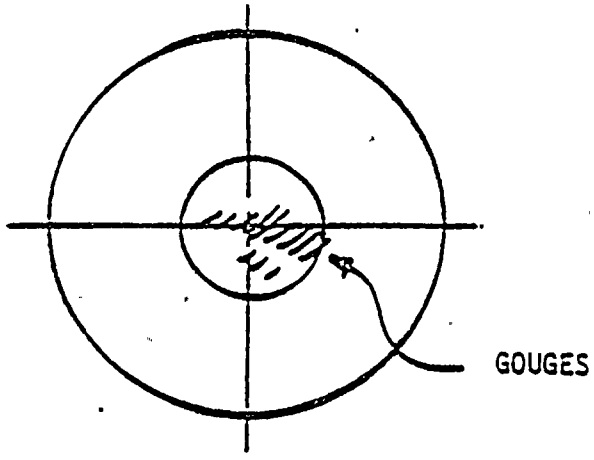

Figure 5.4-27
HARDFACE H (162°)

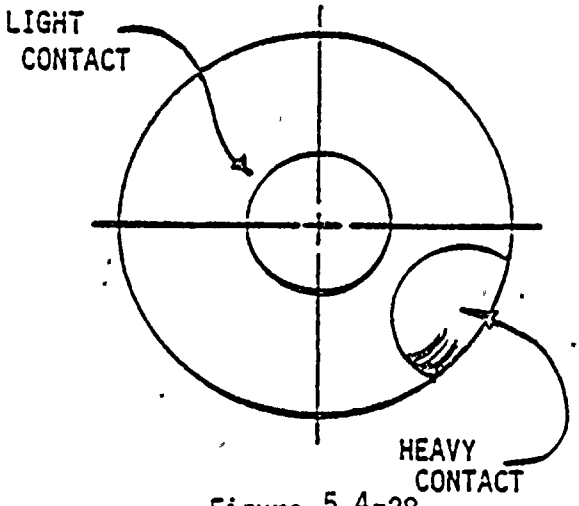

Figure 5.4-28
HARDFACE I (183°)

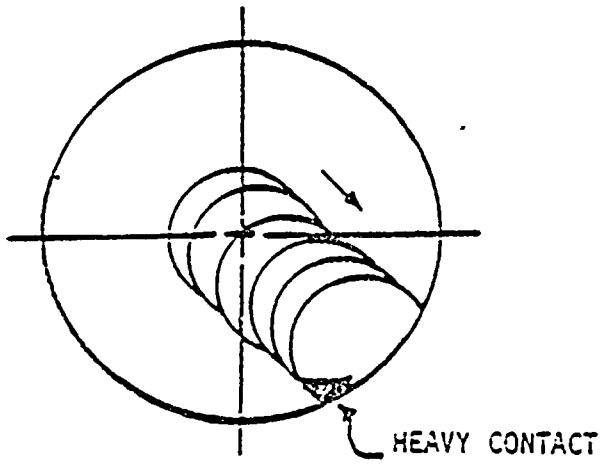

Figure 5.4-29
HARDFACE J (204°)

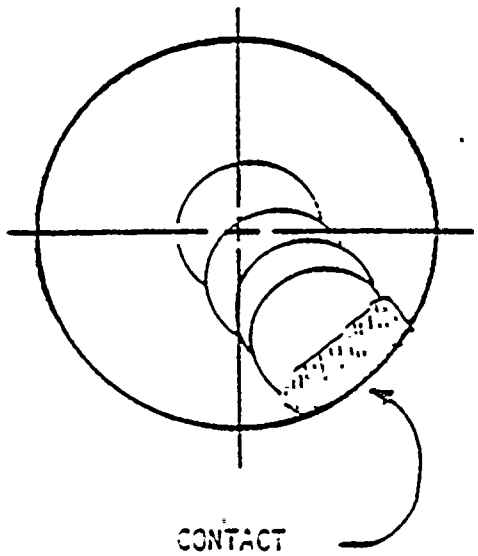

Figure 5.4-30
HARDFACE K (225°)

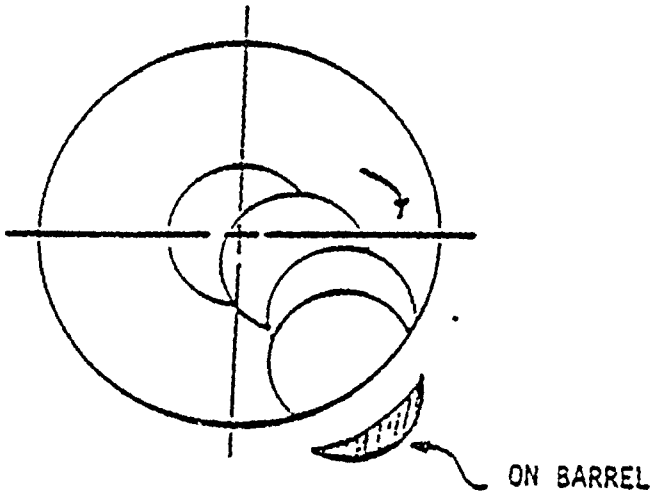

Figure 5.4-31
HARDFACE L (246 °)

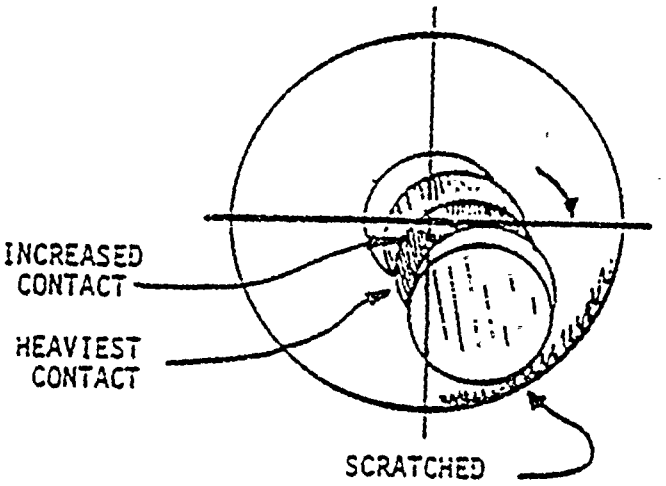

Figure 5.4-32
HARDFACE M (268 °)

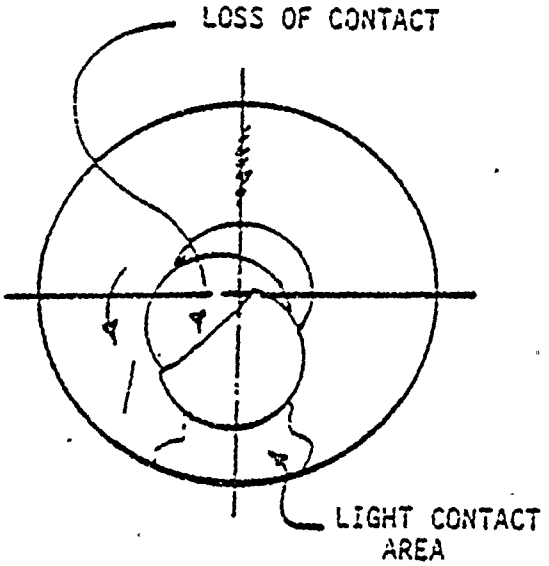

Figure 5.4-33
HARDFACE N (285 °)

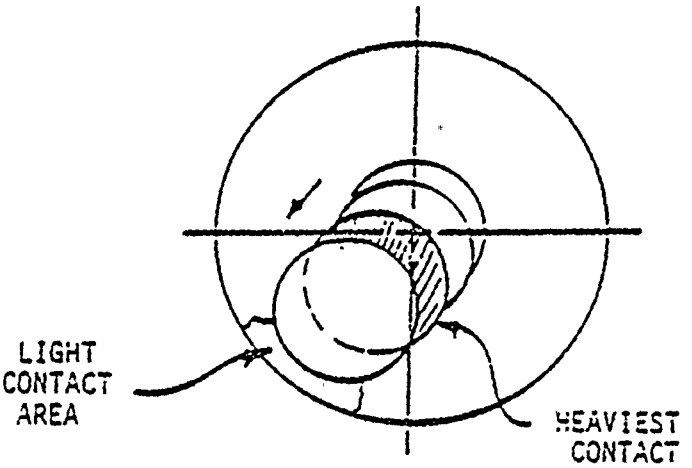

Figure 5.4-34
HARDFACE O (310°)

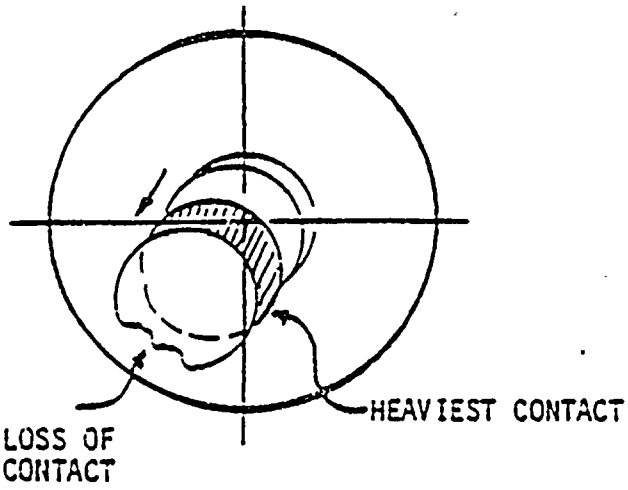

Figure 5.4-35
HARDFACE P (331°)

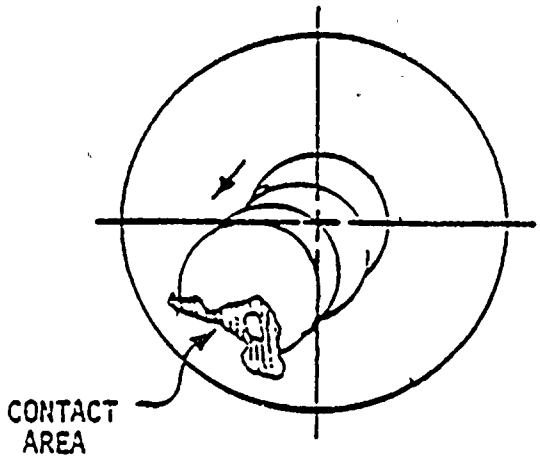

Figure 5.4-36
HARDFACE Q (352°)

6.0 CORE SUPPORT BARREL REPAIR

6.1 CORE BARREL SUPPORT REPAIR MACHINING

6.1.1 Repair Machining Objectives

The objective of the repair machining to the core support barrel was the elimination of the sharp surface discontinuities associated with the cracks and irregular surfaces produced by the degraded thermal shield support system. The machining requirements were established to minimize material removal and reduce the stress concentration effects at the crack tips and surface irregularities by replacing them with more gradual transitions to the unaffected cross section of the core support barrel wall. These goals were accomplished by machining out the surface discontinuities associated with non-through thermal shield support lug tear out areas and cracks which had not penetrated the full thickness of the core support barrel wall. Through wall cracks were repaired with crack arrestor holes providing a generous radius of curvature which were machined through the core support barrel at the crack tips. Lug tear out areas were machined as described above and prepared for a patch plate to cover through wall holes. The patches were held in place by expandable plugs.

6.1.2 Repair Machining Description

The extent of repair machining was determined from the results of nondestructive examination (NDE) of the core support barrel lug area. Cracks which were determined to be through wall over any part of their length were repaired by machining a crack arrestor hole beyond each

end of the crack tip to prevent further running. Cracks which were found to exist on the surface but which did not go through the full thickness were removed by machining a groove into the core support barrel beyond the length and depth of the crack and the edges of the groove were blended for a smooth transition into the full wall thickness.

Four of the nine thermal shield support lugs were torn from the core support barrel, taking with them segments of the core support barrel wall. One of the support lugs which tore out of the core support barrel produced a through wall hole (lug location No. 1). The hole repair process first machined out shallow surface indications. The through wall damage was machined in a triangular in shape, with large radius corners. The triangular shape resulted from the configuration of the damage and was determined to minimize material removal. Other lug areas were machined in a similar manner when it was found that the damage required through-wall machining. The support lug tear out areas which did not penetrate the full core support barrel wall thickness were machined to eliminate the surface discontinuities.

6.1.3 Repair Machining Operations

The repair machining of the core support barrel was closely monitored with eddy current testing to assure that the flaw being machined was eliminated. All non-through wall cracks were eddy current traced over their full length. A shallow groove was then machined, centered on the crack and extending at least one half inch to either side and a quarter to one half inch beyond the tip of the crack. Eddy current examination was then used to verify crack elimination, or the need for additional machining until crack removal was verified.

For through wall cracks, the location of the crack arrestor holes was established by locating the end of the crack with eddy current examinations and ultrasonic examinations. A slot or two inch diameter hole was then machined over the crack, extending one quarter to one half inch beyond the tip of the crack. The machining was carried out in small increments and eddy current testing was used to verify that the crack tip was within the machined area. If the end of the crack could not be located, the machine was shifted one half inch in the direction of the crack tip and the process repeated. Once the crack tip was verified to be within the machined area, a crack arrestor holewas machined. The hole was then spotfaced and back chamfered in preparation for plugging.

Lug tear out areas were machined to partial wall thickness and one quarter inch minimum beyond the edge of the damage. The machined area was then eddy current inspected for the location of discontinuities and the depth of machining was increased again going one quarter inch minimum beyond the damage. This process was repeated as necessary.

6.1.4 Post Repair Machine Description

As discussed in Section 5.4.1 describing the Core Support Barrel Inspection results only lug location number seven did not require repair. The remaining lugs required repair machining to the extent necessary to remove non-through wall cracks and prepare the core support barrel for a patch or crack arrestor hole. A description of the repair machining is found below and in Figures 6.1-1 through 6.1-9.

6.1.4.1 Lug 1/R (30^{o}) (Figure 6.1-1)

The cracks were terminated by three 8 inch diameter holes. The center tear out area was machined to remove the damaged material and four 3 inch diameter holes were machined in preparation for a patch. The patch area was machined in order to provide a seating surface for the patch.

6.1.4.2 Lug 2/S (70^{o}) (Figure 6.1-2)

Machining was performed to remove the non-through wall cracks. The center area was the deepest and decreased as the machining progressed outward from the center area.

6.1.4.3 Lug 3/T (110^{o}) (Figure 6.1-3)

Two 5 inch diameter crack arrestor holes were required to arrest the horizontal crack. The center area was machined through wall and the core support barrel was machined to provide a flat surface for a patch. Three 3 inch diameter holes were drilled for the expandable plugs to secure the patch to the core support barrel. One of the 3 inch diameter holes serves as a crack arrestor hole.

6.1.4.4 Lug 4/U (150^{o}) (Figure 6.1-4)

Three 8 inch diameter holes were used to arrest the cracks. Four 3 inch diameter holes were machined for the expandable plugs to secure the patch to the core support barrel. The core support barrel was machined to provide a flat surface for the patch.

6.1.4.5 Lug 5/V (190°) (Figure 6.1-5)

The core support barrel was machined through wall to remove damaged material. Four 3 inch diameter holes were machined to serve as crack arrestor holes and provide for the expandable plug to secure the patch to the core support barrel. The core support barrel was machined to provide a flat surface for the patch.

6.1.4.6 Lug 6/W (230°) (Figure 6.1-6)

Two 8 inch crack arrestor holes were machined. The center area was machined to remove the damaged material and three 3 inch diameter holes were machined for the expandable plugs to secure the patch to the core support barrel. The core support barrel was machined to provide a flat surface for the patch.

6.1.4.7 Lug 7/X (270°) (Figure 6.1-7)

No repair machining was necessary however the lug was machined off to facilitate non-destructive examination.

6.1.4.8 Lug 8/Y (310°) (Figure 6.1-8)

Two 3 inch diameter crack arrestor holes were machined to terminate the horizontal crack. No further machining was required.

6.1.4.9 Lug 9/Z (350°) (Figure 6.1-9)

The machining required was non-through wall since no cracks penetrated the wall at this location. The machining removed the crack and provided a radius to the wall of the core support barrel.

6.2 CORE SUPPORT BARREL EXPANDABLE PLUG REPAIR

6.2.1 Design Description

6.2.1.1 Design Criteria

The expandable plugs are non-load bearing members designed to be installed in the crack arrestor holes to limit bypass flow leakage through the core support barrel. Patches attached to the core support barrel by expandable plugs were designed to be installed where through holes, not suited to plugging, existed. The expandable plugs and patches were designed to accommodate the loads and thermal transients resulting from normal operation, upset and faulted conditions. The designs have been evaluated and shown to meet the stress criteria of the ASME Code. The design life objective for the plugs and patches is for the remaining life of the plant.

6.2.1.2 Design Description

The expandable plug is a closed end cylinder with a flange at the opposite end (Figure 6.2-1). The flange is a spring member which is pre-deflected prior to installation into the crack arrestor hole. The wall of the expandable plug is then expanded on the back side of the hole locking the plug in place (Figure 6.2-2). The preload in the flange along with the expanded section acts to secure the plug against motion due to operation and provides the flexibility to keep the plug tight under anticipated thermal conditions.

The plugs were made in three nominal sizes to match the corresponding crack arrestor holes in the core support barrel. The plugs were sized to fit 3, 5, and 8 inch diameter holes. A slightly heavier wall 3 inch diameter plug was used to secure the patches to the core support barrel.

The patch is a plate designed to cover the through wall area and limit leakage at a through hole. A representative patch is shown in Figure 6.2-3. Expandable plugs are used to secure a patch over the hole resulting from the repair machining to the damage area. The preload from the plugs acts to preload the patch against the core support barrel, locking it in place.

6.2.2 Thermal and Hydraulic Considerations

The fundamental requirement for the plug repairs was that the plugs remain tight in the core support barrel. Tightness assures that the plugs will seal adequately, limit bypass flow and that vibrations of the plug will not occur. The degree of tightness (preload) which is needed to limit leakage and plug motion is governed by the pressure differential across the core support barrel, the hydraulically induced forcing functions on the plug, and the thermal loads and deformations caused by temperature gradients between the plugs and core support barrel.

6.2.2.1 Thermal Considerations for Plugs During Normal Operation

As shown on Figure 6.2-2, the plug is held in position by a "belleville type" flange on the vessel side of the core support barrel and a swaged section on the core side. The flange deflection and extensional deformations in the plug body provide the preloading needed to keep the plug tightly in position. During normal operation, thermal gradients are generated in the core support barrel due to the difference in coolant temperatures across the core support barrel and by radiation heating. Radiation heating in the plug does not cause significant gradients. The heat transfer analysis described in Section 6.2.2.3 confirms this conclusion.

In general, the core support barrel operates at a higher temperature than the plugs during normal operation. Since the plugs are installed during cold isothermal conditions, this temperature difference causes two components of movement in the core support barrel, one radial from the plug centerline position, and the other transverse (through the thickness of the core support barrel). The resultant movement is therefore dependent on the hole radius and thickness of the core support barrel at the plug. For all plug designs, the hole radius is equal to or greater than the core support barrel thickness at the plug. Since the chamfer and swage angle is 45^{o} to the plug centerline, the net thermal deformations during normal operation act to slightly relax the preload in the plug. Figure 6.2-4 graphically shows this effect. This relaxation has been adequately compensated for in the initial plug preload at installation.

6.2.2.2 Thermal Considerations for Plugs

There are two categories of thermal events which affect plug performance, those which cause the core support barrel to be hot relative to the plug and those which cause the plug to be hot relative to the core support barrel. In the former case, the most severe event would be a large steam line break. During such a hypothetical event, the vessel inlet temperature is reduced by a maximum of 372^{o} F. This reduction in inlet temperature would cause the plug to cool rapidly (because of it's low mass relative to the core support barrel while the core support barrel cools more slowly.

Inlet and outlet coolant temperatures for a transient of this type are shown in Figure 6.2-5. It has been assumed that the plug conservatively follows the inlet coolant temperature instantaneously, while the core support barrel remains at normal operating temperatures. As described in Section 6.2.2.1, this type of temperature difference would cause a net reduction in interference between the plug and core support barrel.

Heatup from cold conditions is the limiting case which can cause the plug to become hot relative to the core support barrel the most severe being a heatup from cold conditions. In this case the coolant inlet temperature is increased at a rate of much smaller than 100^{o}F per hour. The 100^{o}F/hr heatup rate results in a temperature difference between the plug and core support barrel of 8^{o}F. Contrary to the situation described in Section 6.2.2.1, such a temperature difference causes an increase in interference between the plugs and core support barrel.

6.2.2.3 Thermal-Performance Analyses

A two dimensional axisymmetric finite element heat transfer analysis of the plug and core support barrel was performed using the ANSYS computer code (Reference 1). A schematic diagram of the 2-D model is shown in Figure 6.2-6.

A range of core support barrel plug radial gap sizes (0.010, 0.025, and 0.050 inches) were examined with the 2-D model. A natural convection boundary condition was imposed on the inner surface (i.e., surface facing the core) of the core support barrel and plug, based on a coolant temperature. A forced convection boundary condition was imposed on the outer surface of the core support barrel and plug (i.e. surface facing the reactor vessel) based on the vessel inlet coolant temperature.

Heat generation rates associated with full power operation were used in the finite element analysis. Heat generation rates used in determining temperatures for input to stress analysis were based on the alarm limit axial peaking factor. Heat generation rates used in the thermal analysis included a deterministically applied 30% uncertainty allowance.

The same boundary conditions and heat generation rates were used with classical heat transfer methods to evaluate the thermal performance of patches.

As discussed in Section 6.2.2.1, stress analyses which included thermal stresses, verify that the plug and patches will not loosen relative to the core support barrel in the course of reactor operation. Hence, the thermal performance criteria has been met.

6.2.2.4 Hydraulic Loadings During Normal Operation

In addition to the thermal considerations, the other loads to which the plugs and patches are subjected are hydraulic and acoustic. The sources of these loads are:

1. steady state pressure differential across core support barrel
2. pulsating pressure due to pump excitation
3. drag forces on plug or patch protrusions
4. vortex shedding off of plug protrusions and cavities
5. turbulence.

Figure 6.2-8 show how these loads act on a typical core support barrel plug. The steady state static pressure differential across the core support barrel plugs or patch was determined by calculating the pressure drop in the flow path from the elevation of the plugs and patches in the downcomer to the core exit elevation.

Pump-induced fluctuating loads on the plugs and patches were based on the same type of load information as was developed for the core support barrel. A description of the methodology is given in Chapter 7.

The drag and vortex shedding loads are based on the relationships

$$F_D = C_D \frac{\rho V^2}{2g} A_\rho$$

and

$$F_{VS} = = C_L \frac{\rho V^2}{2g} A_\rho$$

where:

F_D = the static drag load on the plug or patch

C_D = drag coefficient of plug or patch

ρ = fluid density

V = downcomer velocity

A_p = projected area of plug flange or patch (looking sideways)

g = gravitational constant

F_{VS} = fluctuating lateral load on plug due to vortex shedding from the plug flange

C_L = Lateral force coefficient due to vortex shedding

The turbulence induced pressure load on the plug or patch was calculated by taking the largest normalized value, Ø, from the PSD plot in Figure 6.2-9 and going through the following operation:

$$F_{turb} = [\text{Ø} \cdot \rho^2 U_{conv}^3 \delta \cdot BW] F_{peak} \cdot A_{plug}$$

where:

F_{turb} = peak load on plug or patch due to turbulence

$\emptyset$ = normalized turbulent pressure PSD from Figure 6.2-9

ρ = fluid density

U_{conv} = turbulence convection velocity

δ = radial gap in downcomer

BW = band width used to generate PSD

F_{peak} = factor to convert RMS pressure fluctuations to peak values, a value of 3 is used.

The resulting magnitudes for these loads are given in Table 6.2-1.

When these loads are applied to the plug designs and are compared to the remaining preload during normal operation, it is clear that sufficient conservatism exists to assure that they have met their functional design objective for tightness.

6.2.2.5 Hydraulic Loadings During Transient Events

In terms of hydraulic loads on the plugs and patches, a large break LOCA is the most severe event that can occur. For the plug and patch design basis a peak pressure differential across the core support barrel was used. This pressure differential is for the conservative double ended guillotine break.

In addition, load tests were performed to show that the plugs remain intact and in position even after potential deformations have occurred and that they cannot be pushed out under these loads.

6.2.3 Structural Considerations

The expandable plugs are fabricated from Type 316 austenitic steel in order to provide a repair material compatible with the Type 304 material of the core support barrel.

The preloads in the expandable plugs were established to provide resistance to the flow, dynamic, and thermal loads which the plugs would experience in normal operation.

The patches and the expandable plugs were designed to meet the normal operating, upset, and faulted (LOCA) loadings.

6.2.4 Testing

A verification test program for the design of the expandable plugs was prepared and has been carried out.

Load-deflection tests were conducted in order to determine the performance of the plugs relative to the design requirements. Measurements of the spring back of the flange were made to establish the preload generated in the plug.

The wall thickness of the cylindrical section was optimized by testing the bulge capability for the various plug sizes. Rebulge tests were performed to determine the viability of retightening the expandable plugs. The tests confirmed this capability.

Thermal cycle, vibration and leak tests were performed on an expanded 2" diameter prototype test plug. The vibration tests were performed with a frequency band ranging from 25 Hz to 2500 Hz and a 1G vertical acceleration. Similar qualification tests were performed for three, five, and eight inch plugs.

A plug leakage test was performed by pressurizing the core support barrel outer surface to the normal operating pressure and measuring the leak rate. The test demonstrated that there was no significant leakage.

The prototype expandable plug was installed in a 1-3/4" thick section of 304 stainless steel simulating the core support barrel. Thermal cycling of the assembly was performed to 100 thermal cycles with an average differential temperature of 70°F between the plug and the core support barrel. Results confirmed that there was no significant loss of preload. Similar tests were performed for three, five, and eight inch diameter plugs.

6.2.5 Expandable Plug Installation

6.2.5.1 Introduction

Installation was performed underwater using remote tooling. The progress of the installation was closely monitored with underwater television cameras and instruments mounted on the tooling to confirm the adequacy of installation. The installation tooling under went testing which verified the installation process and capabilities of the installation tooling design prior to its use on the core support barrel.

6.2.5.2. Installation

With the expandable plug mounted for installation, the tooling was lowered to the approximate elevation of the hole to be plugged. Using an underwater television camera to align the expandable plug in the core support barrel, the plug was guided into the hole by remote manipulation of the installation tool from a work platform located above the core support barrel. Seating of the expandable plug flange against the spotface machined on the core support barrel was monitored with Linearly Variable Displacement Transducers (LVDT). Once the plug was properly located in the hole, the installation tool was actuated to apply a hydraulic load which expanded the plug in place. Following removal of the installation tool, the installed plug was visually inspected and photographically documented to provide a base-line for future inspections.

6.2.6 Conclusions

A conservative assumption has been made regarding loads on the plugs and patches and has been considered in the design. Testing and analysis demonstrated the design objectives were met.

6.2.7 Post-Repair Inspection of Installed Patches and Plugs

Repair hardware includes the appropriate size plugs and patches for each lug location. In addition, several lug locations employ spacer rings to provide clearance from the core shroud located directly behind some plug locations. Table 6.2-2 summarizes the number and

size of plugs used at each lug location and indicates whether or not a spacer ring or patch is required at that location. Figure 6.2-1 shows a typical expandable plug. Figures 6.2-10 through 6.2-15 show schematic representations of the repairs at each lug location requiring plugging or patching. Plugs and patches were installed at lug locations 1, 3, 4, 5, 6, and 8. Locations 2 and 9 did not require plugs or patches and had the non-through wall cracks machined out. Location 7 did not sustain any damage and no core support barrel repair work was done at this location following removal of the thermal shield support lug.

6.2.7.1 Plug Installation (Crack Arrestor Holes)

The plugs were expanded into the holes for the nominal 3, 5, and 8 inch diameters. Personnel were trained to perform the operation underwater in accordance with detailed procedures. The completed installation was examined visually and photographs of each plug were documented. Flange deflections of the installed expandable plug were determined for each plug by an inspection tool. These flange deflections will serve as a baseline data for future inspection.

6.2.7.2 Patch Installation

Each patch was manufactured with a boss protrusion that fit into the through wall machined cut out in the core support barrel. The clearance between the patch boss protrusion and the core support barrel is a close fit maintained at 15 mils maximum. The fit between the patch and the core support barrel was determined by a gauge. The gauge was inserted into the core support barrel machined cut out, and when the proper fit was determined the gauge outline was machined on the patch.

Alignment of the patch to the core support barrel is provided by the boss thereby assuring the proper patch plug installation. The completed installation was examined visually and the installation was photographically documented.

The flange deflections of the patch plugs were measured by an inspection tool. The deflections have been documented and will provide a baseline for future inspections.

6.2.8 Post Outage Testing *

In addition to the normal post refueling outage test program other tests will be conducted to measure the effect of the thermal shield removal. These are:

1) Shape Annealing Factor Test

   The incore to excore detector relationship has changed since the thermal shield was removed. This test will be performed to measure the effect.

2) A containment survey will be performed during power ascension to measure the neutron in gamma fields present as a result of the thermal shield removal.

---

*Discussion provided by Florida Power and Light.

REFERENCES

1. ANSYS Engineering Analysis System, Swanson Analysis Systems, Inc., Elizabeth, PA.

TABLE 6.2-1

NORMAL OPERATING BEST ESTIMATE HYDRAULIC LOADS ON THE CORE SUPPORT BARREL PLUGS AND PATCHES

Type of Load	Load Value
1. Static pressure differential across the plug or patch.	23.2 psi (directed inwards towards core)
2. Pump-induced fluctuation pressures on plug on patch face.	± 0.3 psi @ 15 HZ ± 0.1 psi @ 30 HZ ± 1.2 psi @ 75 HZ ± 0.2 psi @ 150 HZ
3. Static drag load on plug protrusion/flange	10.7 psi x A*
4. Vortex shedding loads on plug protrusion/flange	± 10.7 PSI X A**
5. Turbulence load on plug	± 1.5 psi

* - Projected area of plug or patch flange (when viewing edge of flange)

** - Projected area of plug flange (when viewing edge of flange)

Table 6.2-2

SUMMARY OF REPAIR HARDWARE EMPLOYED AT EACH LUG LOCATION

LUG LOCATION	EXPANDABLE PLUGS	PATCH ASSEMBLY
1	4-3 Inch Heavy Wall 3-8 Inch 2-8 Inch Spacer Ring	1
2*	0	0
3	3-3 Inch Heavy Wall 2-5 Inch 1-5 Inch Spacer Ring	1
4	4-3 Inch Heavy Wall 3-8 Inch 2-8 Inch Spacer Ring	1
5	4-3 Inch Heavy Wall	1
6	3-3 Inch Heavy Wall 2-8 Inch	1
7**	0	0
8	2-3 Inch Standard Wall	0
9*	0	0

* Machined out non-through wall cracks

** No core support barrel damage

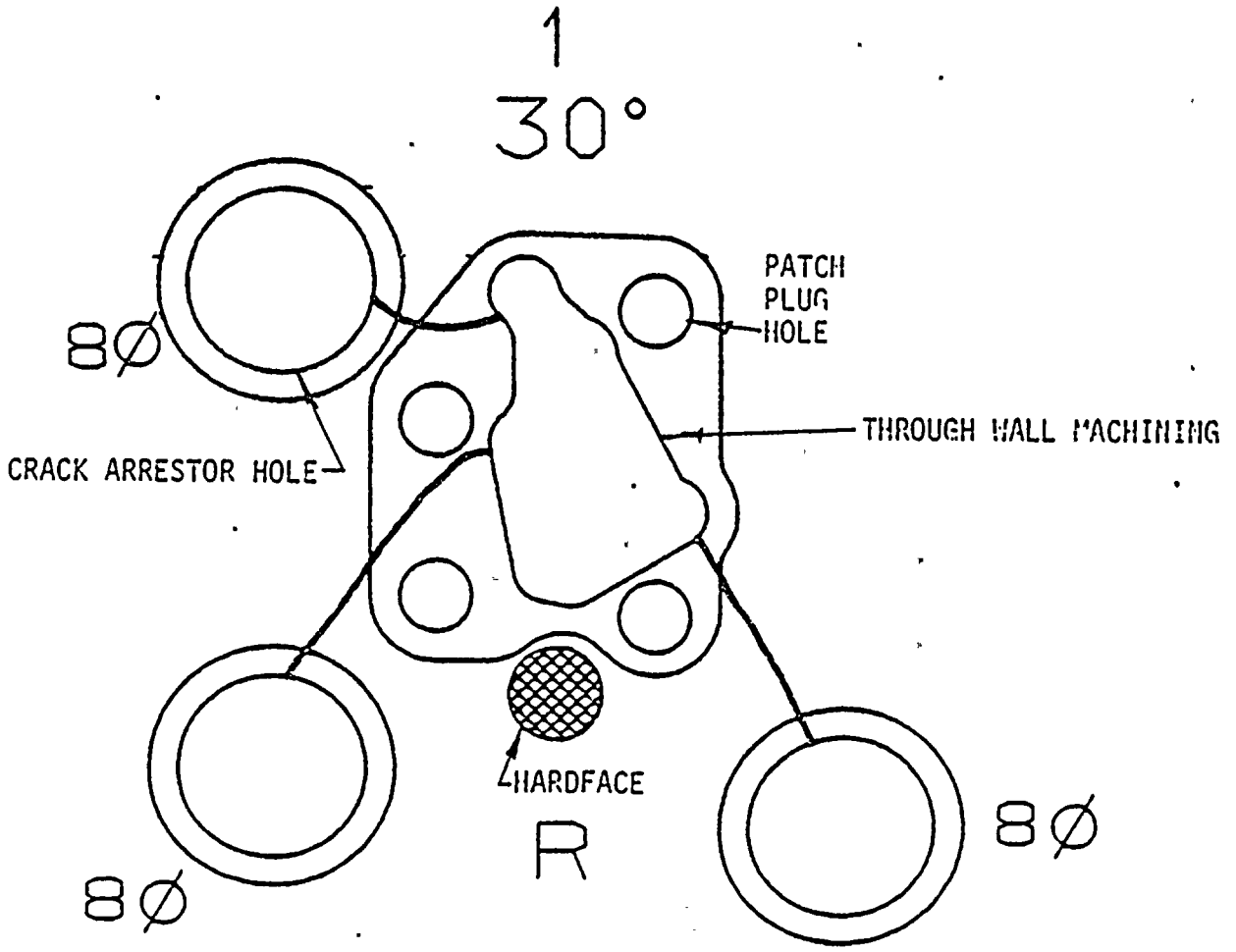
1
30°
PATCH
PLUG
HOLE
8Ø
THROUGH WALL MACHINING
CRACK ARRESTOR HOLE
HARDFACE
R
8Ø
8Ø

FIGURE 6.1-1

2

70°

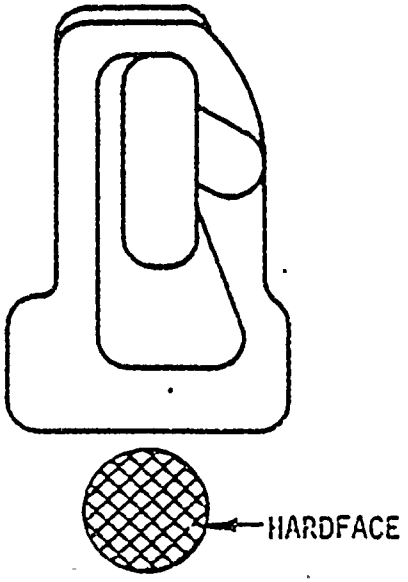

S

NON-THROUGH WALL MACHINING

FIGURE 6.1-2

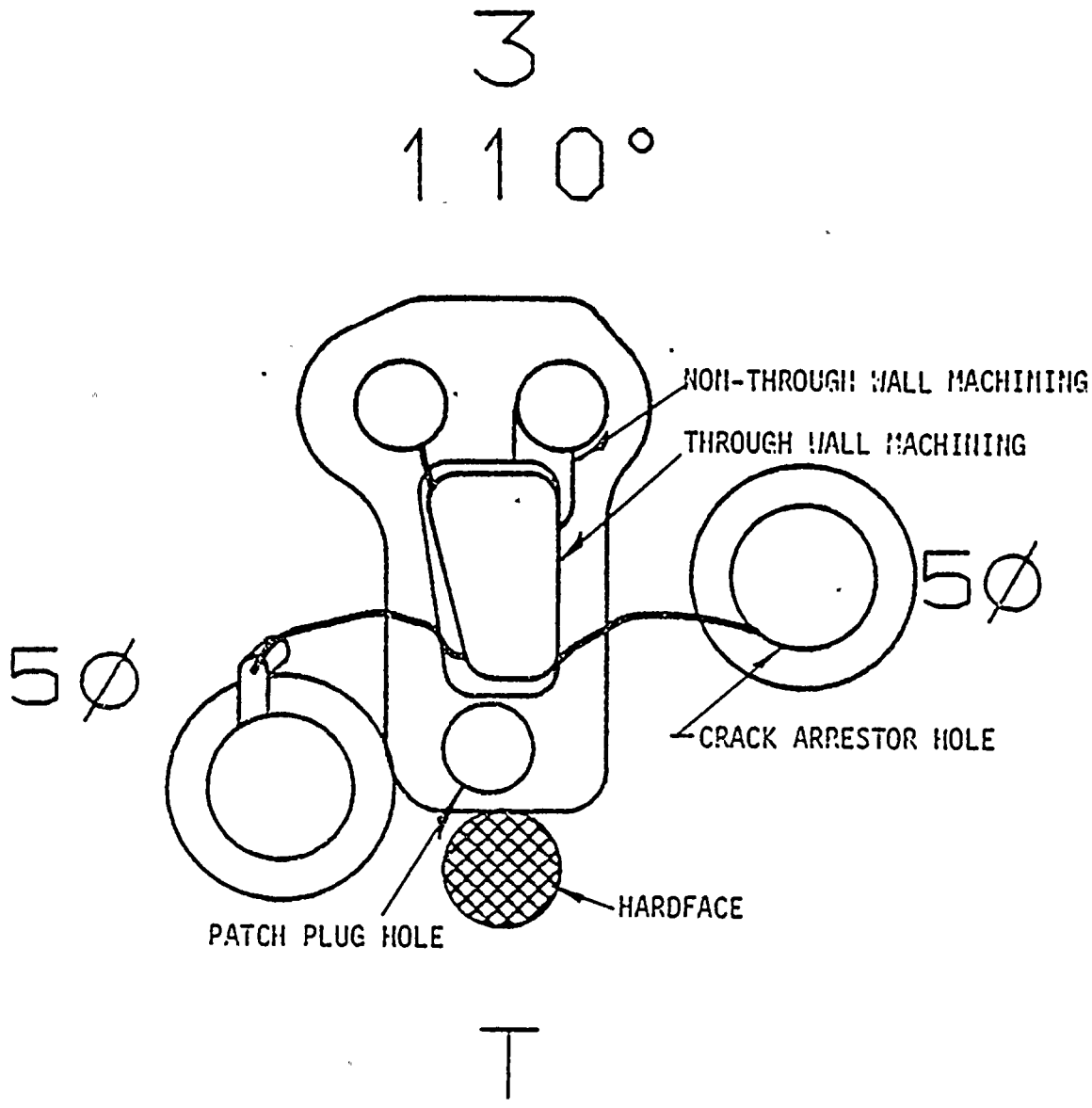
3
110°
NON-THROUGH WALL MACHINING
THROUGH WALL MACHINING
5Ø
5Ø
CRACK ARRESTOR HOLE
HARDFACE
PATCH PLUG HOLE
T

FIGURE 6.1-3

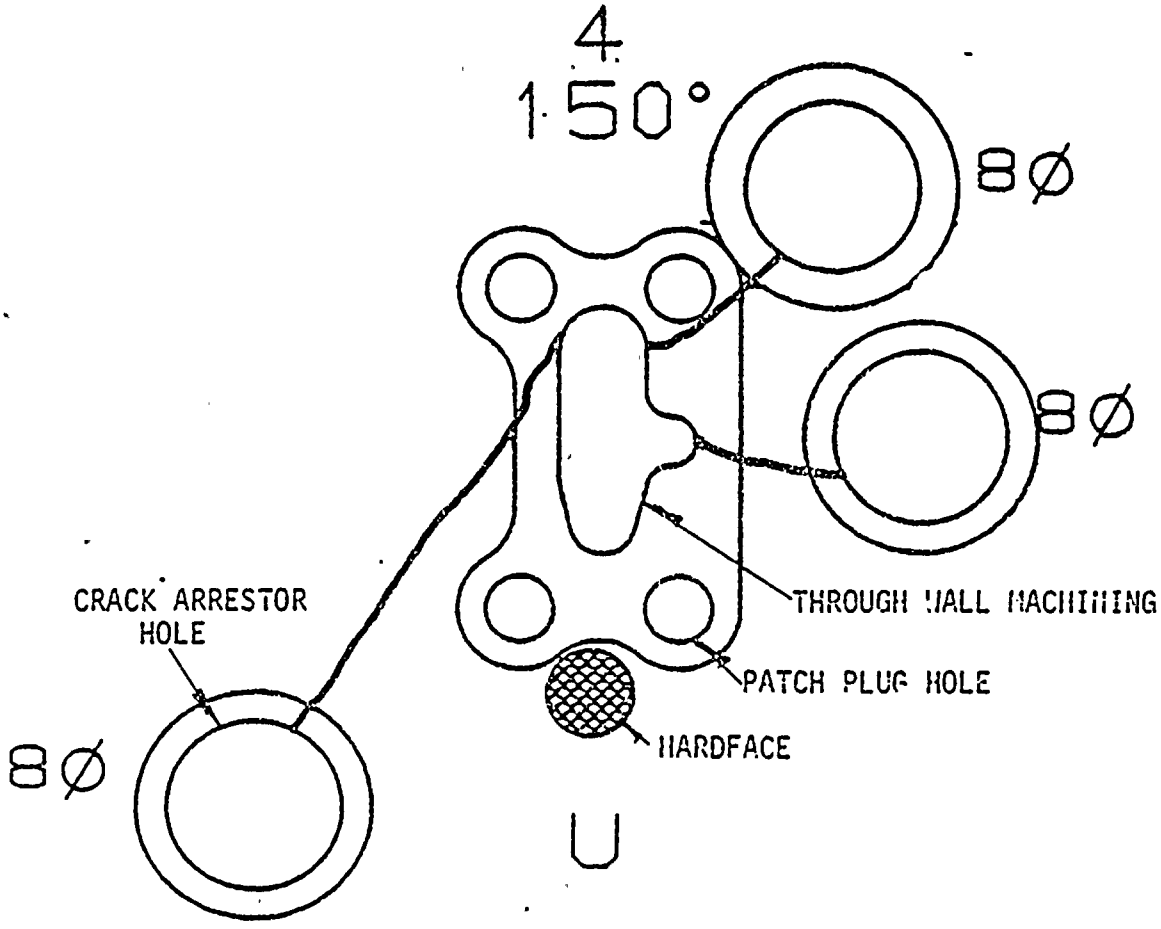
4
150°
8Ø
8Ø
8Ø
CRACK ARRESTOR HOLE
THROUGH WALL MACHINING
PATCH PLUG HOLE
HARDFACE
U

FIGURE 6.1-4

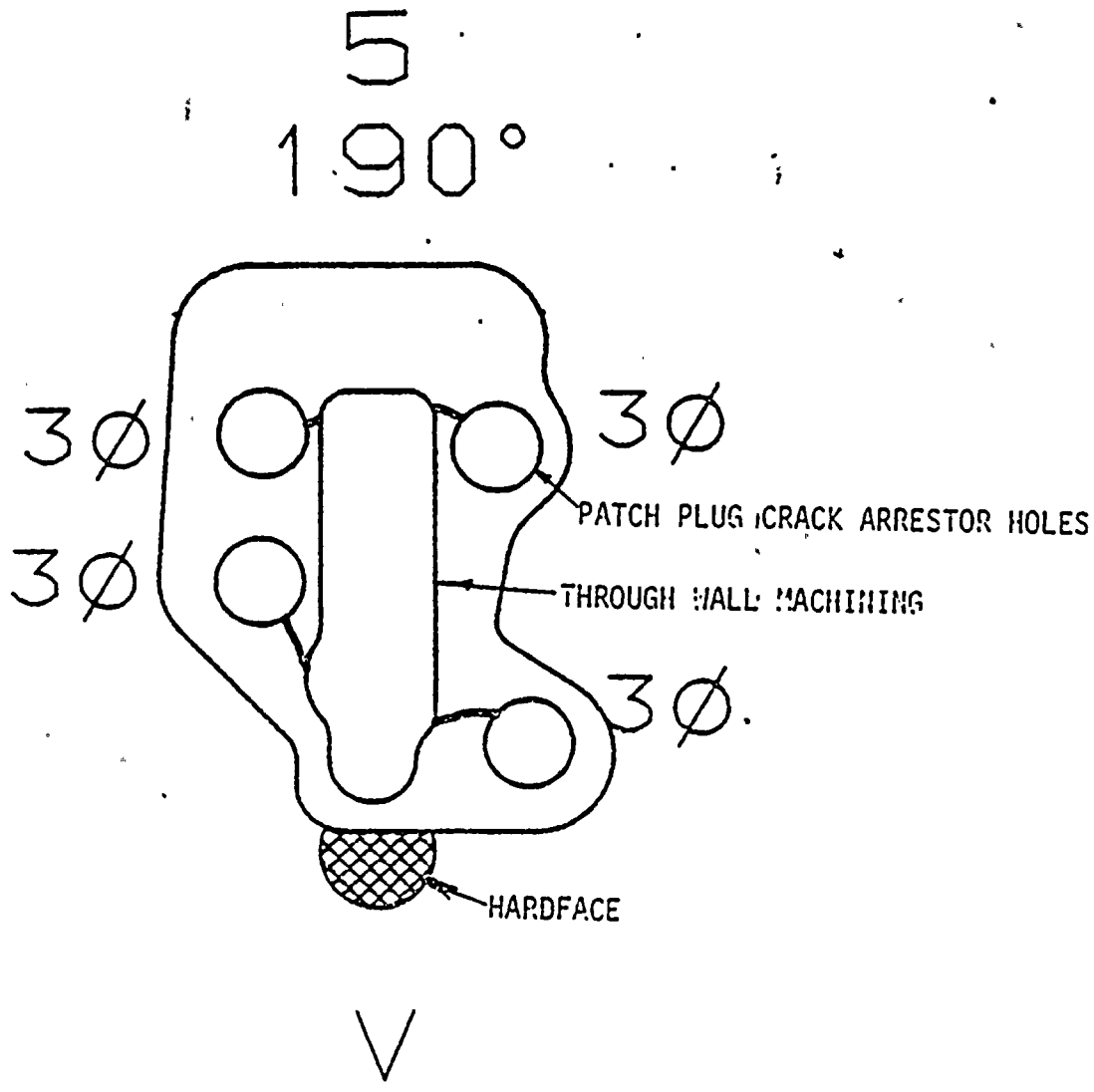
5
190°
3Ø
3Ø
3Ø
3Ø
PATCH PLUG CRACK ARRESTOR HOLES
THROUGH WALL MACHINING
HARDFACE
V

FIGURE 6.1-5

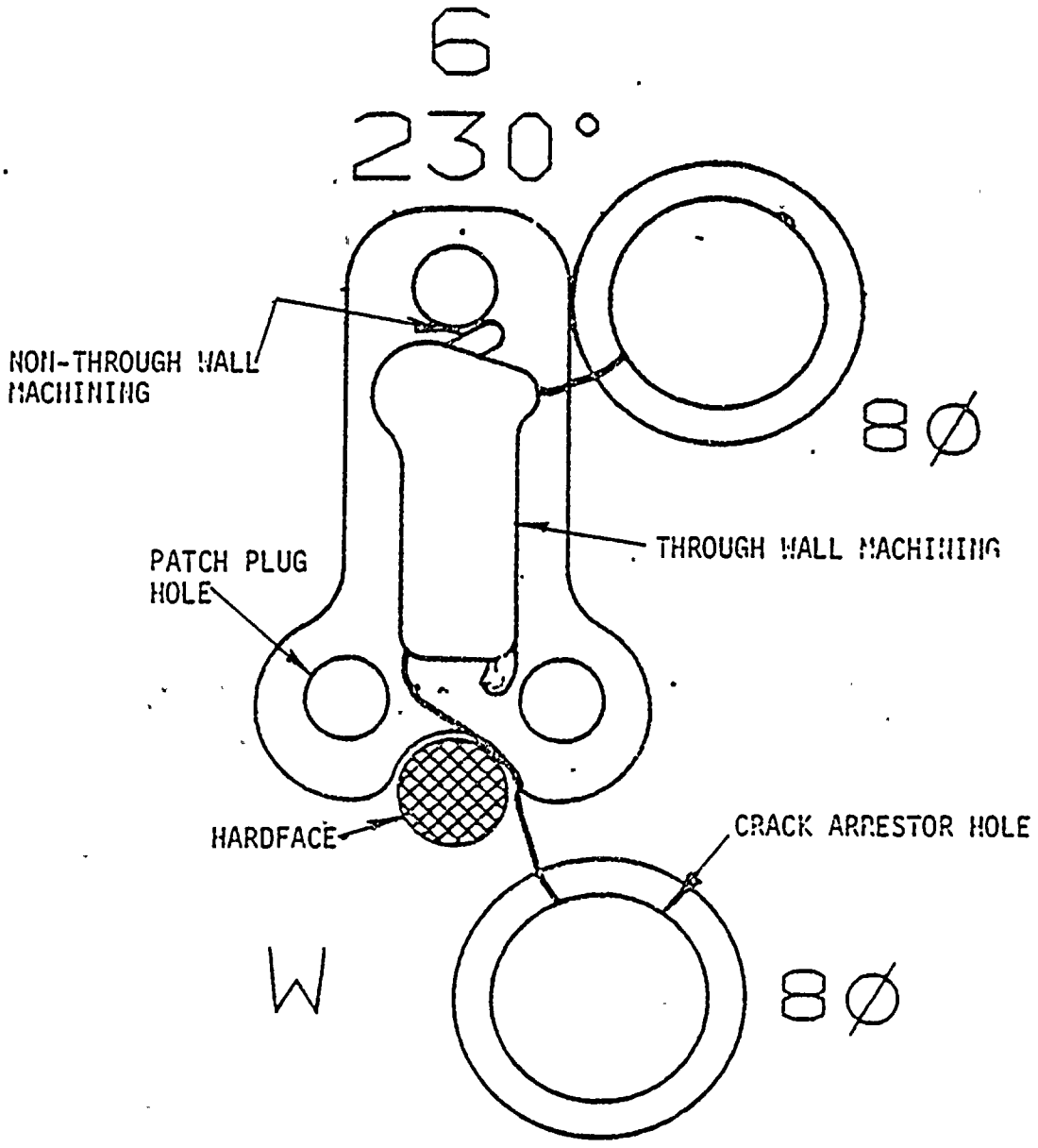
6
230°
NON-THROUGH WALL MACHINING
8Ø
THROUGH WALL MACHINING
PATCH PLUG HOLE
HARDFACE
CRACK ARRESTOR HOLE
W
8Ø

FIGURE 6.1-6

7

270°

NO DAMAGE

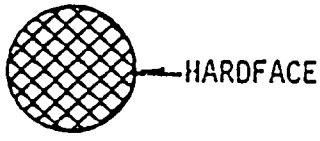

FIGURE 6.1-7

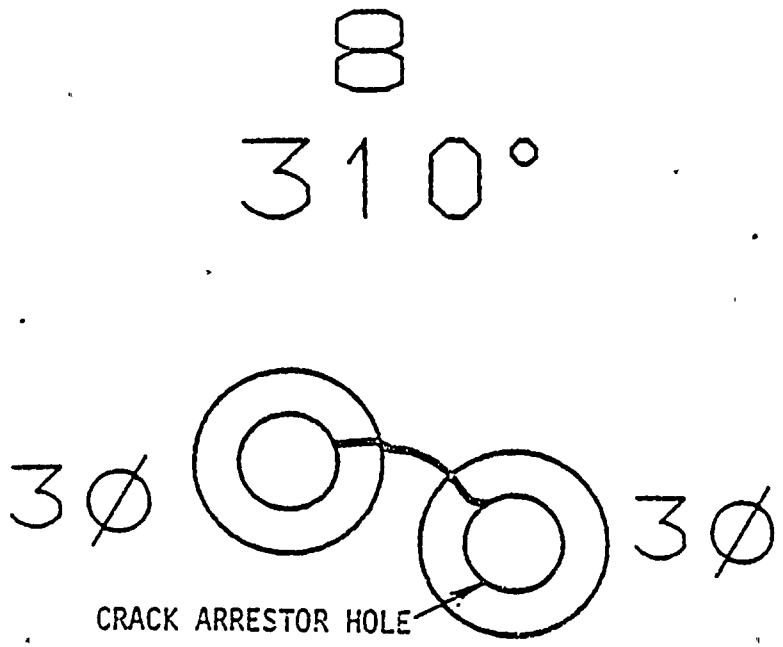

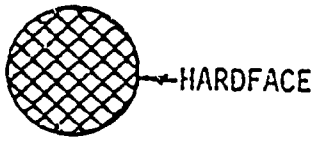

Y

FIGURE 6.1-8

9

350°

NON-THROUGH WALL MACHINING

Z

FIGURE 5.1-9

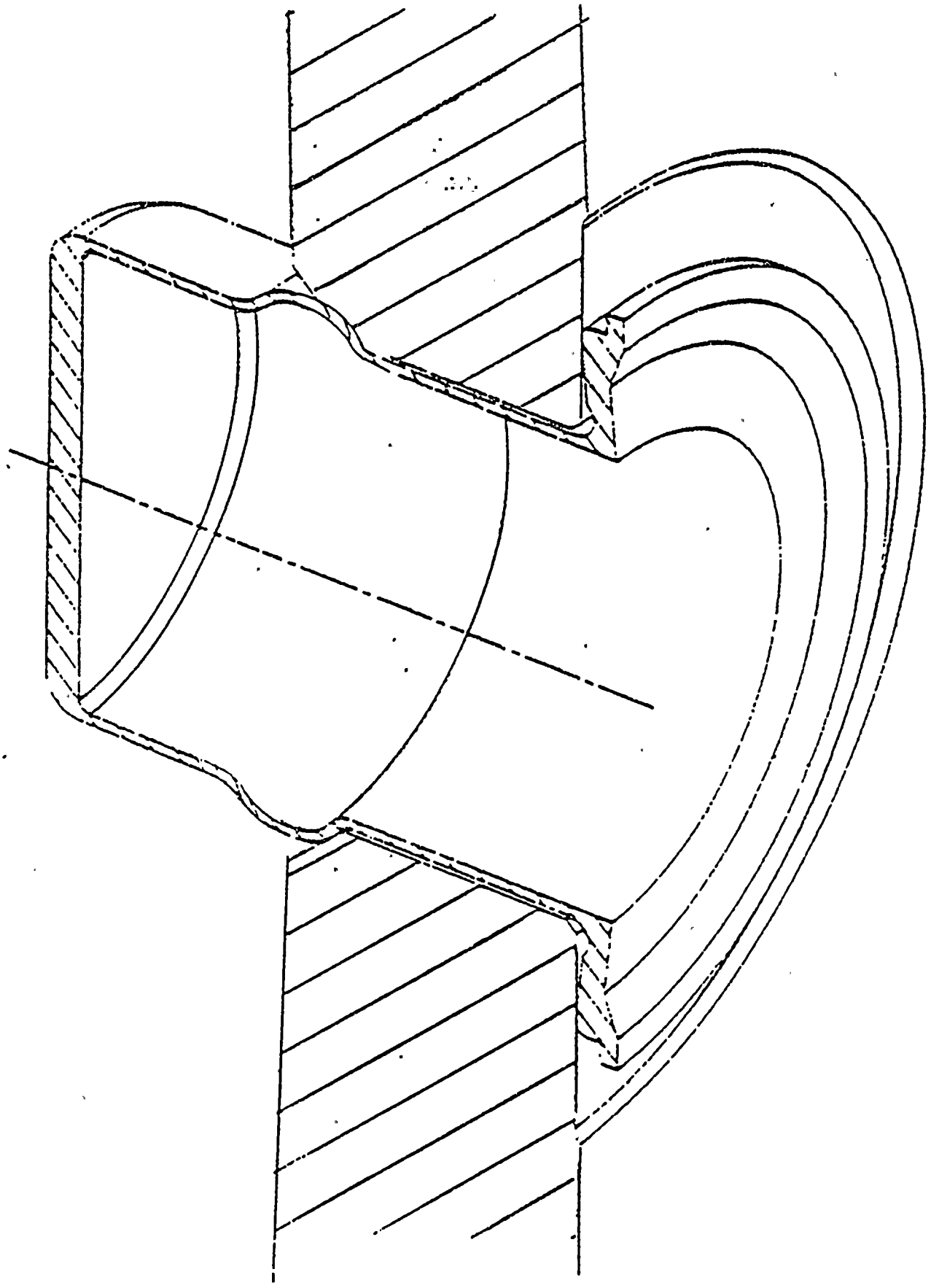

FIGURE 6.2-1

EXPANDABLE PLUG

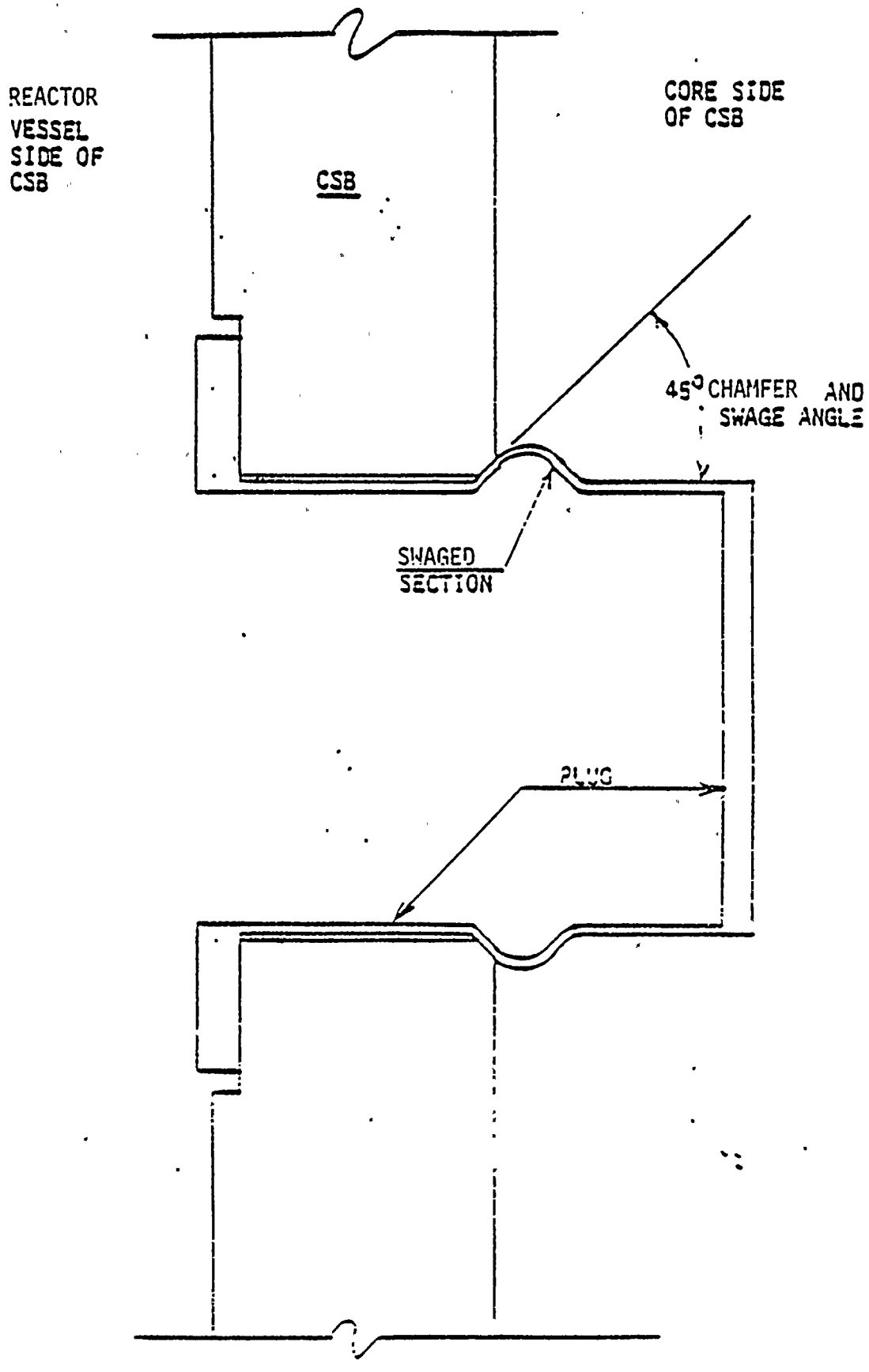

FIGURE 6.2-2

INSTALLED PLUG

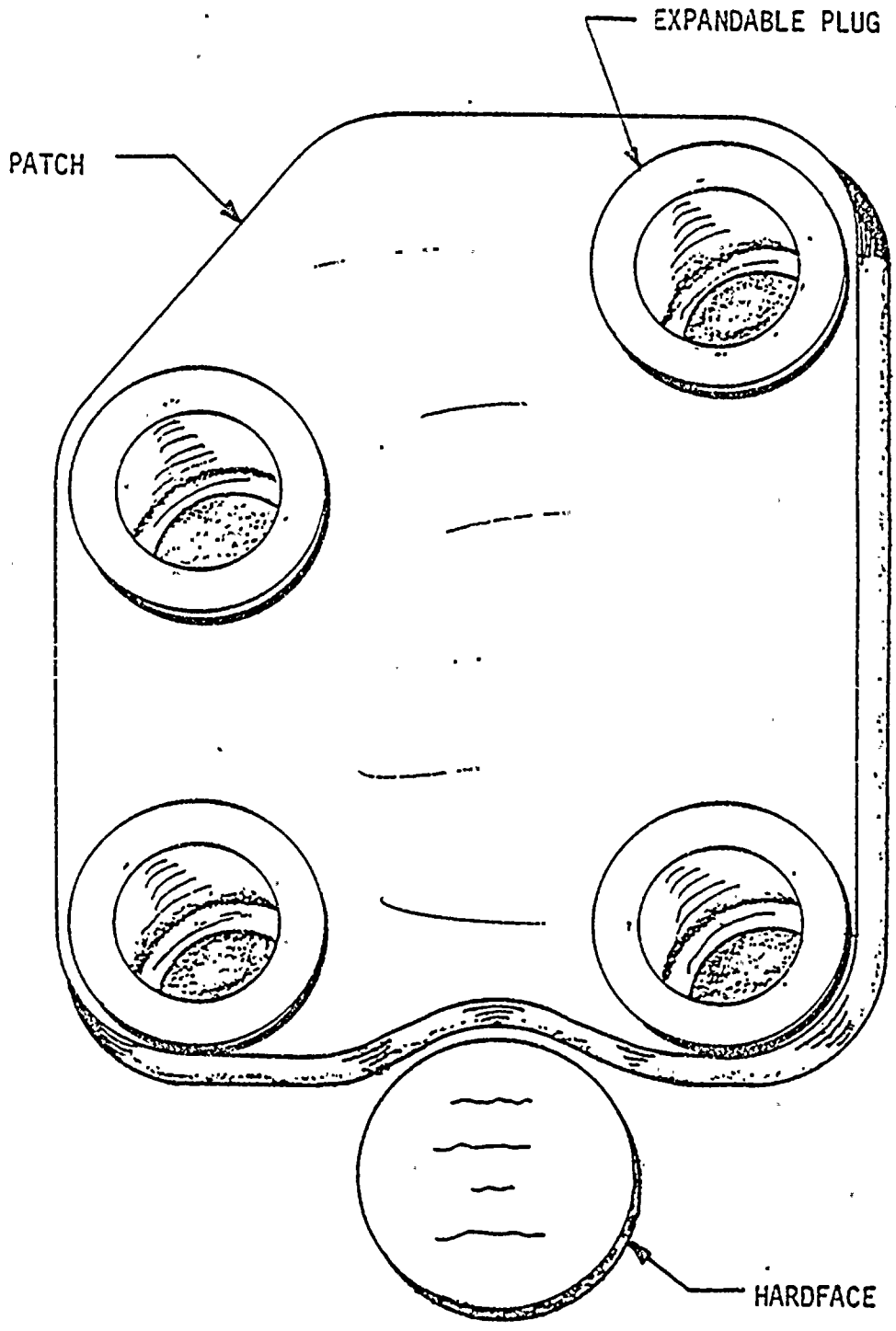

FIGURE 6.2-3

TYPICAL PATCH

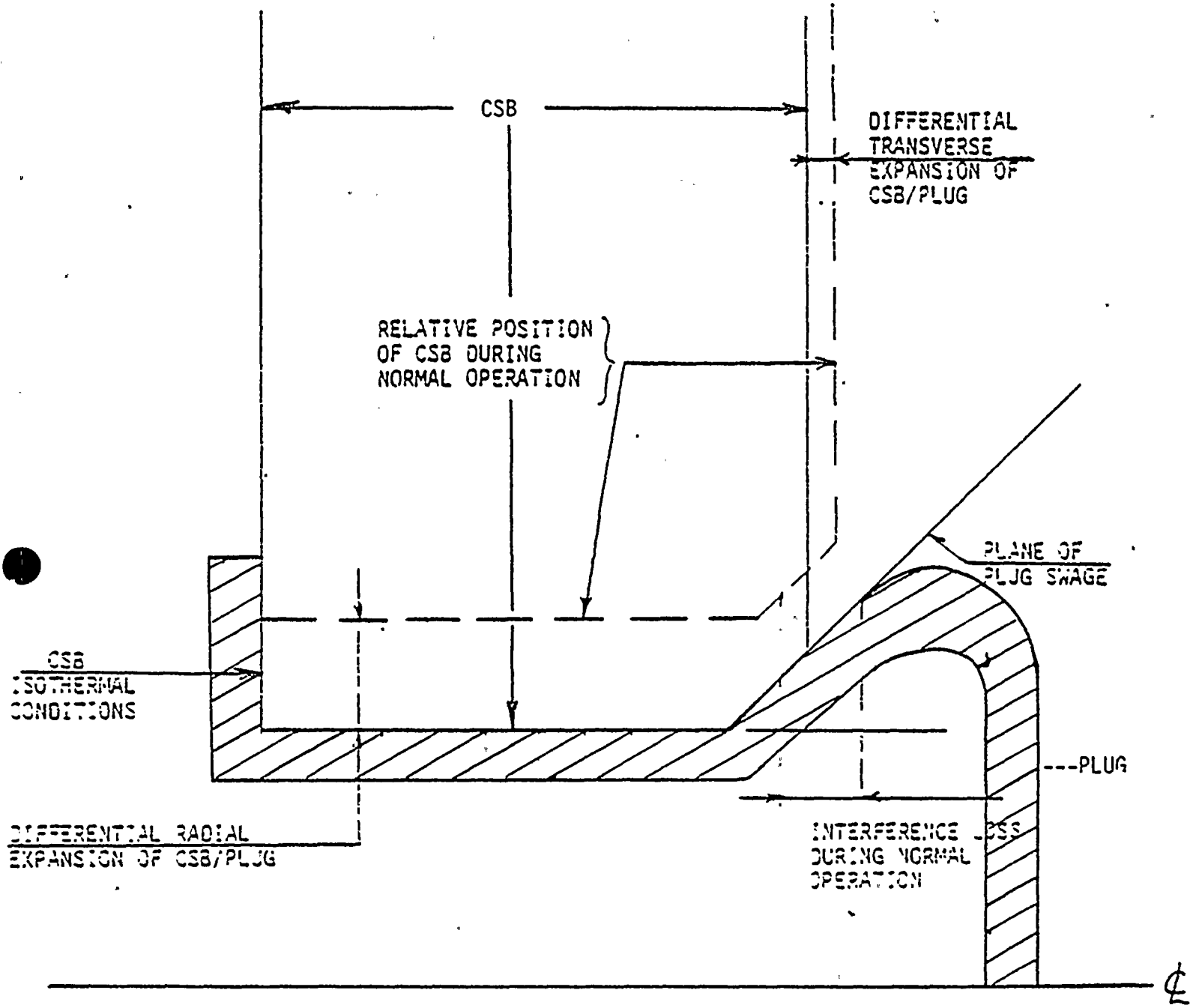

FIGURE 6.2-4

CSB/PLUG RELATIVE THERMAL EXPANSION

FIGURE 6.2-5
COOLANT TEMPERATURES vs
TIME DURING A STEAM LINE BREAK

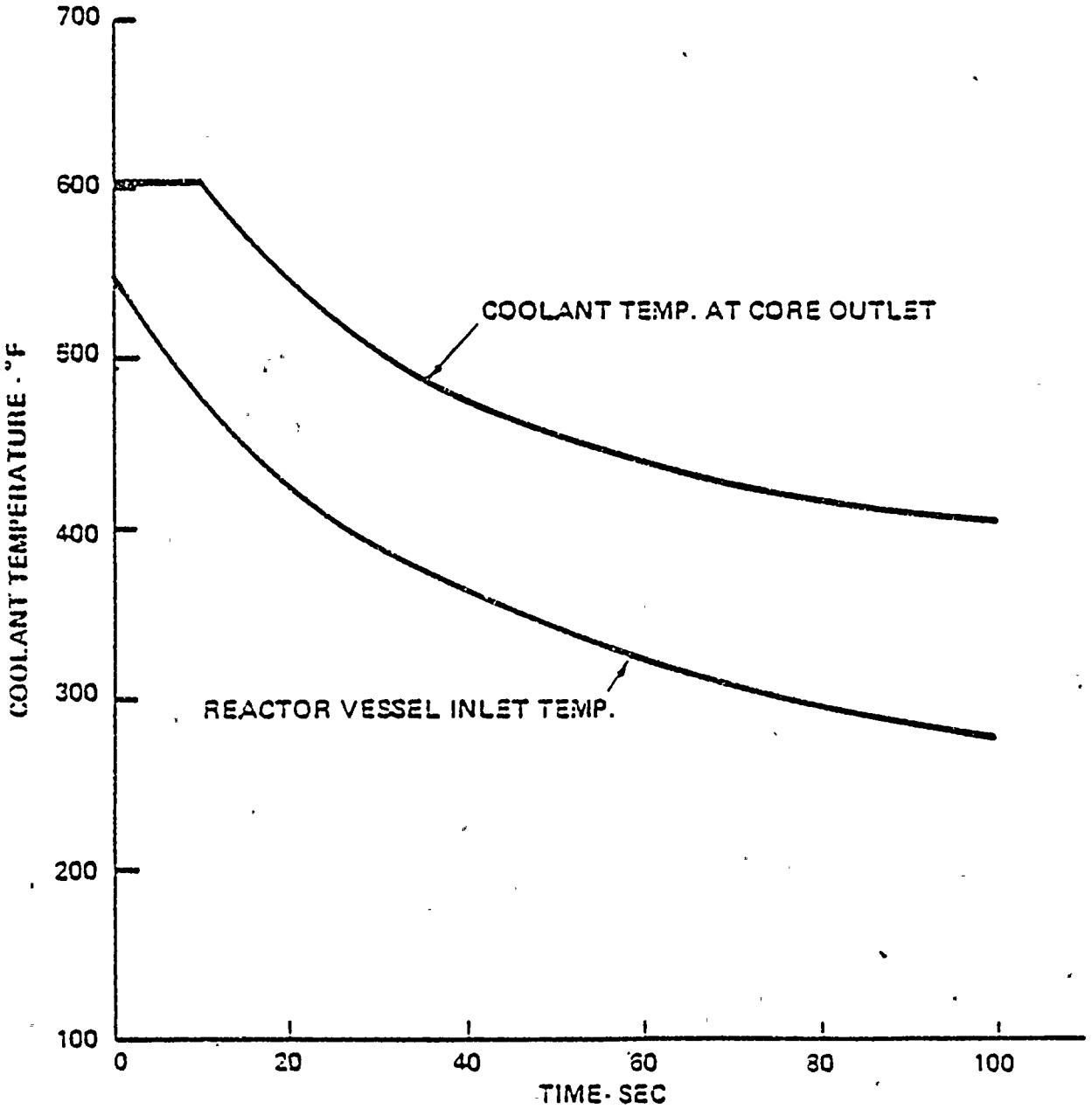

FIGURE 6.2-6
ST. LUCIE I
2 D EXPANDABLE PLUG ANSYS MODEL

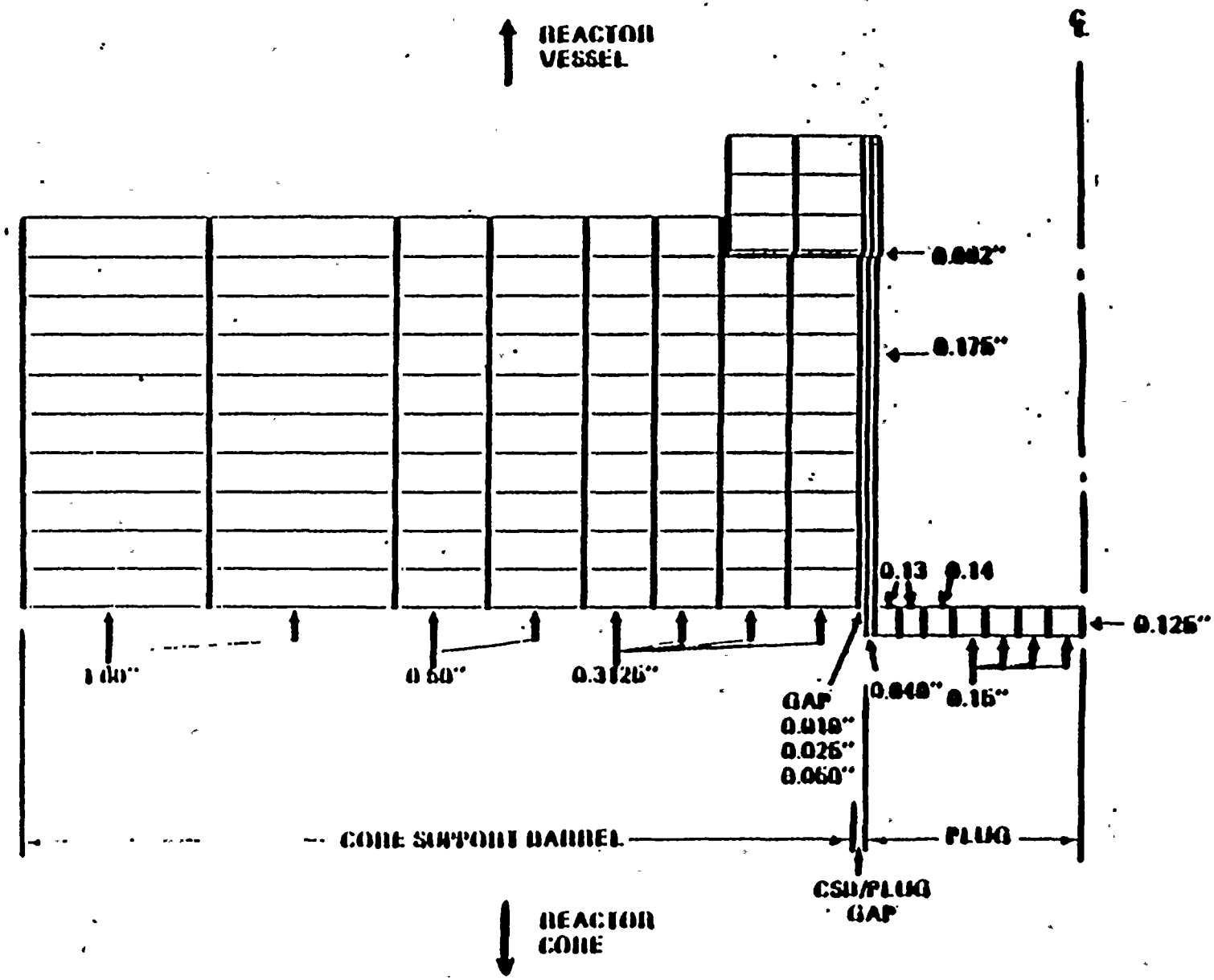

Figure 6.2-7

INTENTIONALLY OMITTED

FIGURE 6.2-8

HYDRAULIC LOADS ACTING ON THE CSB PLUGS

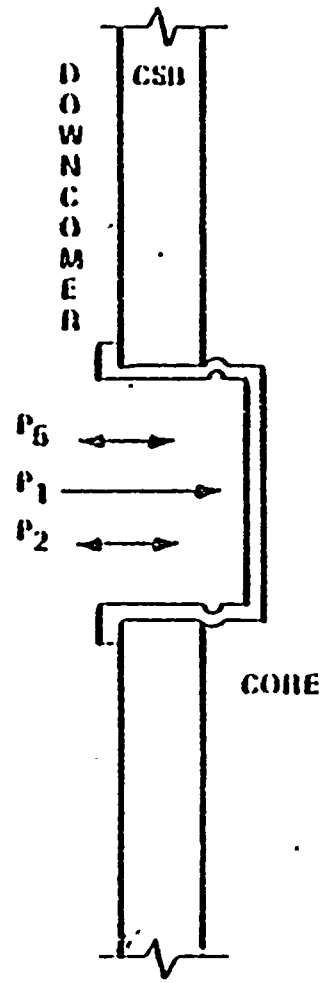

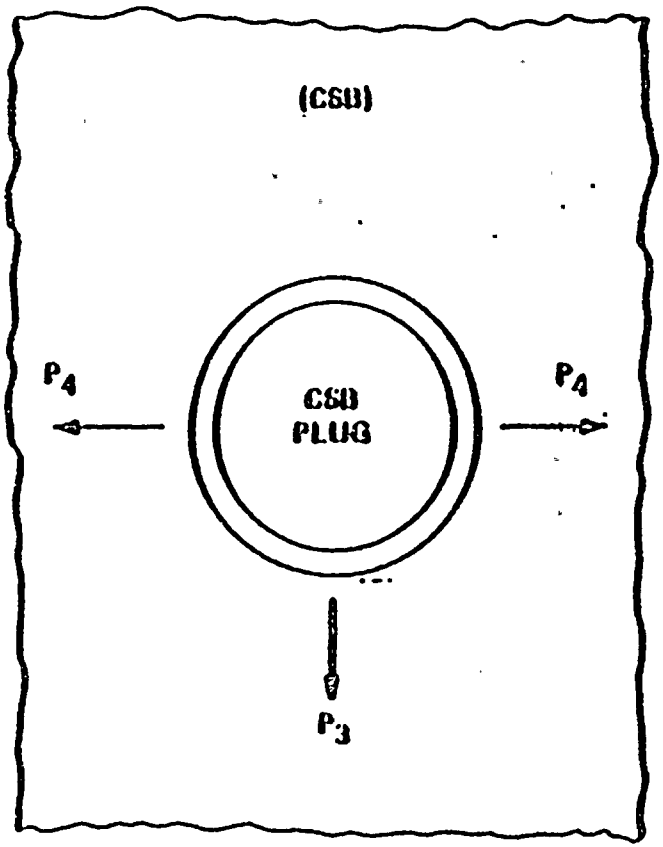

P_1 • STEADY STATE ΔP DURING NORMAL OPERATION

P_2 • FLUCTUATING LOADS DUE TO BLADE PASSING FREQUENCY PUMP SPEED

P_6 • GENERAL TURBULENCE

P_3 • HYDRODYNAMIC DRAG

P_4 • VORTEX SHEDDING

FIGURE 6.2-9
ANNULAR SPACE BETWEEN RV/CSB NORMALIZED
PRESSURE POWER SPECTRAL DENSITY vs
NORMALIZED FREQUENCY

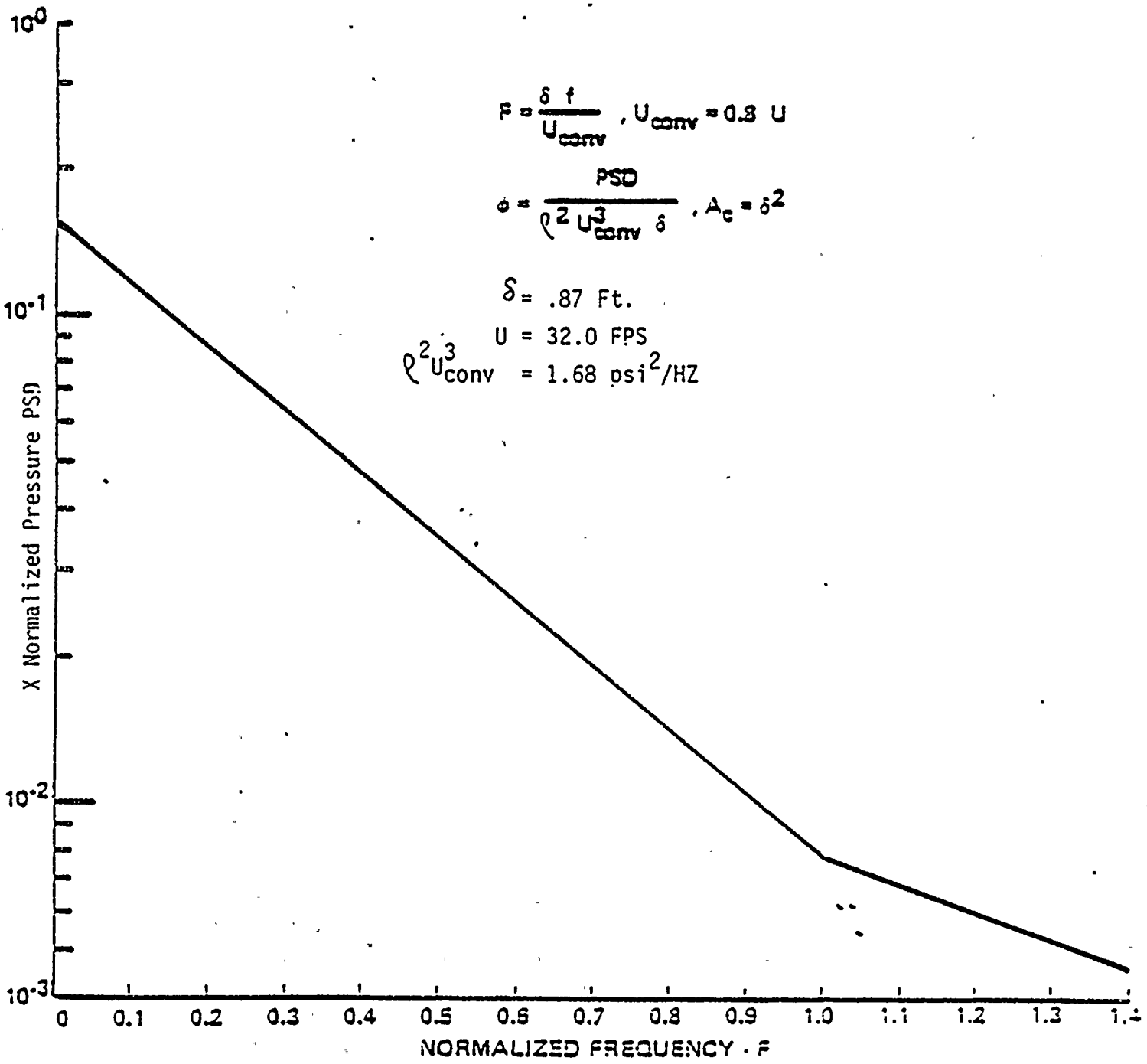

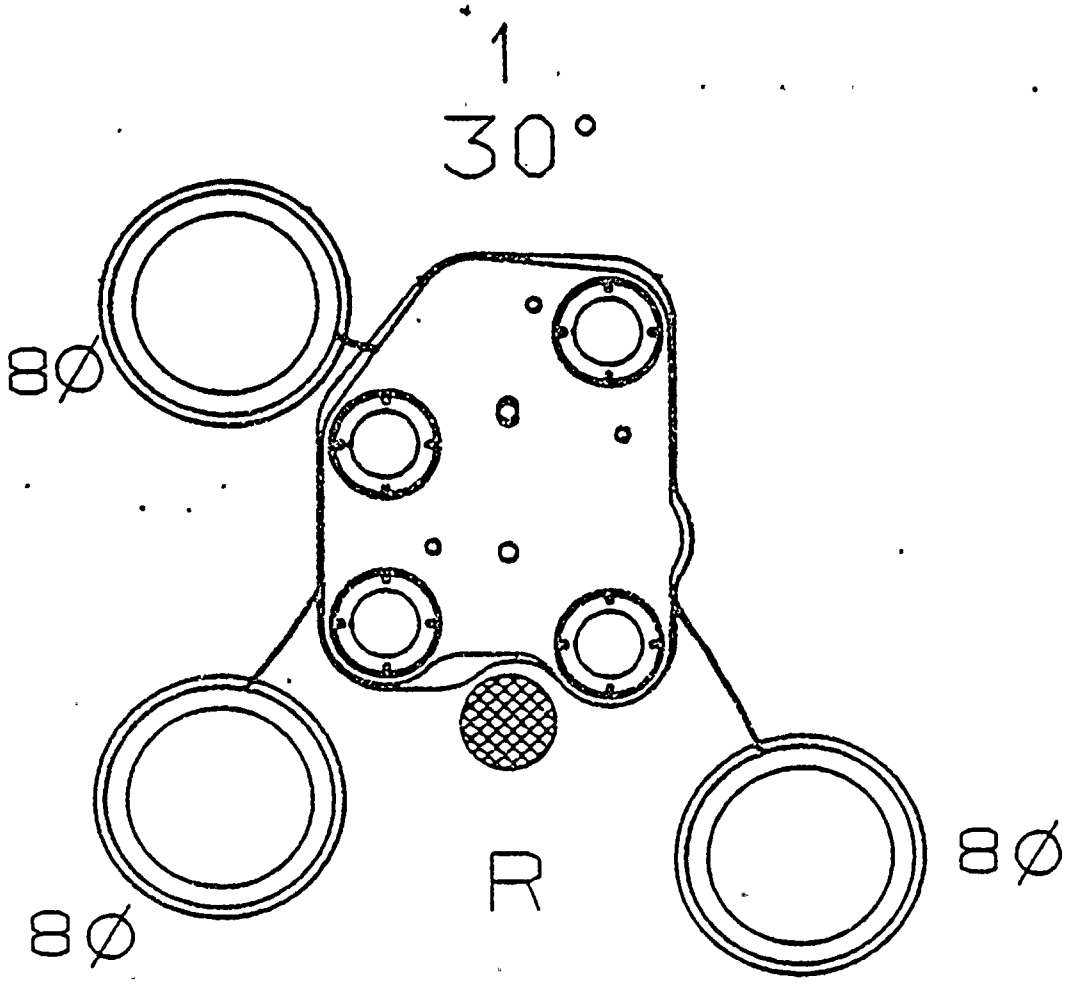

PATCH & PLUGS INSTALLED

FIGURE 6.2-10

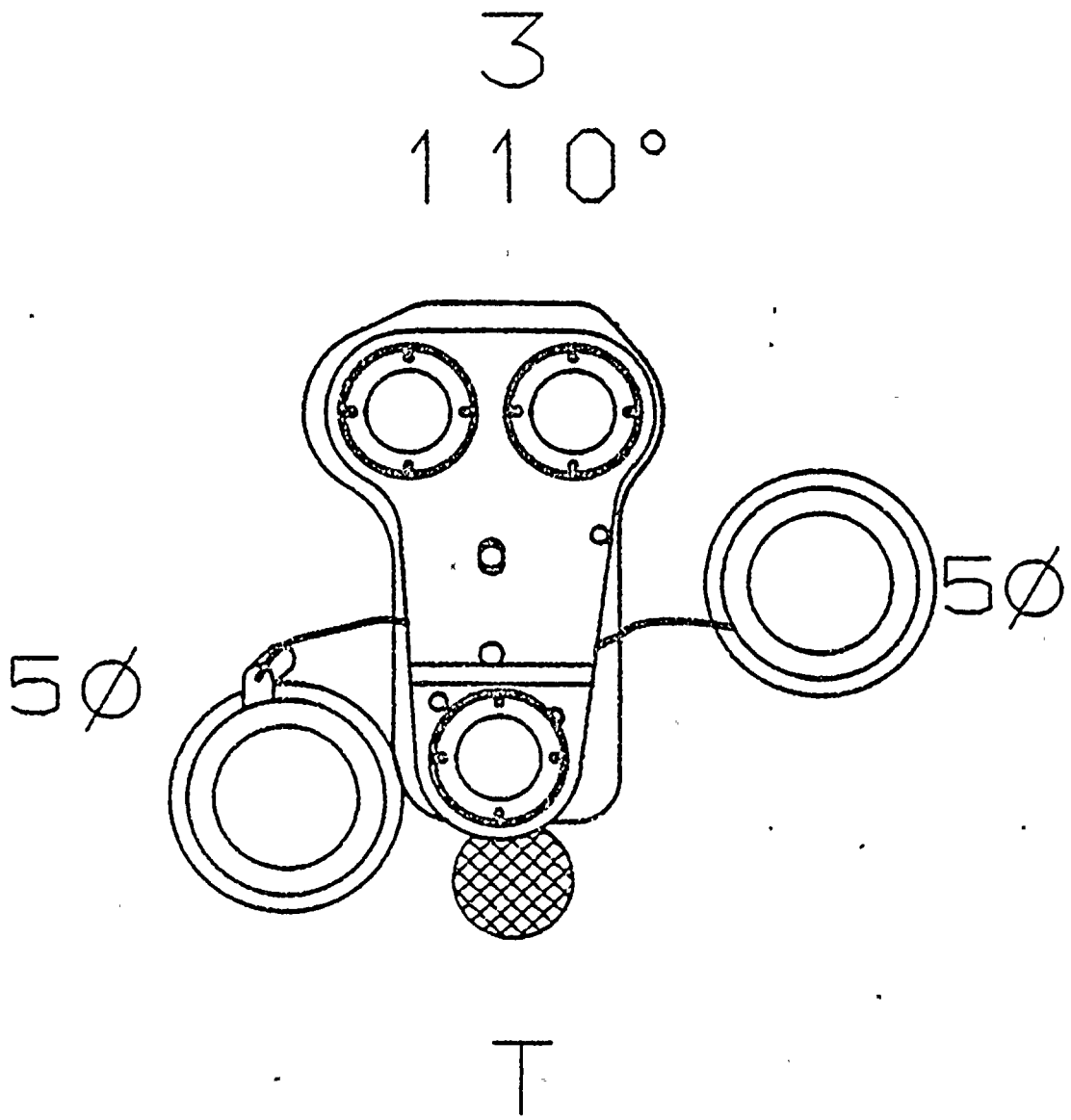

PATCH & PLUGS INSTALLED

FIGURE 6.2-11

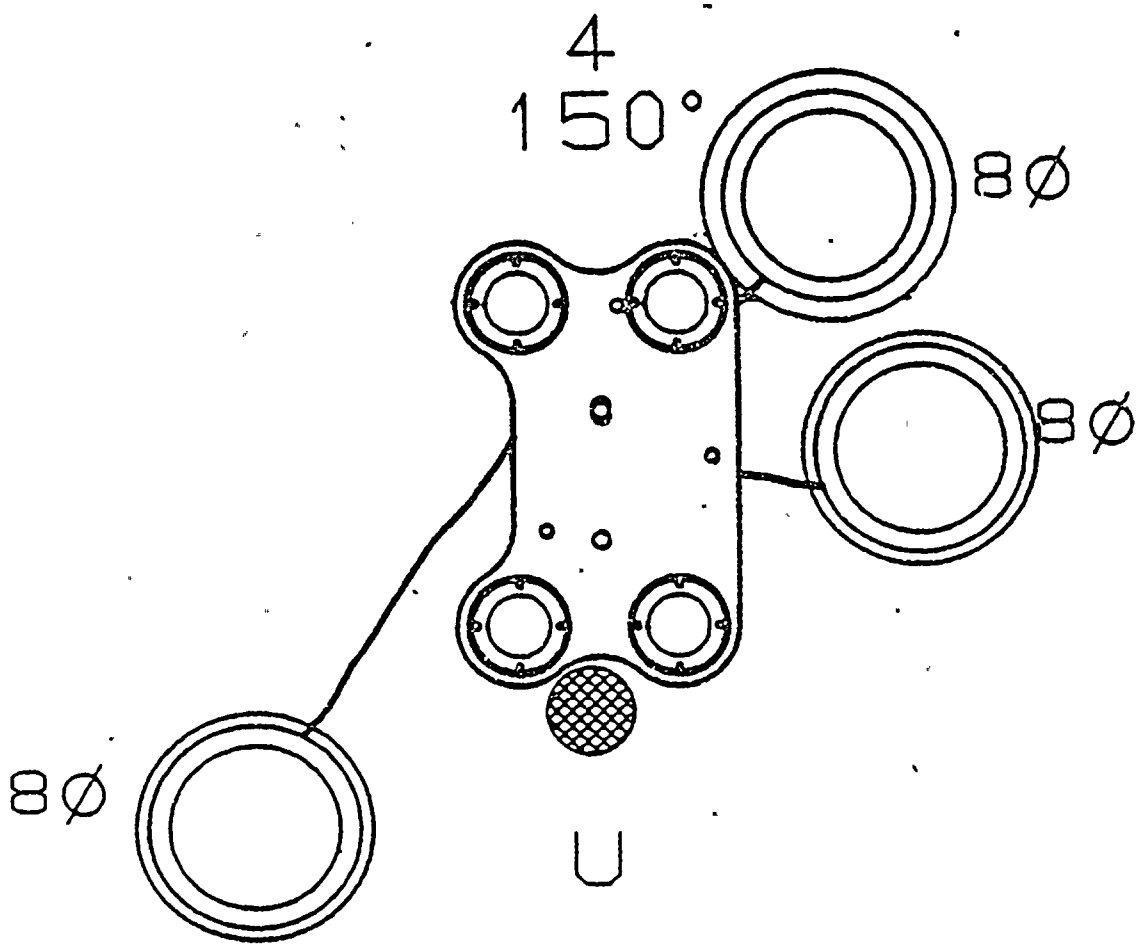

PATCH & PLUGS INSTALLED

FIGURE 6.2-12

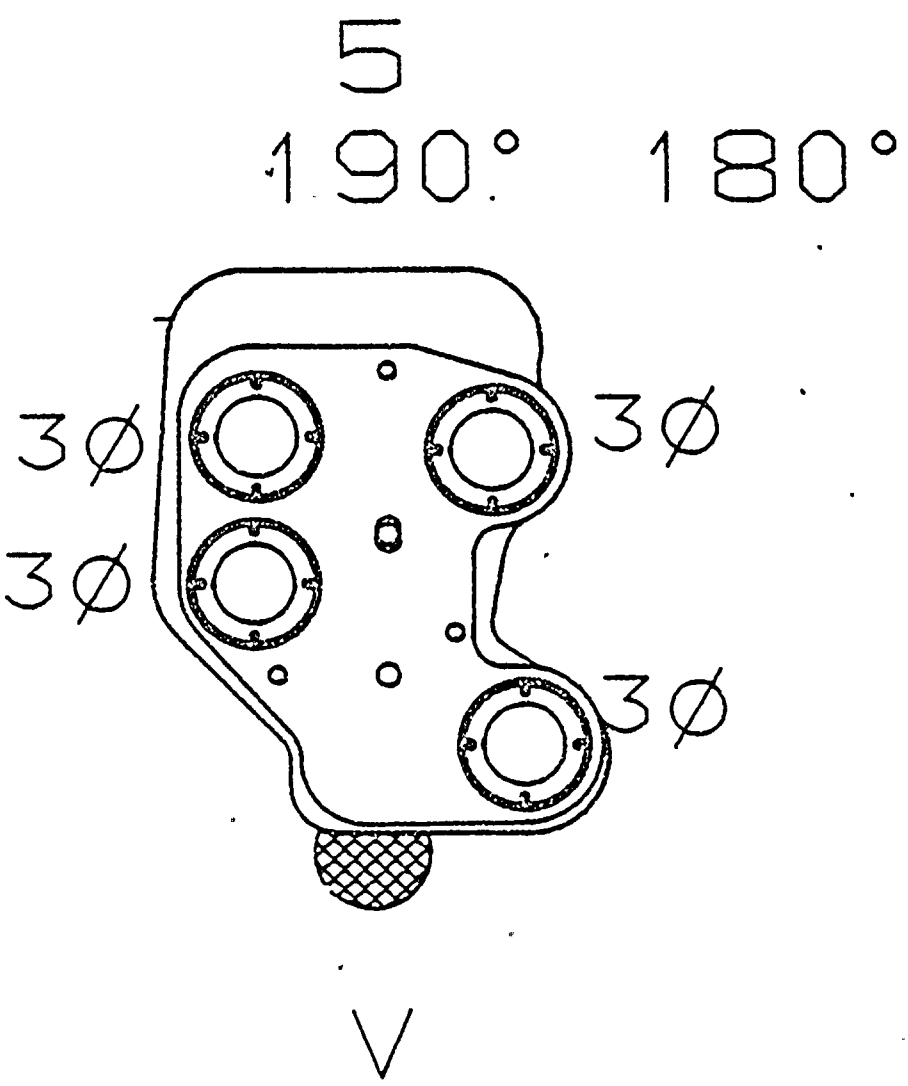

PATCH & PLUGS INSTALLED

FIGURE 6.2-13

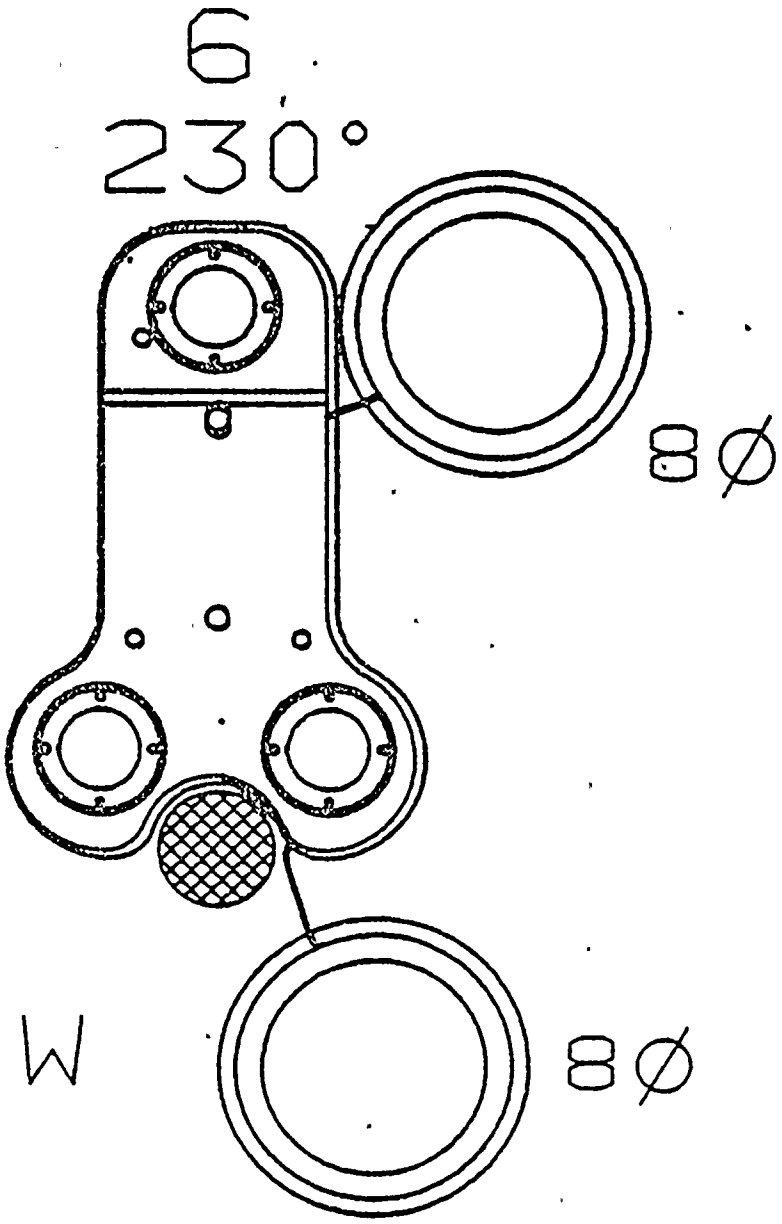

PATCH & PLUGS INSTALLED

FIGURE 6.2-14

8

310°

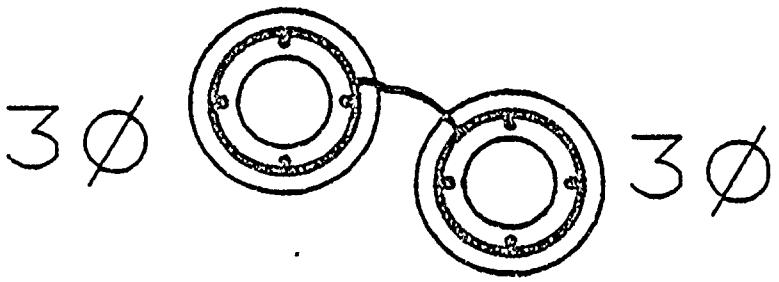

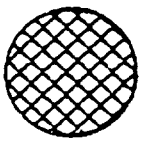

Y

PLUGS INSTALLED

FIGURE 6.2-15

8.0 CORE SUPPORT BARREL STRUCTURAL INTEGRITY

8.1 INTRODUCTION AND CRITERIA

In order to establish the structural integrity of the repaired core support barrel a comprehensive stress analysis was performed utilizing the methods and compared to the original criteria set forth in Section III, Subsection NG of the ASME Code.

The criteria employed were the same as those discussed in the FSAR and generally are:

For Normal and Upset Conditions (Levels A and B), Figure NG-3221-1.
For LOCA Conditions (Level D) Appendix F.

8.2 REACTOR INTERNALS STRESS ANAYSIS RESULTS

In addition to the effects of thermal shield removal on the repaired core support barrel the effects on the reactor internals were investigated and determined to be:

(a) A small change in the hydraulic loads on the reactor internals.

(b) A negligible change in the frequency of the core support barrel assembly.

Evaluation of the above effects were considered in combination with the site specific seismic and asymmetric loads analysis. A seismic analysis was performed considering the thermal shield had been removed and asymmetric LOCA load data were derived based on no thermal shield. The analysis showed that the reactor internals with the thermal shield removed meet the ASME Code allowable stresses using the original design criteria for normal operation, upset (Level A and B), and LOCA (Level D) conditions.

8.3 CORE SUPPORT BARREL (CSB) STRESS ANALYSIS RESULTS

8.3.1 Core Support Barrel Analysis

The analysis was performed for the region of the core support barrel at the thermal shield lug elevation. The conservative assumption was made that at each of the lug regions the maximum length of lateral crack was circumferential and in the same horizontal plane as the cracks in the other lugs. The point of maximum stress in the region was then established by determining the axis in the plane about which the moment of inertia of the cylindrical section in combination with the load resulted in the maximum stress. The fatigue analysis was performed utilizing the stress concentration factors resulting from the crack arrestor hole size analysis. The design fatigue curves used in the analysis are the more conservative fatigue curves published in the Winter 1982 Addenda to Section III, Appendix I, Figures I-9.2.1 and I-9.2.2.

In addition to the Code Analysis, a confirmatory stress analysis of the core support barrel was performed using sophisticated finite element techniques. Overall effects and local effects of cracks in the core support barrel were evaluated by comparing stress distributions to those of an uncracked barrel. Figure 8.2-3 depicts a typical finite element model of the core support barrel used by the ANSYS finite element computer program (Reference 3). The conclusion of the confirmatory analysis was that the analysis considering the horizontal crack length in the same horizontal plane was conservative. A summary of these results are shown in Table 8.3-1.

8.3.1.1 Evaluation Criterion for Cracks in Core Support Barrel Based on Fracture Mechanics Considerations

An evaluation of the cracks in the core support barrel on the basis of fracture mechanics considerations was performed. After discussion with consultants on fracture mechanics it was concluded that insufficient data for the barrel material in a pressurized water reactor environment for service in excess of 10^{11} cycles was available. Because of the lack of materials data and the length of cracks in the core support barrel extremely conservative assumptions would have had to be made. The decision was made to use crack arrestor holes sized to reduce stress concentrations to magnitudes compatible with the ASME Code fatigue limitations.

8.3.1.2 Stress Concentration Factors

The stress concentration factors for a crack with a crack arrestor hole at each end were calculated using available theoretical solutions of stress distributions in plates with openings (References 1, 2, and 3). The adequacy of the solutions was verified through comparisons with finite element analyses of typical crack geometries and loading conditions.

The "equivalent ellipse" concept is useful in calculating stress concentration factors for a crack with crack arrestor holes at each end. For an elliptical hole in an infinite plate in tension, the stress concentration factor, K_t, is given by:

$$K_t = 1 + 2\sqrt{\frac{b}{2r}} \qquad \text{(Reference 2)}$$

where

b = length of crack perpendicular to applied stress

r = radius of crack arrestor hole

Figure 8.3-1 is a plot of the stress concentration factors for a 32 inch crack with various sizes of arrestor holes. The theoretical solution was confirmed by finite element results which are also indicated on the figure. The finite element results were obtained using the CDC-MARC general purpose finite element program Reference 1). Figure 8.3.2 shows a typical finite element model of a crack with arrestor holes under transverse tension.

8.3.2 Core Support Barrel Material Examination Results

The St. Lucie 1 core support barrel material is SA-240 type 304 stainless steel plate. A number of tests, some of which are also described in Chapter 7, Failure Mechanism Analysis, have been performed to verify that the core barrel has not suffered any untoward degradation.

Mechanical properties of the core support barrel (Table 8.3-1) have been verified by performing tensile tests on the core support barrel material attached to thermal shield lug, position No. 1. Tensile tests were performed at room and operating (575^{o}F) temperature.

Metallographic samples described in Chapter 7 indicate no detrimental condition, principally a sensitized microstructure, associated with the core barrel material.

8.3.3 Thermal and Hydraulic Considerations

8.3.3.1 Thermal Considerations

Core support barrel temperature is an important consideration in the integrity analysis since temperatures give rise to thermal stresses that must be considered in the core support barrel analysis.

A one-dimensional slab heat transfer model was used to determine temperatures for evaluation of core support barrel integrity. The results from this model were in good agreement with core support barrel temperatures far from the hole in comparison cases run with the finite element thermal model discussed in Section 6.2.2.3.

A natural convection boundary condition was imposed on the inner surface (i.e., side facing the core shroud) of the core support barrel, based on a conservatively high coolant temperature. A forced convection boundary condition was imposed on the outer surface (i.e., surface facing the reactor vessel) based on the vessel inlet coolant temperature.

Energy deposition rates (e.d.r.) associated with full power operation were used in the 1-D analysis. These e.d.r. were based on the axial peak at the level of core support barrel damage and included a deterministically applied 30% uncertainty allowance.

Stresses based on the results of the thermal analysis have been used in the core support barrel fatigue analysis and provided acceptable results.

Pump-Induced Loads

Pump-induced acoustic loads acting on the core support barrel were calculated at an inlet temperature of 548°F at the following four pump characteristic frequencies:

1. rotor speed, 15 HZ
2. 2 x rotor speed, 30 HZ
3. blade passing frequency, 75 HZ
4. 2 x blade passing frequency, 150 HZ

The pump-induced loads on the core support barrel are determined using two hydrodynamic models:

1. The first model evaluates the propagation of pump-induced pressure pulsations in the cold leg water column from the pump discharge to the inlet nozzle on the vessel.

2. The second model evaluates the propagation of pump-induced pressure pulsations in the downcomer water column in the reactor vessel. The output from the first model is used to drive the second.

The wave equation for a compressible, inviscid fluid is set up and solved for each model. For the case of the downcomer, the series solution for the resulting 3-D wave equation was solved by means of a C-E computer code, DPVIB.

8.3.3.2 Hydraulic Loads

The normal operating loads, generated for use in the integrity analysis, consist of the following categories of loads:

1. Static Hydraulic loads,
2. Pump Induced loads, and
3. Turbulence Induced loads.

These are discussed in detail in the following sections.

Static Hydraulic Loads

The static hydraulic loads acting on the portion of the core support barrel extending from the thermal shield lug elevation down to its bottom are given in Table 8.3-3 and Figure 8.3-5. Loads were calculated for the two sets of conditions given in Table 8.3-4; the most adverse loads were chosen as input to the integrity analysis.

The axial hydraulic load in Table 8.3-3 is based on the operating conditions in Table 8.3-4 and calculated loss coefficients for the flow path segments between the inlet nozzles and the upper region. The maximum radial delta p across the core support barrel wall in Table 8.3-3 is also based on calculated loss coefficients.

The lateral loading distributions on the core support barrel given in Figure 8.3-5, are based on measured total pressures and flow kinetic heads in the downcomer region of a scaled flow model of the St. Lucie 1 reactor.

The output from the downcomer model consists of a description of the pressure distribution on the core support barrel wall, $P_o\ (R_{CSB}, \theta, Z)$. Typically, a pressure distribution is generated at each pump driving frequency for the case of a single operating pump with a nominal unit fluctuating inlet nozzle pressure. The resulting pressure distribution is described by the series:

$$P_o\ (R_{CSB}, \theta, Z) = \sum_m H_m \cos m\theta$$

where:

$$H_m = \sum_n \sum_s C_{nms} \left| J_m\ (\lambda_{nms}\ r) + \eta_{nms} Y_m(\lambda_{nms}\ r) \right| \cos \alpha_n Z$$

m = Circumferential wave number

n = Axial wave number

s = Radial wave number

C_{nms} = Fourier coefficient

η_{nms} = Eigenvalue = $(W_n{}^2{}_{ms}/Co^2 - n^2)^{1/2}$

W_{nms} = Liquid natural frequency

Co = Speed of sound in liquid

α_n = Variable related to the axial waves = n/L

r = Radius

J_m, Y_m = Bessel functions of first and second type

Z = Axial position

θ = Azimuthal position referenced to the zero degree position for the operating pump

L = Length of downcomer annulus

The pressure distribution P_o (R_{CSB}, θ, Z) based on the nominal unit psi inlet pressure, is scaled by the calculated inlet nozzle pressure that is output from the model for the cold leg.

$$P\ (R_{CSB}, \theta, Z) = P_{inlet} \times P_o\ (R_{CSB}, \theta, Z)$$

where:

P_{inlet} = calculated pump-induced pressure fluctuation at the vessel inlet nozzle; values are given in Table 8.3-5

To obtain the overall pressure distribution P (R_{CSB}, θ, Z) on the core support barrel, for multiple pump operation, the pressure distribution for the single pump case was superimposed at the appropriate azimuthal positions for the particular operating pumps. To maximize pressure fluctuations on the downcomer, the phasing between the operating pumps was selected to produce the most adverse loading condition on the core support barrel.

Turbulence-Induced Loads

Hydraulic excitation of the core support barrel due to random turbulence was calculated from a power spectral density vs. frequency plot based on turbulent pressure fluctuation measurement in a scaled PWR model and coherence areas determined from laboratory and field test data inside a PWR.

The normalized power spectral density (PSD) plot developed from those sources for the downcomer annulus is given in Figure 6.2-5. The parameters associated with the PSD are defined as:

$\emptyset$ - normalized power spectral density for the turbulent pressure fluctuations

PSD - power spectral density for the turbulence, PFS^2/HZ

ρ - coolant density, lb/ft^3

U - average coolant velocity, FPS

U_{conv} - turbulence convection velocity, FPS

δ - radial gap of annulus, ft

F - frequency, HZ

$A_{coherence}$ - coherence area, ft^2

The coherence area for the turbulent pressures was calculated from the square of the radial gap of the downcomer annulus.

REFERENCES (Section 8.2)

1. CDC-MARC Finite Element Computer Program

2. R. E. Peterson, Stress Concentration Factors, John Wiley and Sons, N.Y., 1974 .

3. ANSYS Finite Element Computer Program

Table 8.3-1

Normal Operation plus Upset Conditions

Stress Category	Calculated Stress* psi	Allowable Stress psi
P_m	5,500	16,200
$P_m + P_b$	7,300	24,300
$P_m + P_b + Q$	21,000	48,600
Fatigue Usage Factor <1		

* Includes Seismic

Faulted Condition

Stress Category	Calculated Stress psi	Allowable Stress psi
P_m	21,200	38,900
$P_m + P_b$	42,500	50,000

TABLE 8.3-2

MECHANICAL PROPERTIES OF THE CORE SUPPORT BARREL

		Lug#1 Material	
	R.T.	R.T.	575 °F
ULTIMATE TENSILE STRENGTH (KSI)	82.9	92.4	70.5
YIELD STRENGTH (KSI)	40.3	51.4	42.7
UNIFORM ENLONGATION (%)	70	75	33

TABLE 8.3-3

NORMAL OPERATING STATIC HYDRAULIC LOADS
ON THE
CORE SUPPORT BARREL

Type of Load	Loading Value	Loading Condition
Axial Uplift Load	267,000 lb.	(See Table 8.3-4) Condition No. 2
Radial Pressure Differential Across CSB Wall at Thermal Shield Lug Elevation	29.9 PSI (Directed Radially Inwards)	Condition No. 1

TABLE 8.3-4

NORMAL OPERATING CONDITIONS
FOR
CALCULATING HYDRAULIC LOADS

Parameter	Condition No. 1 For Maximum Loading	Condition No. 2 For Minimum Loading
Inlet Temp	500°F	548°F
System Flow Rate	130% of ODES *	116% of ODES *
Power Level	Zero Power	2700 MWT

*Design flow range is based on a ± 7% band about the best estimate measured (Cycle 1) flow rate of 123% of ODES (324,800 gpm).

TABLE 8.3-5

PRESSURE FLUCTUATIONS
AT THE
INLET NOZZLE STATION

$T = 548^{o}F$

	Pump Characteristic Frequency		Peak Pressure Fluctuation, P_{inlet}
	Description	Value	psi
1.	Rotor Speed	15	± 0.15
2.	2x Rotor Speed	30	± 0.05
3.	Blade Passing	75	± 0.64
4.	2x Blade Passing	150	± 0.08

FIGURE 8.3-1

STRESS CONCENTRATION FACTOR
FOR A 32 INCH CRACK WITH END CIRCULAR HOLES

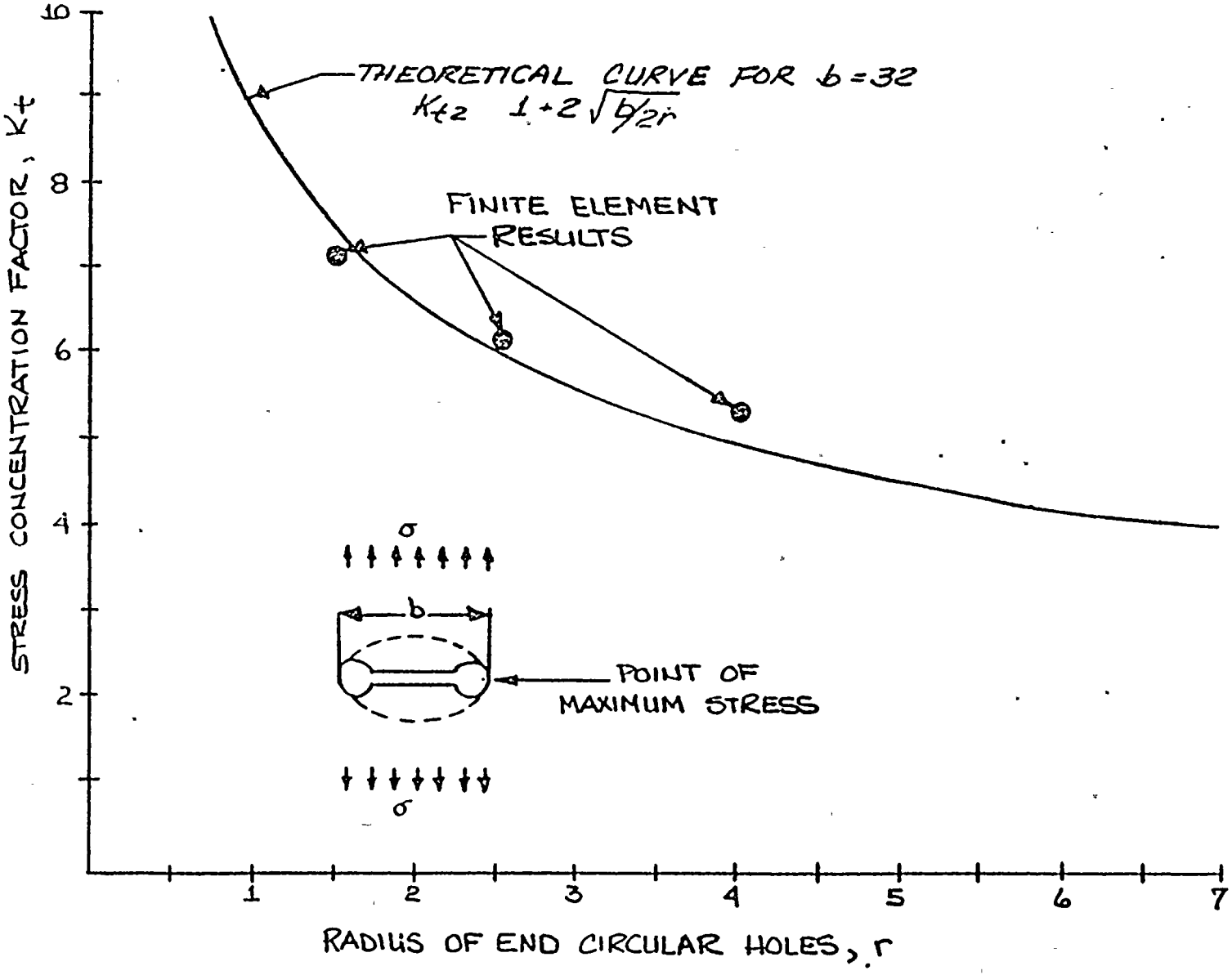

FIGURE 8.3-2

FINITE ELEMENT MODEL OF CRACK WITH TWO END CIRCULAR HOLES

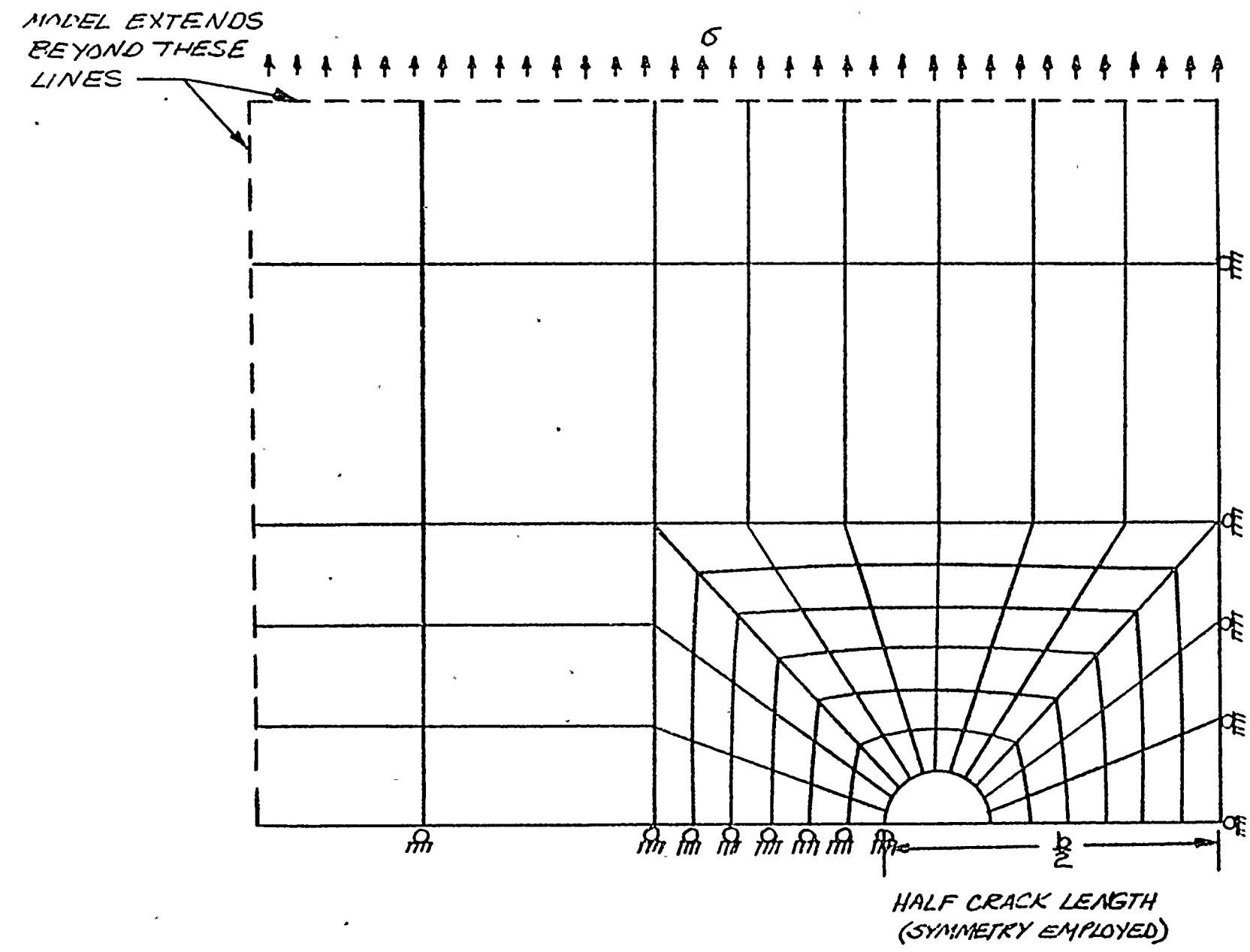

Figure 8.3-3

FINITE ELEMENT MODEL OF THE CORE SUPPORT BARREL (CSB)

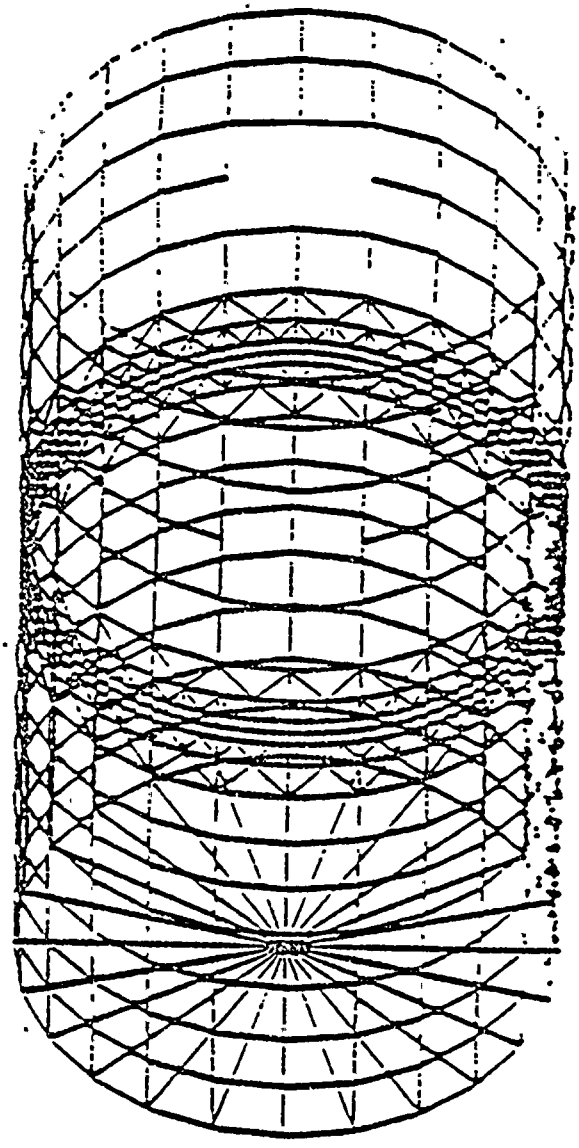

FIGURE 8.3-4

NORMAL OPERATING LATERAL HYDRAULIC LOADS

ON THE CORE SUPPORT BARREL

T_{in} = 500°F; Q = 130% of ODES

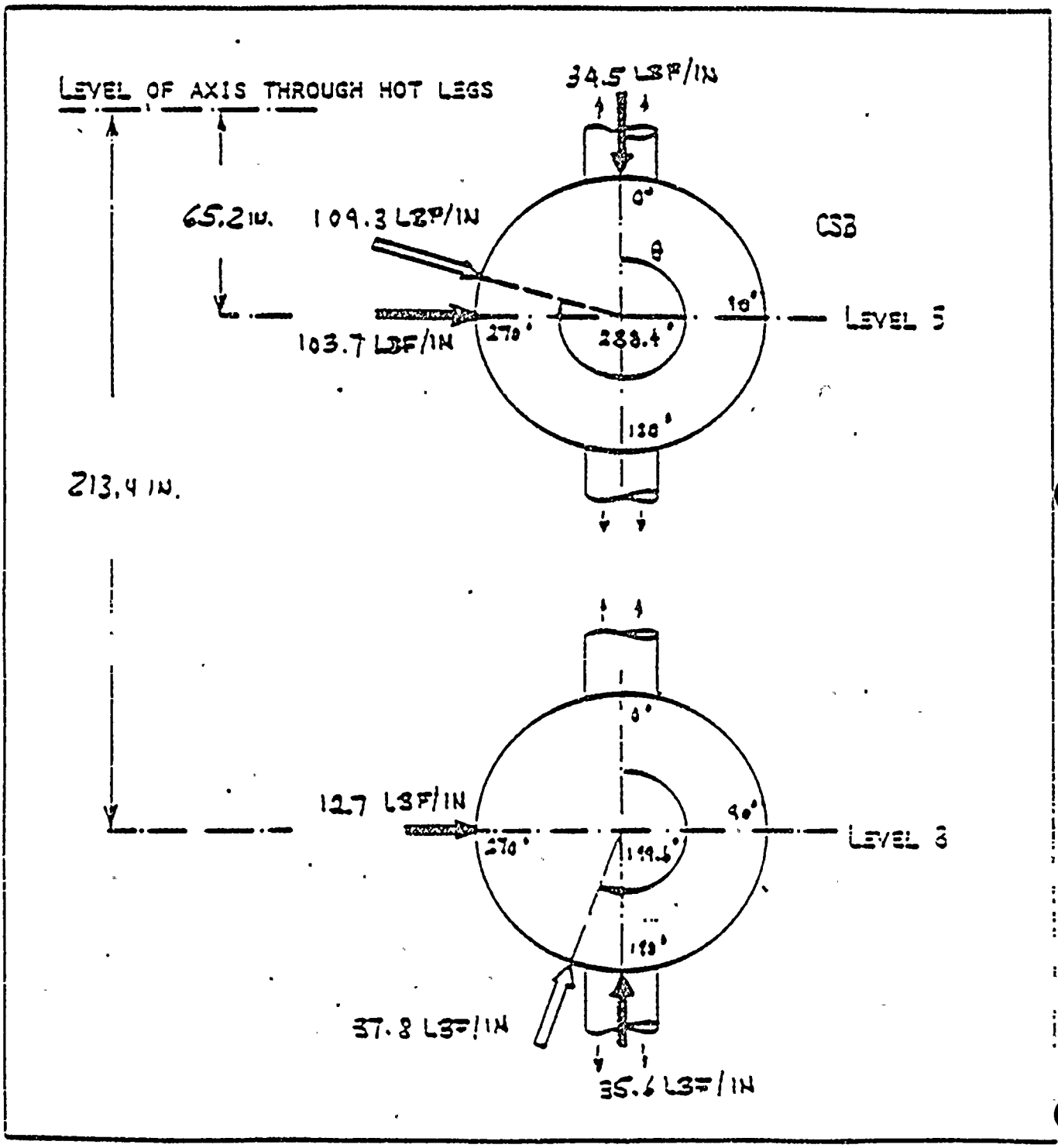

9.0 SAFETY ANALYSIS

9.1 INTRODUCTION

Removal of the thermal shield and repairs to the core support barrel were evaluated for impact on primary system flow rate, core inlet flow distribution, and core bypass leakage rates. The details of these evaluations are discussed in Sections 9.2 and 9.3.

Given that the plugs and patch plates meet their functional objectives, the only effect of the thermal shield removal and the core support barrel repairs on the core thermal and hydraulic conditions is a slightly higher core flow due to the removal of the thermal shield and a slightly lower core flow due to the very small bypass leakage which might exist around the plugs, patch plates, and cracks in the core support barrel. The net result on actual operation is that the core thermal hydraulic conditions change by an insignificant amount.

Although the core support barrel repair functional design objective is for maintenance of plug integrity for all normal and accident conditions, an assessment of the impact of a repair failure is included in Section 9.3 to show that even in the extremely unlikely event that a patch assembly fails, the consequences of transients and accidents remain acceptable. The low probability of such failures is based on the conservative design assumptions and testing discussed in Chapter 6.0.

Material in Section 9.4 shows that the removal of the thermal shield and the core support barrel repairs do not significantly impact the core thermal hydraulic conditions and that the Cycle 6 safety analyses submitted in References 1 and 2 remain applicable.

Neither the assessment assuming that the plugs remain intact nor the assessment in which a repair thermal shield assumed to fail, take credit for the additional system flow resulting from thermal shield removal.

REFERENCES

1. XN-NF-82-81 Rev. 1, St. Lucie Unit 1 Cycle 6 Safety Analysis Report, January, 1983.

2. XN-NF-82-99, Plant Transient Analysis for St. Lucie Unit 1, January, 1983.

9.2 EFFECT OF THERMAL SHIELD REMOVAL

9.2.1 Primary System Flow Rate

Removal of the thermal shield results in a net decrease in reactor vessel pressure drop of 1.1 psi at normal operating conditions with a total reactor system coolant flow rate of 370,000 gpm (minimum guaranteed). The reduced resistance in turn results in an increase in reactor coolant system flow rate by +0.5% of design flow rate.

9.2.2 Core Inlet Flow Distribution

Removal of the thermal shield has negligible impact on the core inlet flow distribution. This conclusion is reached based on examination of scaled reactor flow model test results and on operating experience with several C-E reactors that do not have thermal shields.

Scaled flow model tests have been run on a C-E 4-loop reactor configuration, both with and without a thermal shield. Examination of the core inlet flow distributions show that resulting differences in the assembly inlet flow factors are very small. Further, there are no systematic trends in the changes in the flow factors that could be related to the removal of the thermal shield. It is concluded from these test results that the thermal shield removal has no systematic impact on core inlet flow distribution.

In other reactor flow model tests on C-E 3410 MWT class reactors, which are very similar in geometry and layout to St. Lucie Unit 1, the core inlet flow distribution was also measured without a thermal shield. The resulting core inlet flow distribution was relatively uniform and indicated that an acceptable flow distribution can be achieved without the presence of a thermal shield. The

relatively uniform core inlet flow distribution is attributed to the flattening effects of (1) the hydraulic resistance of the flow skirt, (2) the lower support structure bottom plate, and (3) the core support plate, all located between the exit of the downcomer annulus and the core inlet plane.

Finally, successful operation of other 2560 Mwt class reactors, which are similar in construction to St. Lucie Unit 1 and also operate at 2700 Mwt ("stretch" rating) as well as the 3410 MWT class reactors indicates no unusual or unacceptable thermal hydraulic performance for C-E reactor designs without thermal shields.

9.3 EFFECT OF CORE SUPPORT BARREL REPAIRS

9.3.1. Bypass Leakage Rates

9.3.1.1 Revised Total Core Bypass Leakage - Normal Operation

As discussed earlier, following removal of the thermal shield, close inspection of the core support barrel revealed cracks and holes requiring repair. To prevent further propagation of cracks under continued service conditions, crack arrestor holes were machined through the core support barrel at the tips of the cracks. An expandable plug was then inserted into each of these holes and tightly swaged at the inside surface of the core support barrel. The radial gap size through the shank portion of the flow path was conservatively estimated to be .050" maximum and has relatively little hydraulic resistance compared with the balance of the flow path. The plug flange was designed to function as a belleville spring with the outboard undersurface seating on the core support barrel spotface. Because the plug flange contains four alignment monitoring holes which are inboard of the flange contact line, the controlling hydraulic resistance is the gap at the plug swage. The bypass leakage analysis assumed a maximum radial gap at the plug swage of 0.001 inches. Using this assumption, the bypass leakage through expandable plugs is calculated to be 70.1 lbm/hr per inch of plug hole perimeter. The hole schedule given in Table 9.3-1 tabularizes cumulative plug hole perimeter of 427.4 inches giving a total plug bypass flow of 29,970 lbm/hr at normal operating conditions. Plug testing demonstrated significantly less leakage than the calculated 70.1 lbm/hr per inch plug hole perimeter.

The tear out at lug location No. 1 was too extensive to repair with plugs alone. As described in Chapter 6, a special patch assembly was designed which was anchored to the core support barrel by four expandable plugs. The interface between the patch boss and the periphery of the core support barrel through hole was conservatively assumed to have a maximum average gap of .015. Other smaller patch assemblies were used at lugs 3, 4, 5, and 6. The total patch bypass flow is calculated to be 205,490 lbm/hr during normal operation.

Those portions of the core support barrel through wall cracks which have not been removed for plugs or covered by the patch are estimated to be no more than 115 inches in cumulative length. All through wall cracks have been appropriately terminated by either patches or plugs. Visual examinations have indicated the crack widths to be quite small. Assuming a conservative average width of .005", the bypass flow is calculated to be 29,175 lbm/hr during normal operation.

The total additional bypass leakage at a flow rate of 370,000 gpm due to core support barrel cracks and repairs is thus:

Bypass Flowpath	Leakage, lbm/hr @T_{IN} 549^{o}
All Expandable Plugs	29,970
Patch Plates at Lug Nos. 1, 3, 4, 5, and 6	205,490
Remaining Cracks	29,175
TOTAL	264,635

A summary of the core bypass flow at normal operating conditions following core support barrel repairs is given in Table 9.3-2, and shows that the additional bypass flow resulting from the repairs is less than 0.3%.

9.3.1.2 Core Bypass Leakage with Failed Core Support Barrel Patch Assembly

Table 9.3-3 provides a summary of the core bypass leakage flow distribution that is predicted if the Lug No. 1 patch assembly is assumed to fail. It was assumed that the four 3" heavy wall plugs used to anchor the patch plate also fail. The core flow rate will decrease by 2.94% over that for normal operation (Table 9.3-4). Since the patch assembly covers the largest through wall area in the core support barrel, the core bypass leakage flow given in Table 9.3-3 would be the maximum value predicted for failure of a single repaired area. Note that this failure would require the extremely unlikely failure of four expandable plugs simultaneously.

9.3.1.3 Impact of Hypothetical Core Support Barrel Patch Assembly Failure on Core Flow Rate

The assumed failure of the core support barrel plug or patch assembly reduces the hydraulic resistance of the reactor; the net effect being that the reduced system resistance intersects the pump performance curve at a larger system flow rate. The larger system flow rate partially offsets the increased core bypass leakage flow due to the failed patch assembly.

Table 9.3-4 compares the resulting predicted best estimate reactor vessel flow rate ratios and core flow rate ratios for normal operation and a failed patch assembly. The listed reactor vessel flow rate ratios are based on measured pump performance curves and calculated system resistance data.

9.3.2 Assessment of Core Support Barrel Repair Failure on Transients and Accidents*

Chapter 6 discusses the core support barrel repairs design assumptions and the testing behind the conclusion that failure of an expandable plug is a highly unlikely event. Exxon Nuclear Company (ENC) has examined effects on the St. Lucie 1 Design Basis Events (DBEs), the Limiting Conditions for Operation (LCOs) and the Limiting Safety System Settings (LSSSs) assuming an increased core bypass flow which envelopes the loss of the largest core support barrel repair (patch and lug no. 1). The assumed consequent reduction in core flow for Cycle 6 was 3.1%. This value conservatively envelopes the 2.94% value calculated in Table 9.3-4. These analyses demonstrate that the predicted effects of a hypothetical failure of the core support barrel patch are acceptable. The event was analyzed to radiation criteria; should LCOs and LSSSs provide protection of Safe Acceptable Fuel Design Limits (SAFDLs), the dose criteria are automatically satisfied.

For verifying the current LCOs, the Control Element Assembly (CEA) drop event and the Loss of Coolant Flow (LOCF) event were reanalyzed using the same statistical methods, and initial conditions as were used in the setpoints determination previously forwarded as Reference (1) of Section 9.1, but with a 3.1% core flow reduction. The allowable LCO boundaries are reduced approximately 3% of rated power from those previously calculated by Exxon and reported in Reference (1) of Section 9.1, but still provide significant margins to the actual LCO limits imposed by current Technical Specifications. This is shown in Figure 9.3-1.

---

*Discussion provided by Florida Power and Light and Exxon Nuclear Company.

For verifying the current LSSSs, only the Thermal Margin Low Pressure (TMLP) trip need be examined in detail. Other LSSSs would not be adversely affected by the core flow degradation because they are triggered by other system parameters (e.g. nuclear instrument signals, system pressures, etc.), and their adequacy was demonstrated by the deterministic transient calculations discussed later.

The TMLP trip verification previously forwarded in the Cycle 6 Reload Safety Evaluation (Reference 1 of Section 9.1) demonstrated 70 psi margin to DNB at the system state point closest to the DNB limit from all cases analyzed. Exxon has determined that the assumed 3.1% additional core flow degradation would reduce this margin by 92 psi. For the core support barrel patch failure, then, the TMLP trip might not have prevented DNB. Therefore, transients protected by the TMLP trip have been further examined.

The most limiting Design Basis Events (DBE's) which would be adversely affected by the core flow degradation (including those which needed to be examined due to the concern with the TMLP trip) were determined to be:

a) Loss of Coolant Flow
b) CEA Drop
c) Excess Load
d) Depressurization
e) Steam Generator Tube Rupture
f) Seized Rotor

Other DBE's have been previously shown in Cycle 6 and earlier Reload Safety Evaluation submittals to produce less restrictive DNB ratios than the transients listed above, or else would not be affected by the flow redistribution in the core/bypass area.

ENC has analyzed all of the listed DBE's using their PTSPWR2 code to obtain system characteristics. (These system analysis results for all but the Steam Generator Tube Rupture SGTR have already been submitted to the NRC in Reference (2) of Section 9.1. These analyses were performed by applying uncertainties deterministically and therefore conservatively. The methods were fully described in these previous submittals.

Under the assumption of failure of a core support barrel patch, the core flows were further degraded by 3.1%. The degraded flows have been used by ENC as inputs to a detailed subchannel analysis using the XCOBRA-IIIC code and the XNB correlations to predict DNBR. The inputs used are summarized on Table 9.3-5. Even under the new, more adverse core flow constraints, only three of the transients listed (LOCF, Depressurization, Seized Rotor) breached the DNB limit. Further, as discussed previously, a statistical rather than deterministic calculation for LOCF has already demonstrated no breach of DNB with the loss of the core support barrel patch. Of the two remaining events, the Seized Rotor is most severe, predicting 1.8% of all rods to be experiencing DNB. Conservatively assuming all rods at DNB will fail and ratioing the damage calculated here to predicted damage and doses from prior cycles submittals, ENC has determined that the predicted offsite doses remain a small fraction of 10CFR100 limits. Results of the ENC calculations are provided in Table 9.3-6.

Based on the ENC analysis, and considering the core support barrel patch failure as a highly unlikely event it is concluded that;

a) Any DBE coupled with a core support barrel repair failure is a highly unlikely event where some fuel damage and offsite dose is acceptable.

b) LCO's and LSSS as found in current Technical Specifications need not be changed.

c) In cases where DNB limits are breached and fuel damage is possible, the worst predicted damage remains at an acceptable level and offsite doses remain an acceptably small fraction of 10CFR100 limits.

9.4 APPLICABILITY OF CYCLE 6 SAFETY ANALYSIS *

Exxon Nuclear Company has reassessed the safety conclusions previously forwarded in the Cycle 6 Reload Safety Evaluation and concluded that they remain valid for normal operation in light of the proposed plug repair and consequent increases in bypass flow for the St. Lucie 1 core barrel.

The calculated core bypass leakage increases during Cycle 6 as a result of flow around the plugs and through cracks in the barrel. The increase in bypass flow has been conservatively estimated to be less than 0.3%, based on an all Exxon Nuclear core, such as is anticipated for Cycle 8.

Prior to the discovery of cracks in the core support barrel, Exxon Nuclear had completed the Reload Safety Analysis for Cycle 6, and Florida Power and Light (FP&L) submitted it to the Nuclear Regulatory Commission. Exxon Nuclear had already applied appropriate core flow penalties to Exxon Nuclear assemblies to account for cross flows in the fixed core and higher burnable poison rod loadings for Cycle 6.

In light of possible increases in bypass flow, Exxon Nuclear has reassessed their Reload Safety Evaluation and has concluded that:

1. Prior LOCA submittals prepared by Exxon Nuclear already assumed a bypass flow in excess of that anticipated with the repaired core support barrel. Therefore, the LOCA analyses remain valid.

---

* Discussion provided by Florida Power and Light and Exxon Nuclear Company.

2. The verification of the LCO curves and TM/LP trip setpoints performed by Exxon Nuclear would exhibit only a slight reduction in the demonstrated margins. Florida Power and Light chose to continue using the curves shown in the present Technical Specification (based on C-E Cycle 4 and Cycle 5 "stretch" power submittals) and the allowable operating region for Cycle 6 is still well within safe limits because the Technical Specifications are more limiting than those required by the Exxon Nuclear analysis.

3. A detailed recalculation of the transient analyses performed by Exxon Nuclear using the increased bypass flow values would result in a DNBR reduction of not more than 0.01 from that previously calculated. With the exception of the seized rotor event, all transient events analyzed have greater than a 0.01 margin to the MDNBR limit.

4. For the seized rotor event, two cases were analyzed; one to maximize the pressure peak, and the second to minimize predicted DNBR. Since the seized rotor event is terminated by low flow differential pressure sensors on the loops, the calculation to maximum pressure would be unaffected by any flow redistribution occurring in the core/bypass area. The calculation to minimize DNBR previously performed by Exxon Nuclear showed an MDNBR = 1.189 and significantly less than 1% fuel damage. As with the other transient calculations mentioned above, a recalculation would show a further decrease in the MDNBR by less than 0.01, which would not appreciably increase the level of fuel damage.

All four conclusions stated are based on the Technical Specification minimum loop flow of 370,00 gpm and take credit for neither the expected increase in system flow resulting from removal of the thermal shield nor for the actual plant flow measurements, which are in excess of the required minimum.

Table 9.3-1

St. Lucie Unit 1

Inventory, Areas, and Perimeters of
Core Support Barrel Holes

Device	Hole Size (in)	No. of Holes	Total Area (in^2)	Total Plug Perimeter (in)	Patch Perimeter (in)
Plug	8.0D	8	402.1	201.1	-
Plug	5.0D	2	39.3	31.4	-
Plug	3.1D	2	15.1	19.5	-
Patch Lug No. 1 with Plugs 3.1D(1)		1	85.2(2)	-	40.0
		4	30.2(2)	39.0	-
Patch Lug No. 3 with Plugs 3.1D(1)		1	26.3	-	27.6
		3	22.6	29.2	-
Patch Lug No. 4 with Plugs 3.1D(1)		1	46.1	-	29.7
		4	30.2	39.0	-
Patch Lug No. 5 with Plugs 3.1D(1)		1	55.3	-	34.4
		4	30.2	39.0	-
Patch Lug No. 6 with Plugs 3.1D(1)		1	53.1	-	37.2
		3	22.6	29.2	-
				427.4	168.9

(1) Plugs used to anchor lug patch plate

(2) Maximum credible size of repair failure (requires simultaneous failure of all four plugs holding in the patch and loss of the patch itself)

$85.2\ in^2$
$30.2\ in^2$

$115.4\ in^2$

Table 9.3-2

St. Lucie Unit 1

Best Estimate Core Bypass Flow Distribution
With All Core Support Barrel Plugs and
Lug Patch Assemblies Installed
Normal Operation

Leakage Path	Bypass Flow Rate (% of Vessel Flow Rate)
Alignment Keys	0.09
Outlet Nozzle Gap	1.18
Core Shroud:	
Holes	0.27
Seams	0.23
Guide Tubes	1.61
Surveillance Holes in Core Support Barrel Flange (6)	0.08
Core Support Barrel Plugs/Patch Assembly and Crack Clearances	0.19
Total Bypass Flow	3.65

Table 9.3-3

St. Lucie Unit 1

Best Estimate Core Bypass Flow Distribution
With Failure of Lug No. 1 Patch Assembly
Cycle 6

Leakage Path	Bypass Flow Rate (% of Vessel Flow Rate)
Alignment Keys	0.09
Outlet Nozzle Gap	1.17
Core Shroud:	
Holes	0.25
Seams	0.19
Guide Tubes	1.56
Surveillance Holes in Core Ssupport Barrel Flange (6)	0.08
Core Support Barrel Plugs/Patch Assembly and Crack Clearances	0.14
Failed Lug No. 1 Patch Assembly	3.45
Total Bypass Flow	6.93

Table 9.3-4

St. Lucie Unit 1

Predicted Best Estimate Reactor Vessel
And Core Flow Rate Ratios

Operational Description	Ratio of Vessel Flow Rate to Normal Operating Vessel Flow Rate	Ratio of Core Flow Rate to Normal Operating Vessel Flow Rate
Normal Operation	1.0000	.9635
Lug No. 1 Patch Assembly Missing ($115.4\ in^2$) (See Table 9.3-1)	1.0036	.9341

Difference in Core Flow
Normal Operation Versus Largest Repair Failure

Normal Operation	96.35%
Lug No. 1 Patch Assembly Missing	-93.41%
	2.94%

Table 9.3-5

XCOBRA-IIIC Input Summary

Transient	Pressure[1] (psia)	T_{inlet}[2] (°F)	Core Flow (Mlb/hr)	Power[3] (MW)
Loss of Coolant Flow	2260	551	106.3	2789
CEA Drop[4]	2230	547	131.0	2761
Excess Load	1939	531	131.7	2832
RCS Depressurization	1941	551	130.8	2885
Pump Seizure	2266	551	99.4	2811
Steam Generator Tube Rupture	1843[5]	551	130.7	2754

1) Includes a 50 psi error for the operating band and a 40 psi adjustment to go from pressurizer pressure to core exit pressure.

2) Includes 2°F error

3) Based on heat flux; for 102% of rated power

4) Uses a 10% hot channel peaking augmentation

5) Conservative value with respect to trip minimum

Table 9.3-6

Summary of Transient Results
with Core Support Barrel Patch Failure

TRANSIENTS	Minimum DNB Ratio	Percent of Rods in DNB
Previously Analyzed as AOOs for Cycle 6*	1.131	0.28
Loss of Coolant Flow		
CEA Drop	1.361	0.0
Excess Load	1.486	0.0
Rapid Depressurization	1.144	0.22
Analyzed as PAs for Cycle 6		
Pump Rotor Seizure	0.97	1.80
PA Not Analyzed for Cycle 6		
Steam Generator Tube Rupture	1.212	0.05

*Treated as PAs for Core Support Barrel Patch Failure.

FIGURE 9.3-1

LCO VERIFICATION FOR PSL-1 W FAILED CSB PLUG

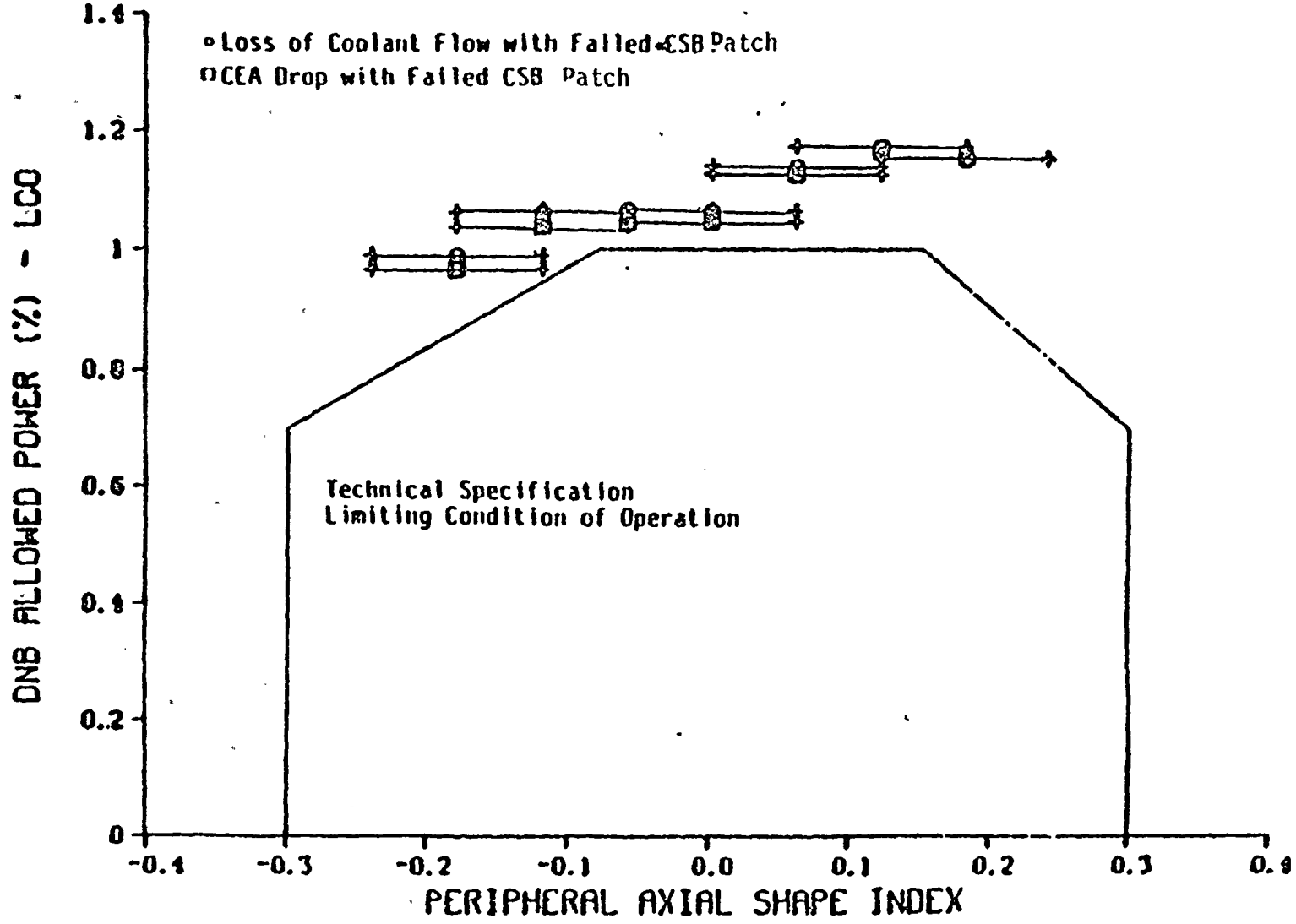

10.0 MONITORING AND INSPECTION PROGRAMS

10.1 INTRODUCTION

Two diagnostic systems are used for monitoring the integrity of the reactor coolant system internals during normal power operation. These diagnostic systems are the Internals Vibration Monitoring (IVM) system and the Loose Parts Monitoring (LPM) system.

The IVM system monitors the signal output or "noise" from six summed (upper plus lower) linear power range excore flux detectors. The out of phase signal component from two pairs of detectors on opposite sides of the reactor provide a reliable indicator of coupled reactor core and core support barrel vibrations. The IVM system provides the signal conditioning and statistical processing necessary to provide estimates of core/CSB vibration.

The LPM system monitors the output from accelerometers mounted on the external surface of the reactor vessel and steam generators. This system has proven to be an indicator of loose and free parts within the primary system. Metal to metal impacting within the primary system causes high frequency impulse vibrations on the reactor system shell which are detected by the LPM system.

10.2 MONITORING OBJECTIVES

Both the IVM and LPM systems provide accurate and reliable diagnostic information about the integrity of the reactor internals. The primary monitoring objective is to use this information to provide as early an indication as possible of degradation or failure of reactor internals components.

The state of the art for these monitoring systems has not progressed to the point where they can provide an immediate and absolute indication of an internals failure. However, the systems can provide considerable information to personnel trained and experienced in diagnosis of "reactor noise monitoring."

There is a trade off between monitoring sensitivity and the incidence of expected false indications. The monitoring philosophy described here is to maintain a high degree of sensitivity and accept some false indications which will require disposition by an experienced diagnostician.

10.3 EXCORE MONITORING

Excore monitors are used with the Internals Vibration Monitoring (IVM) system. St. Lucie 1 technical specifications adequately direct the type and frequency of monitoring with this system.

10.3.1 SYSTEM DESCRIPTION

The IVM is an automated, computer based system specifically designed to acquire, analyze, and interpret small variations in excore nuclear detector signals for the purpose of identifying reactor core and core support barrel motion. The system is based on a Hewlet Packard 5451-A Fourier Analyzer capable of accepting analog information, digitally converting it and processing it in both the time and frequency domains. The IVM system provides descriptors of the frequency region of motion, its amplitude probability distribution, the azimuthal character of the motion, and a quantitative measure of the root mean square (RMS) vibration amplitude. The system also provides the capability of selecting a wide range of statistical analysis functions providing considerable flexibility when diagnosing anomalous signals.

The IVM system has been programmed for three modes of operation; 1) continuous monitoring of internals motion by comparison of calculated RMS values of excore signal amplitude to preset limits, 2) calculation and plotting of amplitude probability density (APD) functions for each of the six excore signals, and 3) Fourier analysis consisting of calculation and plotting of power spectral density (PSD), cross PSD, coherence, and phase measurements for each of three pairs of excore detector signals. All measurements are capable of being made over a frequency range of 0.1 to 17 HZ.

10.3.2 DATA ACQUISITION SCHEDULE

Baseline APD and Fourier analysis data is obtained at 20, 50, 80, and 100 percent power after each refueling outage. APD and Fourier analyses are planned at monthly intervals during the first cycle after the core support barrel repair and at four month intervals during subsequent fuel cycles if no significant change in internals motion is observed.

10.3.3 DIAGNOSTICS

Baseline data will be reviewed and interpreted as to the mechanical significance of detected internals motions. Preferential frequencies and the amplitude of measured core and core support barrel motion will be compared to predicted analytical values.

APD and Fourier analysis data obtained during the cycle will be reviewed as to its significance to the integrity of the reactor internals. Recommendations with respect to any special visual examination of reactor vessel internals that are required will be the objective of the data review.

10.4 LOOSE PARTS MONITORING

The Loose Parts Monitoring (LPM) system detects vibrations on the external surface of the reactor vessel and steam generators. In addition to normal "background" vibration caused by mechanical and flow induced sources, the system detects impulse like variations caused by metal to metal impacting within, on, or near the primary system.

10.4.1. SYSTEM DESCRIPTION

The signals from eight accelerometers mounted on the primary system are monitored by the LPM system. Each of the eight channels has a frequency response of 5 to 5000 HZ and is conditioned by a preamplifier located in containment. The signals terminate at an electrical cabinet in the control room. The cabinet contains an amplifier, peak detector, and alarm module for each channel. The alarm setpoint is compared against the instantaneous peak value of an accelerometer signal. When exceeded, an alarm status indicator is lighted and remains lighted until manually reset.

The LPM system also contains audio output for listening to a selected channel. Since the signals are in the audio range, changes in the signals are easily detected by the human ear.

The primary readout device on the system is an oscillographic recorder. It produces time history strip chart recordings of all eight accelerometer signals on light sensitive paper at chart speeds of up to 160 in/sec. The eight signals are also available for monitoring by external equipment such as an oscilloscope or magnetic tape recorder.

10.4.2 DATA ACQUISITION

Normal monitoring consists of the LPM system continuously comparing the instantaneous peak value of each accelerometer signal to its individual setpoint. An alarm is indicated for the channel or channels which exceed the setpoint(s).

For the LPM system to be effective as a diagnostic tool when a possible loose part is detected, information about the response of the accelerometers to a loose part must be known. This information has already been obtained from an impact calibration test at St. Lucie 1.

Since the accelerometers are also sensitive to normal mechanical and flow induced vibrations of the primary system, these "background" vibration levels are used to determine the minimum setpoint levels which will not cause an excessive number of spurious alarms. Typically, the background levels vary with the number of reactor coolant pumps running. For effective operation of the LPM system, setpoints must be as low as possible to detect small impacts and yet high enough to eliminate excessive spurious alarms.

After removal of the thermal shield and during initial power operation, the LPM system setpoints will be determined from baseline data. If any changes in the setpoints are required, the new values will be recorded as well as the reason for the change. During cycle 6 normal power operation, the LPM system alarm status will be recorded at least once per day.

10.4.3 DIAGNOSTICS

Since the LPM is sensitive to external vibrations of the primary system, it will generate alarms for many events besides the occurence of a loose part. The setting of absolute alarm limits which require plant shutdown would tend to limit the effectiveness of the early indication of an internals failure, because the alarm limits would have to be rather insensitive to preclude unacceptability frequent false alarms. However, if persistent LPM system alarms should occur, the source will be evaluated if at all possible by plant personnel. Experienced diagnosticians may also be consulted to evaluate such alarm indications.

10.5 INSPECTION PROGRAM

The design and testing of the expandable plugs has been directed toward a repair that has a service period from cycle six to the end of plant life. The inspection program is designed to provide a means to detect if the crack arrestors and/or expandable plugs are no longer performing their intended design function.

10.5.1 SHORT TERM INSPECTION

10.5.1.1 Core Support Barrel

The cracks in the core support barrel have been machined out or, in the case of through wall cracks, have been arrested via nominal 3", 5", or 8" diameter crack arrest holes which were subsequently plugged. Analysis has shown that these holes are sufficient to prevent crack propagation. During the refueling outage following Cycle 6, FP&L will perform Non Destructive Examinations (NDE) on the core support barrel to verify that the crack lengths have not increased.

10.5.1.2 Core Support Barrel Plug and Patch Inspection

The patches and expandable plugs used in the core support barrel repair have been designed to be effective for the remaining life of the plant. FP&L will assess plug tightness during the refueling outage following Cycle 6. A comparison to baseline readings will then be made to demonstrate plug integrity has been maintained.

10.5.2 LONG TERM INSPECTION

After the Cycle 6 inspections outlined above the next scheduled inspection is the 10 year inservice inspection. Future inspections during the interim period between the end of cycle six and the ten year in-service inspection examination will of course be considered contingent upon the inspection results from cycle six.